Spring 5-15-2019

Dissemination of the apicomplexan parasite, Toxoplasma gondii

Lisa L. Drewry
Washington University in St. Louis

WASHINGTON UNIVERSITY IN ST. LOUIS

Division of Biology and Biomedical Sciences
Molecular Microbiology and Microbial Pathogenesis

Dissertation Examination Committee:
L. David Sibley, Chair
John A. Cooper
Tamara L. Doering
Daniel E. Goldberg
Robyn S. Klein
Gwendalyn G. Randolph

Dissemination of the Apicomplexan Parasite, *Toxoplasma gondii*

by

Lisa LaRhea Drewry

A dissertation presented to
The Graduate School
of Washington University in
partial fulfillment of the
requirements for the degree
of Doctor of Philosophy

May 2019
St. Louis, Missouri

Table of Contents

List of Figures

Chapter 1: Introduction

Chapter 2: *Toxoplasma* actin is required for efficient host cell invasion

Chapter 3: The secreted kinase ROP17 promotes *Toxoplasma gondii* dissemination by hijacking monocyte tissue migration

Chapter 4: Conclusions and future directions

List of Tables

Acknowledgments

The work presented here would not have been possible without extensive support and guidance. I wish to especially thank my mentor, David Sibley. David was a selfless mentor, always generous with his time, ideas, and perspective. Throughout my PhD, David's dedication and enthusiasm for science never failed to impress, and I hope to emulate his example one day. My thesis committee was consistently an excellent source of guidance, experimental suggestions, and scientific collaborations. I have immensely enjoyed working with my colleagues in the Sibley Lab. In particular, Kevin Brown and Bang Shen always patiently answered my most naïve Toxo questions. Nathaniel Jones and Quiling Wang trained me to up my game and work with mice. Alex Rozenberg's boundless optimism for the potential of my project was always a welcome boost to my spirits. Lisa Funkhouser-Jones may have stolen my status as the only Lisa, but also brought contagious enthusiasm to the lab. Georgia Wilke inspired me with her industriousness and resourcefulness. All of my experiments were much less daunting with Jenn Barks providing never-ending fibroblasts for parasite culture. The finishing touches of my research would never have happened without the expertise and tireless assistance of Mark Miller and his colleagues at the IVIC. My many imaging studies would not have been feasible without the resources and assistance provided by Wandy Beatty. My classmates Christina Mikulka, Prachi Bagadia, and Rachel Wong have been wonderful colleagues and dear friends. My parents Don and Deb have always been amazing role models of hard work and supported me in all my endeavors. Most importantly, I need to thank my husband Tyler for being so supportive of my career but also devising adventures that forced me to better prioritize my experiments so that they did not fill every weekend.

Lisa Drewry, Washington University, May 2019

Dedicated to my family.

ABSTRACT OF THE DISSERTATION

Dissemination of the apicomplexan parasite, *Toxoplasma gondii*

by

Lisa LaRhea Drewry

Doctor of Philosophy in Biology and Biomedical Sciences

Molecular Microbiology and Microbial Pathogenesis

Washington University in St. Louis, 2019

Professor L. David Sibley, Chair

The parasitic protist *Toxoplasma gondii* is a common pathogen of rodents and felines that also infects humans. The most severe clinical manifestations of toxoplasmosis in humans derive from the systemic dissemination of *T. gondii*, during which the parasite penetrates biological barriers and accesses protected host compartments such as the central nervous system. *T. gondii* dissemination is enabled by the intrinsic gliding motility of extracellular parasites, which allows for travel to new host cells and tissues, and also powers the invasion of diverse host cells including migratory leukocytes. Dissemination is further advanced when migrating infected leukocytes shuttle intracellular parasites to new locations as they traffic throughout the host.

All *T. gondii* gliding motility and host cell invasion was long presumed to be powered by the work of a parasite actin-myosin motor. The possibility of alternative gliding and invasion mechanisms was suggested by the development of inducible Cre-Lox technology that facilitated inducible disruption of genes thought to encode critical components of the *T. gondii* invasion machinery, including the parasite actin gene *ACT1*. To determine whether ACT1-independent

invasion was likely, inducible *Δact1* parasites were examined for uniformity of ACT1 protein depletion. Individual parasites with residual ACT1 protein persisted long after inducible *ACT1* excision. Suggesting the residual ACT1 content of these parasites was functionally relevant, the invasion of *Δact1* parasites was highly sensitive to an actin polymerization inhibitor. Parasite invasive ability was also found to negatively correlate with the length of time parasites were subjected to ACT1 depletion. Although the existence of ACT1-independent invasion mechanisms cannot be formally excluded, they do not appear to comprise robust alternatives to actin-dependent gliding and invasion in *T. gondii*.

As the most abundantly infected circulating leukocyte during murine toxoplasmosis, monocytes have been theorized to be poised to deliver intracellular *T. gondii* across the blood-brain barrier and into the central nervous system. However, *in vivo* evidence supporting this theory was scarce. *In vitro* models had demonstrated that infection could alter the motility of monocytes when interacting with endothelial vasculature. However, whether infected monocytes could efficiently traverse the specialized endothelium that comprises the blood-brain barrier had not been tested, nor had the ability of infected monocytes to migrate through the tissue environments where *T. gondii* is first encountered. Models of peripheral and blood-brain barrier endothelium were used to show that infection markedly inhibited monocyte transendothelial migration. In contrast, infected monocytes and macrophages migrated through three-dimensional matrices *in vitro* and collagen-rich tissues *in vivo* with enhanced efficiency. Enhanced tissue migration relied on host Rho/ROCK and formin signaling, and the secreted *T. gondii* kinase ROP17. In a murine model, infection with *Δrop17* parasites that fail to enhance tissue migration resulted in delayed dissemination and prolonged mouse survival. These results implicate monocytes in advancing the tissue spread of *T. gondii* during *in vivo* dissemination.

Chapter 1: Introduction

This chapter was composed by LLD and revised according to comments from LDS.

Apicomplexan parasites

Many diseases of medical and veterinary significance are caused parasites belonging to the Apicomplexa phylum. *Plasmodium* species cause malaria, which infects about 200 million and kills over 500,000 annually (1). Cryptosporidiosis was recently realized to be one of the most common causes of severe diarrheal disease in young children (2,3). *Eimeria* (4,5) and *Theileria* species (6) infect poultry and ruminant livestock, leading to substantial economic losses. *Toxoplasma gondii* infection causes toxoplasmosis in a wide array of human and animal hosts (7).

Life cycle of *T. gondii*

Like most of the Apicomplexa, *T. gondii* is an obligate intracellular parasite. However, unlike most of the Apicomplexa, *T. gondii* replication is not restricted to a narrow range of hosts or cell types. *T. gondii* is primarily a pathogen of rodents and felines, but can infect essentially any warm-blooded vertebrate (8). Within these hosts, *T. gondii* can invade and replicate within any nucleated cell type.

T. gondii infections are typically orally acquired upon ingestion of parasite cysts. Ingested cysts can be either sexual stage oocysts or asexual tissue cysts. As the definitive host of *T. gondii*, felines are the only hosts in which the parasite can undergo sexual reproduction (7). Felines are very sensitive to infection with asexual tissue cysts (9), and shed oocysts in their feces after primary *T. gondii* infections (10). Shed and sporulated oocysts contain eight sporozoites, are highly resistant to environmental stresses, and remain infectious for months (11,12). Intermediate hosts can acquire toxoplasmosis through the oral-fecal contact, by ingesting water contaminated with oocysts, or through the consumption of other intermediate hosts harboring tissue cysts (7,11).

Once ingested, the bradyzoites contained within tissue cysts or sporozoites contained within oocysts invade the intestinal lamina propria and differentiate into tachyzoites. Tachyzoites undergo rapid asexual reproduction in many host compartments and their proliferation causes the symptoms of acute toxoplasmosis (7). Immune pressure leads tachyzoites to differentiate into bradyzoites. Bradyzoites form tissue cysts, in which they are largely quiescent but undergo periods of cyclical replication (7,13). Tissue cysts resist immune clearance and can persist for the life of the host, causing a life-long asymptomatic infection. Tissue cysts can be formed in many tissues, but are predominantly found in long-lived tissues such as those of the central nervous system (CNS) and skeletal muscle (7,14,15). Whether cysts are preferentially formed in the CNS or simply persist there more efficiently due to the immuno-specialized nature of the CNS remains a matter of active debate (16).

To replicate during tachyzoite proliferation, *T. gondii* enters host cells using an active penetration mechanism that relies on parasite actin and myosin (17). This process results in the creation of a non-fusogenic parasitophorous vacuole derived from the host cell membrane (18). The internalized parasite replicates within the parasitophorous vacuole via endodyogeny and emerges about 48 hours later via an active egress process that lyses the host cell (19). After egress, extracellular tachyzoites use gliding motility to locomote to a new host cell and begin the invasion and replication cycle anew.

Toxoplasmosis in humans

Humans contract toxoplasmosis primarily though the consumption of undercooked meat harboring tissue cysts or by ingesting food or water contaminated with oocysts. Although the specific route of infection cannot usually be established, epidemiological studies show that water and meat harboring *T. gondii* oocysts or tissue cysts is relatively common in the United States

(7,11). Interestingly, a study of congenital toxoplasmosis cases in the United States indicated that the majority of the mothers were infected with oocysts as evidenced by the presence of antibodies specific to sporozoite stages (20). Infections can also be transmitted from pregnant mothers to the developing fetus, and within transplanted organs (7).

In immunocompetent individuals, acute toxoplasmosis is a relatively benign infection that often goes unnoticed as it presents with minor flu-like symptoms (7). However, the infection is a major risk to the immunocompromised. In such patients, toxoplasmic encephalitis is one of the most severe disease manifestations and lethal if not promptly treated (7,21,22). Maternal-fetal transmission, particularly in the first and second trimesters, causes congenital infections that can result in severe birth defects or fetal death (7). Both congenital and postnatal infections can also lead to ocular disease (7). The parasites' ability to spread beyond its initial intestinal niche thus poses substantial risk to human hosts.

Even immunocompetent hosts capable of suppressing the growth of tachyzoites during acute toxoplasmosis do not actually clear the infection and instead harbor lifelong asymptomatic chronic infections. Chronic infections are wide-spread, with seropositivity rates suggesting over half the human population in parts of South America and Europe to be infected (23). If chronically infected individuals become immunocompromised, tissue cysts can lead to a recrudescent infection caused by the dedifferentiation of bradyzoites into proliferative tachyzoites (7). In this scenario, the preponderance of CNS-localized tissue cysts leaves the host at risk for toxoplasmic encephalitis.

Although there is no vaccine against toxoplasmosis, treatments options are available for patients experiencing severe acute disease. The most common regimen is combination sulfadiazine and pyrimethamine, supplemented with folinic acid (7). Unfortunately, the high

therapeutic doses of these agents required for toxoplasmosis treatment yields substantial host toxicity. In addition, none of the available regimens have any activity against the bradyzoite tissue cysts that cause chronic infections. Moreover, these regimens are not suitable for use during pregnancy. Spiramycin is used in Europe to treatment maternal infections, but its efficacy remains highly uncertain (7). Accordingly, the identification of therapeutics suitable for use during pregnancy and with efficacy against chronic infections would be a significant clinical advance.

Dissemination kinetics

T. gondii infections initiate when hosts ingest encysted parasites in the form of either bradyzoite tissue cysts or oocysts shed by felines (24). The acidic environment of the stomach triggers excystation (25), during which sporozoites emerge from oocysts and bradyzoites from tissue cysts (Fig. 1.1). Both sporozoites and bradyzoites enter the small intestine and access the lamina propria by traversing intestinal epithelial enterocytes (Fig. 1.1). In mice orally infected with high doses of oocysts, sporozoites were detected in the apical ends of intestinal enterocytes by 2 hours post infection (14). By 6 hours post oocyst feeding, sporozoites were primarily detected in the lamina propria, but also found in the basal portion of enterocytes (14). The rapidity with which parasites reach the lamina propria suggests that *T. gondii* is capable of directly traversing the intestinal epithelium without replicating within enterocytes. This interpretation is supported by more recent i*n vitro* and *ex vivo* studies that showed that *T. gondii* tachyzoites were capable of both invading and traversing through intestinal epithelium (26). In mice orally inoculated with bradyzoites liberated from tissue cysts, parasites were similarly detected within intestinal enterocytes and in the lamina propria within 3 hours (15). Although parasites are liberated from cysts in the stomach, invasion seems to be concentrated in the ileal

distal portions of the intestine, as indicated by studies examining parasite distribution in mice fed oocysts (14,27) or bradyzoites (15). The mechanistic basis for parasites' preferential invasion of distal small intestine remains unexplored.

Although able to directly traverse intestinal epithelium, once in the lamina propria, *T. gondii* is primarily intracellular and replicative. Transmission electron microscopy analysis showed that parasites in the lamina propria 12-18 hours post oocyst feeding were morphologically consistent with tachyzoites and had replicated. These parasites were primarily intracellular and contained within parasitophorous vacuoles. They were found within essentially all cells of the lamina propria, including lymphocytes, plasma cells, macrophages, neutrophils, eosinophils and fibroblasts (14). More recent work used flow cytometry to quantify parasite distribution 3 days after tissue cyst feeding. Parasites were again detected in a wide range of cells including macrophages, monocytes, neutrophils, B cells, $CD4^+$ T cells, $CD8^+$ T cells, $CD11b^+$ DCs, $CD8\alpha^+$ DCs, $CD4^-/CD8\alpha^-$ DCs, and plasmacytoid DCs, but most abundantly in non-leukocytes, macrophages, monocytes, and neutrophils (28).

Parasites continue to replicate in the lamina propria but also rapidly spread to secondary lymphoid tissues. Parasites were detected within Peyer's patches and mesenteric lymphoid nodes with 8 hours of feeding mice heavy doses of oocysts (14,27) or bradyzoites (15). Studies using more moderate doses of tissue cysts detected parasites within mesenteric lymph nodes and Peyer's patches 2-3 days post inoculation (28,29).

After spreading to secondary lymphoid tissues, *T. gondii* goes on to invade essentially all distal organs of the host. Various studies report detection in the lungs at 4-5 days post oral infection with bradyzoites or tissue cysts (14,15,27). First infection of the brain is consistently placed at 6-8 days post oral infection with either oocysts or tissue cysts (14,15,27,29,30).

Whether oocyst- and tissue cyst-initiated infections closely mirror each other in dissemination routes has not been rigorously explored. However, both infection modes seem to result in central nervous system invasion in similar time frames, with minimal influence from the size of initial inoculum on the eventual CNS burden. The disconnect between inoculum dose and CNS burden likely stems from the peak burden during acute infection being primarily determined by the effectiveness of host immune control.

Experimental models of toxoplasmosis often infect mice through intraperitoneal tachyzoite injection as this easily cultivated stage does not tolerate the acidic environment of the stomach. Curiously, such intraperitoneal tachyzoite injections also lead to parasites accessing the central nervous system on the 6-8 day time-frame (30,31) typical of oral cyst inoculation. However, a different route to the CNS may be used as this infection model bypasses the intestinal lamina propria and migratory leukocytes initially encountered in natural infections.

Basis of systemic and CNS dissemination

The impressive spread of *T. gondii* from its initial nidus in the intestinal lamia propria to essentially all tissues and organs of the host likely relies on both the gliding motility of extracellular parasites (32) and the shuttling of intracellular parasites by motile host cells (33). Circulatory and lymphatic vasculature could both serve as conduits that enable intracellular and extracellular parasites to rapidly access tissues highly distal to the initial infection nidus in the intestinal lamina propria.

Several early studies speculated that rapid dissemination following cyst feeding must be driven by travel through lymphatics as they failed to detect *T. gondii* present in the bloodstream (34,35). However, these same authors reported early infection of the spleen (34), which would presumably result from hematogenous spread as the spleen lacks afferent lymphatics. Several

other studies confirmed early infection of the spleen (14,15,27). Moreover, a contemporaneous study using a more sensitive cat bioassay detected infectious parasites in the blood one day following bradyzoite feeding, albeit with heavy inoculum doses (15). More recent studies fed mice physiological doses of tissue cysts and detected parasitemia within 4-5 days of inoculation using quantitative PCR (29) or flow cytometry (30). Hematogenous or lymphatic spread of *T. gondii* from the lamina propria to distal sites thus are both plausible dissemination routes.

Defining the route by which *T. gondii* accesses the central nervous system has been of high interest due to the severe clinical consequences of toxoplasmic encephalitis. Within the brain, *T. gondii* cysts are primarily found in the cerebral cortex and more frequently in grey matter than white matter (36,37). Early *in vitro* studies suggested that *T. gondii* might efficiently and even preferentially invade astrocytes (38,39). However, *in vivo* studies in mice showed that CNS cysts are overwhelmingly found within neurons, and very occasionally oligodendrocytes, and this pattern is unlikely to derive from clearance of parasites within astrocytes (36,40,41). A study of recrudescence in mice reported that re-activating parasite cysts are found primarily near microvasculature (37). *T. gondii* cysts were also noted to predominantly localize to the brain parenchyma and not meninges or circumventricular areas. This distribution led to the proposal that *T. gondii* accesses the brain by traversing the blood-brain barrier (37). However, these studies considered cyst location weeks to months after initial CNS entry (36,37). Whether cysts form and mature at or near the initial site of CNS entry by the founder parasite is unknown, and evidence suggests that bradyzoites do occasionally escape tissue cysts and migrate to new sites (42). Moreover, no rigorous studies have yet examined whether the blood-CSF barrier (43) or recently described brain lymphatics (44,45) could be used by *T. gondii* to access the CNS or

spread once within it. The blood-brain barrier is thus currently the most promising possible portal for *T. gondii* to enter the CNS, but other avenues are also possible.

Actin-dependent parasite gliding motility

T. gondii and other apicomplexans use a parasite-powered process termed gliding motility to both move as extracellular parasites and invade host cells. Briefly, in this process, rearward translocation of transmembrane adhesin proteins secreted from the parasites' micronemal organelles powers forward movement. If this process is coupled to host cell attachment at the parasites apical (anterior) end, the power of gliding motility can propel the parasite into the cell. Gliding motility promotes dissemination both by enabling parasites to spread while extracellular and by powering productive invasion of diverse host cells, including highly motile leukocytes.

Extracellular gliding

Extracellular tachyzoites use gliding motility to locomote between host cells. Early descriptions of this behavior noted three distinct forms of tachyzoite gliding on glass surfaces: corkscrew-like helical gliding, circling gliding, and twirling (46). Because helical gliding most efficiently produces net displacement of the parasite, it has been speculated to constitute productive gliding while circling and especially twirling may simply be failures to helical glide. Consistent with this idea, helical gliding is the only form that leads to invasion (46). Furthermore, parasites embedded in three-dimensional matrigel matrices meant to model extracellular matrix overwhelmingly glide in helical corkscrews (47). Forward translocation via helical gliding motility is quite efficient, occurring at rates of 1-10 micron/sec (46,48,49).

During gliding, forward movement is produced by the rearward translocation of transmembrane parasite adhesins. The adhesins are discharged at the apical end of the parasite

from micronemal secretory organelles in a calcium-regulated process (50-52). Micronemal adhesins are transmembrane proteins that possess extracellular domains that interact with surface substrates and cytoplasmic tails that interact with the parasite's cytoskeleton (53). The linkage of substrate-contacting micronemal adhesins to the cytoskeleton allows a complex termed the glideosome to power forward movement by translocating the adhesins in the reverse direction (54,55). Power for this process is produced by concerted action of a small parasite myosin (56) with parasite actin (17).

Invasion

In contrast to most intracellular pathogens, *T. gondii* invasion of host cells is primarily a pathogen-driven process. Invading *T. gondii* parasites do not enter host cells via endocytosis or phagocytosis or induce dramatic host membrane rearrangements. Instead, the parasite uses gliding motility to actively propel itself into host cells (49). This process is very rapid and typically occurs in under a minute (57). As parasites enter the host cell, they undergo a dramatic constriction at their interface with the host cell. This constriction appears as a ring through which parasites appear to squeeze and is often termed the moving junction (58). Some subtle rearrangements of cortical host actin are also observed at the parasite-host moving junction interface (59,60). Whether the redistribution of host actin at the moving junction facilitates parasite entry or simply reflects rearrangements in cortical actin forced by the dramatic inversion of the host membrane during invasion remains unclear. However, the force for entry appears to primarily derive from the parasite ACT1-MYOA glideosome (17).

Invasion is mediated by adhesive events enabled by sequential secretion from the parasites microneme and rhoptry organelles (61,62). The micronemal adhesins involved in gliding motility facilitate initial attachment to the host cell. Following initial attachment,

rhoptries are discharged. The rhoptry proteins RON2, RON4, and RON5 are secreted into the host cell and localize to the moving junction (63). RON2 traverses the host cell membrane and at an ectodomain contacts the micronemal adhesion AMA1 (64,65). The cytosolic portion of RON2 forms a complex with RON4 and RON5, which engages the host cell's cytoskeleton (66). This linkage allows the parasite to exert the force of gliding motility to penetrate into the host cell, as evidenced by the dual reliance of gliding and invasion on parasite but not host actin polymerization (61,67). The host cell's membrane is inverted where the parasite engages and transformed into the parasitophorous vacuole in which *T. gondii* will replicate. During this process, the membrane is modified to produce a non-fusogenic vacuole that protects the replicating parasites from endosomal or lysosomal-mediated destruction (18,49).

Potential for alternative invasion mechanisms

The adaptation of inducible Cre-Lox technology for use in *T. gondii* enabled the creation of stable knockout parasite lines for several genes thought to be essential, including *T. gondii* myosin (*MYOA*) and the micronemal adhesin AMA1 (*AMA1*), as well as an inducible knockout line for *T. gondii* actin (*ACT1*) (68-70). The lytic growth cycle of *T. gondii* cannot proceed without invasion (19). Accordingly, the ability of *ΔmyoA* and *Δama1* parasites to grow in cell culture was initially speculated to comprise evidence of an intact invasion pathway that functioned independently of the MYOA-ACT1-powered glideosome (68,69). As the sole actin present in *T. gondii* (67), *ACT1* plays critical roles in cytoskeletal function and division and is thus, not surprisingly, truly essential (68). However, residual motility and invasive ability in inducibly *Δact1* parasites were suggested to be further evidence of alternatives to glideosome-powered invasion in *T. gondii* (68,69). Given the ability of *T. gondii* to invade an unusually diverse array of host cells and penetrate nearly all biological barriers (71), the concept of the

parasite maintaining multiple motility and invasive strategies was intriguing. In particular, an alternative invasion pathway that does not lead to host cell lysis could plausibly help *T. gondii* to more effectively exploit leukocyte trafficking for dissemination by allowing parasites to be shuttled within migrating leukocytes for time periods longer than the typical lytic cycle.

Initial investigations of glideosome-dependent invasion quickly identified functional redundancies in the *T. gondii* genome as likely explanations for the dispensable nature of *MYOA* and *AMA1*. In addition to diminishing the efficiency of *T. gondii* invasion, *MYOA* deletion prevented the subsequent excision of the gene encoding for splice variants of an alternative parasite myosin, MYOB and MYOC (69). Following studies determined that an alternative glideosome based on the MYOC splice variant compensated for *MYOA* loss and allowed invasion in *ΔmyoA* parasites (72). Similarly, analysis of *Δama1* parasites found that upregulated homologs compensated for the loss of function of AMA1-RON2 linkage in the glideosome (73).

The pleiotropic roles for ACT1 in the life cycle of *T. gondii* complicate establishing whether *ACT1* is specifically required during invasion. All studies agree that *Δact1* parasites exhibit severe defects in both gliding and invasion, with both processes reduced at least 10-fold relative to wild-type parasites (68,69). However, *ACT1* has proven refractory to stable deletion. Accordingly, these studies have examined parasites following rapamycin induction of Cre-mediated excision of a floxed $ACT1^f$ allele, in which a YFP reporter is used to identify parasites that have undergone $ACT1^f$ excision. Complicating analysis, this system often yields rather low rapamycin-induced excision frequency (68,69) and can also produce spontaneous excision events at a low rate. How effectively the pools of inducible *Δact1* parasites that have been studied approximate true phenotypic nulls was thus unclear. Initial studies used immunostaining as a rough qualitative estimate for the completeness of ACT1 depletion in inducible *Δact1* parasites

and showed marked reduction, albeit to an unquantified degree (68,69). Notably, *T. gondii* actin polymerizes in an unusual isodesmic manner that lacks a critical concentration required to support the generation of F-actin (74,75). Accordingly, it is plausible that even very low levels of residual ACT1 might suffice to support invasion.

ACT1 function has also been interrogated by perturbing polymerization dynamics, rather than direct genetic knockout. Such approaches showed that conditional depletion of the *T. gondii* formin FRM1 (76), actin depolymerizing factor ADF (77), and profilin (76) disturbed gliding and invasion. Expression of ACT1 transgenes mutated to produce longer and more stable filaments than that typical of the parasite's natural isodesmic filaments also led to aberrant parasite gliding (78). These studies all point to an important role for parasite actin in gliding and invasion. Whether the residual gliding and invasion observed in inducible *Δact1* parasites reflect an alternative motility pathway or simply the incomplete removal of ACT1 protein in some parasites in the analyzed pools thus remained uncertain.

Trojan horse dissemination

Immune responses are obviously critical to controlling microbial infections. However, many pathogens have evolved the ability to exploit leukocyte trafficking as a means of promoting dissemination. This strategy can enable enteric pathogens to spread beyond the gastrointestinal tract (79). For example, *Salmonella* bacteria can rapidly escape their initial intestinal niche and enter the bloodstream within CD18-expressing monocytes by using the secreted effector SrfH to stimulate motility (79-81). Pathogen-harboring Trojan horses can also breach the blood-brain barrier, providing access to the immuno-specialized CNS compartment (33). *Listeria monocytogenes* invades the CNS when infected phagocytes traffic to the brain while carrying intracellular bacteria (33,82-84). The pathogenic yeast *Cryptococcus neoformans*

can also cross the blood-brain barrier within monocytes and macrophages acting as Trojan horses (85-89). Among protozoan parasites, *Leishmania* species modulate adhesion and chemokine receptor expression in phagocytes including macrophages and dendritic cells, which is theorized to promote dissemination through host tissues (90-92).

Throughout *in vivo* infections, *T. gondii* parasites encounter and invade a plethora of motile leukocytes that could be co-opted as dissemination-promoting Trojan horses. Various reports propose DCs, neutrophils and monocytes as potential Trojan horses. Given the diverse tissue compartments and biological barriers invaded by *T. gondii*, each of these leukocyte types may contribute to systemic *T. gondii* spread by advancing dissemination at distinct stages of the infection.

Dendritic cells as Trojan horses

Of all leukocytes, the ability of DCs to promote *T. gondii* dissemination has been explored in the most detail. DCs are antigen presenting cells that are primarily positioned in peripheral tissues, where they acquire antigens that they subsequently deliver for presentation to T cells in secondary lymphoid tissues (93).

The distribution of DCs suggests that they would be well-poised to promote *T. gondii* dissemination by advancing spread through tissues. Consistent with this idea, an analysis of parasite distribution after mice were orally inoculated with tissue cysts reported that *T. gondii* was primarily detected associated with $CD11c^+$ cells in intestinal lamina propria and mesenteric lymph nodes early in infection, but then switched to preferential association with $CD11b^+$ monocytes when in the bloodstream at 1 week post infection (29). Curiously, though, another study reported that at three and six days post inoculation with oral tissue cysts, parasites in the intestinal lamina propria were predominantly found within non-leukocytes (37-52%), followed

by monocytes, macrophages and neutrophils, which cumulatively accounted for about 1/3 of infected cells at both time points (28). In this study, infected DCs were quite scarce, comprising less than 5% of all infected cells in the intestinal lamina propria, Peyer's patches, and mesenteric lymph nodes at both three and six days post inoculation (28).

Several independent studies point to a role for DCs in promoting dissemination. In mice infected intraperitoneally with *T. gondii*, peritoneal $CD11c^{+}$ $Gr\text{-}1^{+}$ DCs were preferentially infected and then recruited to the spleen, where they comprised more than half of the infected cell population, suggesting these cells might have delivered parasites to the spleen (94). Another report showed that *T. gondii* infection of human monocyte-derived DCs and murine bone marrow-derived DCs induced an *in vitro* hypermotility phenotype characterized by increased DC migration across plastic transwell membranes, and increases in the velocity and distance traveled by DC crawling on 2-D substrates (95). Mice inoculated intraperitoneally with *T. gondii*-infected bone marrow-derived DCs exhibited higher parasite burdens and more rapid detection in the brain (1 *vs* 3 days post infection), compared to intraperitoneal inoculation with a matched quantity of extracellular parasites, suggesting that the migration of infected DCs can promote dissemination *in vivo* (95). Further studies established that the magnitude of the DC hypermigration phenotype varied with parasite genetic lineage (96), such that a less pronounced enhancement was observed upon infection with parasites of a hypervirulent type I lineage that possess higher rates of intrinsic motility as extracellular parasites (26). Adoptive intraperitoneal transfer of DCs infected with less intrinsically motile type II and III *T. gondii* strains (26) led to mice exhibiting parasite burdens similar to that caused by infection with type I lineages expected to exhibit a virulence advantage (96). This suggests that DC-aided dissemination might be more

important for *T. gondii* lineages with less robust extracellular motility, particularly type II and III lineages (96).

The precise mechanistic basis for hypermigration in *T. gondii*-infected DCs remains unclear. However, the DC hypermigration phenotype has been shown to be accompanied by rapid cytoskeletal changes that start within ten minutes and include dissolution of adhesive podosomes, redistribution of integrins and F-actin, and moderate upregulation of CCR7 expression (97). The enhanced migration of infected DCs requires signaling through GABA receptors to a Cav1.3 voltage-dependent calcium channel (98,99). The rapid onset of the hypermigration phenotype suggests control at the level of signaling rather than transcription or translation. Consistent with this, one study reported that heterologous expression of a *T. gondii* 14-3-3 protein was sufficient to induce hypermigration in DCs, as was treatment of DCs with recombinant Tg14-3-3 (100). Unfortunately, Tg14-3-3 is likely an essential gene (101) and proved refractory to deletion (100). Accordingly, it is unclear whether Tg14-3-3 is required for parasites to enhance DC migration. Moreover, 14-3-3 proteins are adaptor proteins expressed by mammalian cells and play extensive roles in cytoskeletal regulation (102). Accordingly, it is uncertain whether enhanced DC migration in response to treatment with recombinant Tg14-3-3 or ectopic expression of Tg14-3-3 reflects specific physiological involvement of Tg14-3-3 in enhancing DC motility, or simply the artificial induction of processes regulated by host 14-3-3 proteins.

Monocytes and macrophages as Trojan horses

Monocytes are myeloid cells that circulate in the blood and are recruited to tissues during resting and inflammatory states, where they differentiate into macrophages and monocyte-derived DCs (103,104). Because of their routine trafficking from blood to tissue, monocytes have

been keenly investigated as potential Trojan horses that could deliver *T. gondii* across the blood-brain barrier and into the CNS (87).

Highlighting the potential for infected monocytes to deliver *T. gondii* into the CNS, monocytes were identified as the most abundantly infected leukocyte in the blood of mice following oral infection with *T. gondii* tissue cysts (29). Blood monocytes are known to separate into two subsets: inflammatory $CCR2^{+}$ $Ly6C^{hi}$ cells and patrolling $CCR2^{-}$ $Ly6C^{lo}$ CX_3CR1^{hi} cells (104,105). However, the distribution of *T. gondii* among these two subsets was not assessed (29). Similar to the phenotype reported upon adoptive transfer of DCs, intravenous introduction of *T. gondii*-infected monocytes hastened dissemination to the brain, relative to transfer of extracellular parasites (29). Investigations modeling monocyte extravasation with an *in vitro* system using human umbilical vein endothelial cells reported that *T. gondii* infection inhibited integrin-mediated adherence of monocytes to endothelium (106,107), moderately enhanced the velocity of monocytes subsequently crawling over the endothelium (108), and had no significant impact on monocyte transmigration through the endothelium (108). Whether these phenotypes would apply if assessed in an endothelial system that models the highly-specialized blood-brain barrier (109) remains untested, as does the mechanistic basis that would allow parasites to enhance vascular crawling after blocking the prerequisite step of integrin-mediated adherence (110). An analysis of migration across transwell membranes found that infection enhanced migration in DCs but not human peripheral blood monocytes, suggesting that monocyte and DC motility is differentially perturbed by *T. gondii* infection (111).

During *in vivo* infections, *T. gondii* parasites encounter monocytes and macrophages in the intestinal lamina propria well before entering the blood. Monocytes and macrophages encountered in the tissue of the lamina propria include $Gr1^{+}$ $Ly6C^{hi}$ $CCR2^{+}$ inflammatory

monocytes recruited to the infection site (112-114) and highly abundant resident CX_3CR1^+ macrophages that are relatively short-lived and continuously replenished from inflammatory monocytes recruited via CCR2 signaling (115). Once disseminated to other tissues, *T. gondii* also encounters self-renewing macrophages that are not replenished from circulating monocyte populations (116). The motility of infected macrophages has not been as extensively studied as that of monocytes and DCs. However, one study reported that *T. gondii* infection inhibits the adherence of peritoneal macrophages to integrin ligands present in extracellular matrix (117), similar to the faulty integrin-mediated adherence of monocytes. Further supporting the potential for infected macrophages to advance dissemination, the same study reported that peritoneal macrophages infected *in vitro* and then transferred back into mice traffic to mesenteric and cervical lymph nodes, although not as quickly as LPS-activated macrophages (117). Similar to DCs, another study reported that *T. gondii* infection enhanced the migration of human monocyte-derived macrophages across plastic transwell membranes (111).

Neutrophils as Trojan horses

T. gondii infection elicits a massive influx of both inflammatory monocytes and neutrophils to the intestinal lamina propria. Only the recruited inflammatory monocytes appear critical for controlling acute toxoplasmosis (112,113). However, one study noted that 5-7 days following oral cyst infection, parasites preferentially associated with neutrophils over inflammatory monocytes in the intestinal lamina propria (118). Infected neutrophils retained high rates of motility and could be captured traversing intestinal epithelium in explanted tissue sections. Unlike the phenotypes described for DCs and monocytes, *T. gondii* infection did not enhance neutrophil motility, but infected neutrophils were capable of establishing infection in new mice upon intraperitoneal transfer (118). Notably, the observed phenotypes in this study

occurred after the typical window in which *T. gondii* is first detected in the bloodstream. Neutrophils might thus act as Trojan horses that enable *T. gondii* to spread to new sections of intestinal lamina propria but seem unlikely to mediate parasite escape into the circulation.

Shortcomings of existing Trojan horse models

Several independent lines of evidence thus suggest that monocytes and DCs might act as Trojan horses that promote *T. gondii* dissemination. *In vitro* studies have convincingly shown that *T. gondii* infection alters the motility of monocytes (106-108) and DCs (95,97,98). Adoptive transfer experiments are supportive of a role for infected monocytes and DCs in promoting *in vivo* dissemination (29,95). However, adoptive transfer involves extensive *in vitro* manipulation of the leukocytes which may induce artificial phenotypes. Transfer of infected cells to naïve recipient mice also fails to capture the inflammatory state that monocyte or DC Trojan horses would encounter during a physiological *T. gondii* infection. In addition, advantages in the infectivity of parasites harbored within monocytes or DCs relative to extracellular parasites after adoptive transfer might derive from the intracellular parasites being protected from attack by complement or IgM defenses (30) in the blood, rather than any particular connection to leukocyte motility. Whether leukocyte Trojan horses meaningfully contribute to *T. gondii* dissemination during physiological infections thus remains unclear.

Because inflammatory monocytes (112,113) and $CD11c^+$ DCs (119) are critical for controlling acute toxoplasmosis, ablation of these cell types alters infection progression in many areas besides dissemination and is thus not a tractable tool for analyzing parasite dissemination. However, *T. gondii* secretes a wealth of effectors known to manipulate innate immunity and intracellular signaling (120). If the altered motility of infected monocytes and DCs is important for their proposed roles as Trojan horses, a more tractable approach to testing this model *in vivo*

could be the identification of parasite effectors required for manipulation of leukocyte motility, and subsequent analysis of dissemination after infection with such mutants. Tg14-3-3 is the only *T. gondii* protein currently implicated in these phenotypes, and as an essential gene, not a candidate for this approach (100). However, the DC hypermigration phenotype is influenced by *T. gondii* lineage (96), suggesting that relevant effectors could be identified by genetic crosses. Genome-wide CRISPR screening technology was also recently developed for *T. gondii* (101) and could alternatively be used to screen for effectors.

Modes of leukocyte migration

Much of the interest in Trojan horse-aided dissemination was motivated by the severe clinical consequences of toxoplasmic encephalitis. Accordingly, most studies have focused on the ability of infected leukocytes to deliver *T. gondii* across the blood-brain barrier. However, the most promising Trojan horse candidates are first encountered within the intestinal lamina propria rather than the blood stream. The confined three-dimensional nature of tissue interstitial spaces has recently been appreciated as enabling modes of leukocyte migration that are not possible on endothelial vasculature (121,122). Analysis of the migration of *T. gondii*-infected leukocytes has largely ignored the distinctions between leukocyte motility within tissues and on endothelial vasculature. One study reported that the hypermigration of infected DCs is capable of mediating migration through collagen matrices that model tissue interstitium (123). Whether this is also true of the monocytes and macrophages frequently infected in the lamina propria (28) remains untested.

Integrin-dependent leukocyte migration

Early studies of leukocyte motility used two-dimensional cell culture systems to establish a detailed cascade that mediates leukocyte motility on the endothelium that lines circulatory

vasculature (110). In this cascade, interactions between leukocyte L-selectin and endothelial P- and E-selectin and other glycosylated substrates are strengthened by shear stress (124) and mediate capture of circulating leukocytes onto endothelial surfaces (110,125). The resultant rolling of leukocytes is slowed and eventually arrested by engagement of activated transmembrane integrins expressed by leukocytes with endothelial ligands including ICAM-1 and VCAM-1 (110,126,127). Integrin-mediated adherence enables leukocytes to proceed to crawling over the endothelial vasculature, presumably to identify preferred sites for the final step of this cascade, transendothelial migration. Transendothelial migration can occur through transcellular and paracellular routes, and is delayed if crawling is inhibited (110).

Integrins serve two critical functions in the transendothelial migration cascade: enabling stable leukocyte-endothelial adherence as described above, and acting as crucial force transducers that convert retrograde actin flow into forward movement (128). In this system, force is primarily generated by actin polymerization at the leading edge of migrating leukocytes. This actin polymerization drives forward protrusion of the cell membrane and rearward translocation of actin filaments via treadmilling (129). Myosin-driven contractility supports this system by pulling the cell cortex rearwards. If these retrograde forces are coupled to the external environment, the leading edge of the migration cell can pull the cell forward (129). This coupling is achieved by linkage of the actin cytoskeleton to ligand-engaged integrins via the adaptor protein talin (128). Integrin-talin linkage of the cytoskeleton to external ligands essentially provide traction that prevents the treadmilling actin cortex from slipping backward in relation to the adhesive substrate (129).

Interstitial leukocyte migration

In stark contrast to the integrin-dependent motility leukocytes deploy to migrate over and through endothelial vasculature, leukocyte migration through tissue interstitium does not require any integrin functionality whatsoever. Although this idea was initially controversial, elegant genetic studies in mice established the *in vivo* feasibility of integrin-independent migration by showing that ablation of either the universal integrin adaptor talin or all relevant integrin heterodimers did not cause any defects in DC interstitial migration (122). Further work established that integrin-independent motility is not restricted to DCs by showing robust integrin-independent interstitial migration in neutrophils (130) and T cells (131).

The precise mechanisms of polarization and force generation that enable migration in the absence of stable integrin-mediated adherence are a topic of active investigation, with a variety of models proposed including membrane flow, polarized blebbing, and deformation-based movement (129,132,133). In general, these models propose that adherence is only required for migration in that it promotes prolonged interaction with a substrate. In confined three-dimensional environments such as tissue interstitium, migrating cells do not passively disengage from their substrates and thus do not require active adhesion to produce traction and convert forces into movement (129). Intriguingly, such systems are theorized to produce migration more efficiently than adhesive-based systems, as there is no need for migrating cells to devote extensive energy to cycles of adhering and de-adhering to substrates (129).

The circumstances that prompt leukocytes to use integrin-independent migratory strategies remain uncertain. Integrin-independent migration can be forced through either genetic ablation of integrins or talin or the provision of artificial environments inhospitable to integrin-mediated adhesion **(**134**)**. However, all mammalian cell types except erythrocytes express

functional integrins (135). Moreover, integrins bind a wide repertoire of ligands that are present in essentially every tissue of the body (136). Accordingly, the extent to which leukocytes rely on integrin-independent strategies during physiological scenarios remains unclear **(**134**)**. To date, the most conclusive evidence that leukocytes migrate *in vivo* without using stable adhesion is the ability of integrin-deficient dendritic cells to migrate through interstitium at normal velocity **(**122**)**. Identification of *in vivo* scenarios where integrin-independent migration is exclusively or preferentially performed would provide much more compelling evidence of the physiological relevance of integrin-independent migration.

Leukocytes also appear capable of switching their migratory strategy to match their physical environment. For example, *in vivo* wound healing studies showed that neutrophils can switch from deformation-based migration to adhesion-based motility upon reaching the wound transition zone **(**130**)**. Dendritic cells presented with different substrates will shift their migratory strategy to match the availability of integrin ligands; this change is rapid and does not alter migration velocity **(**137**)**. Matrix geometry was also shown to determine whether macrophages migrating in 3-D used a deformation-based lowly-adhesive migratory mode or a proteolytic highly-adhesive mesenchymal mode **(**138**,**139**)**. The mechanisms controlling switching between migratory modes *in vivo* remain unelucidated. Dissecting the ability of *T. gondii* to manipulate leukocyte migration may provide insights into the regulation of leukocyte migratory modes.

Aims and scope of thesis

The overarching goal of this thesis was to further understanding of *T. gondii* dissemination by investigating two major mechanisms of parasite spread. The first aim was to establish whether *T. gondii* possesses functional and robust alternatives to actin-dependent gliding motility that would aid extracellular parasites in invading cells and tissues. The second aim was to determine whether and how monocyte Trojan horse promote systemic parasite dissemination, with particular emphasis on assessing whether monocytes are best suited to deliver intracellular parasites to any specific host environments.

Abundant evidence suggests that *T. gondii* uses a parasite actin-myosin motor to power a gliding motility process that enables both the locomotion of extracellular parasites and invasion of host cells. At the outset of this study, provocative data generated by new tools for inducible genetic deletions in *T. gondii* had suggested the possibility of motility and invasion processes that did not require parasite actin. However, the essential and pleiotropic nature of *T. gondii* actin (*ACT1*) complicated assessment of the consequences of inducible *ACT1* deletion. This study used live cell microscopy of parasite motile behaviors, immunofluorescence estimation of the of ACT1 protein abundance, and inhibitors of actin polymerization to test whether the phenotypes of inducible *Δact1* parasites suggested that robust actin-independent motility or invasion pathways exist.

T. gondii is also theorized to coopt the migration of infected leukocytes to promote dissemination. During murine toxoplasmosis, monocytes and macrophages are commonly infected in the blood and intestinal lamina propria, suggesting they would be well-poised to promote *T. gondii* dissemination in several host compartments. Supporting this idea, a collection of *in vitro* studies showed that *T. gondii* infection altered the motility of monocytes interacting

with endothelial vasculature. However, the mechanisms controlling this altered motility were unknown. In addition, whether infected monocytes could effectively traverse the specialized endothelium that comprises the blood-brain barrier or migrate through tissue environments had not been tested. This work used *in vitro* models of tissue and vascular environments to assess whether the aberrant motility of *T. gondii*-infected monocytes supported efficient blood-brain barrier traversal or interstitial tissue migration. This aim also identified monocyte signaling pathways and a secreted parasite effector required for *T. gondii* to manipulate monocyte migration *in vitro*, and murine models to evaluate the *in vivo* relevance of monocyte-aided dissemination.

Toxoplasmosis is a common infection in humans and a serious threat to the immunocompromised. The most severe manifestations of toxoplasmosis derive from the ability of *T. gondii* parasites to systemically disseminate and invade protected host tissues such as the central nervous system and developing fetus. This thesis work examines how *T. gondii* is able to spread from an initial enteric infection nidus and invade diverse host tissues. Better understanding the basis of *T. gondii* dissemination will inform efforts to control or prevent the most severe clinical consequences of toxoplasmosis.

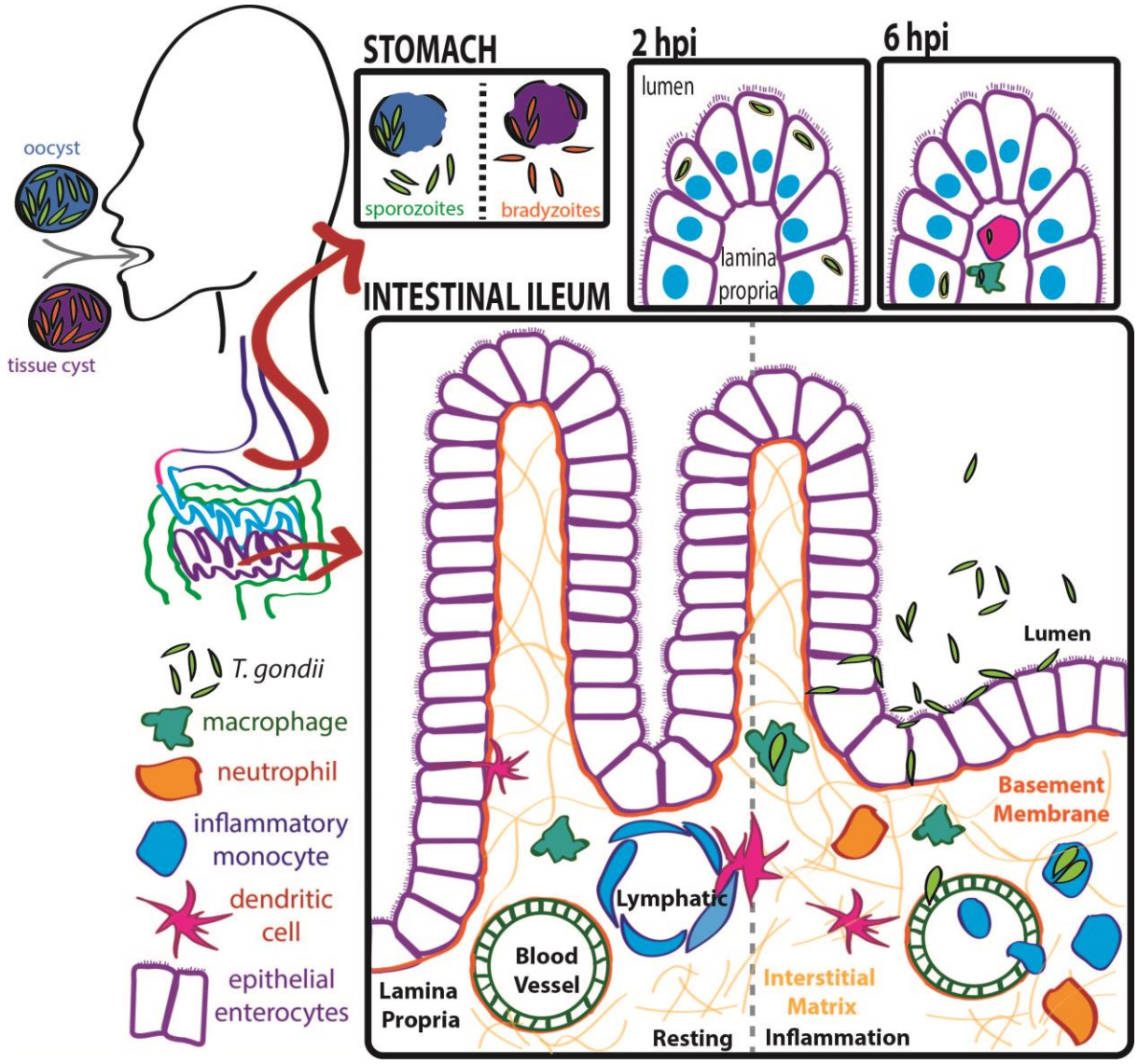

Figure 1.1: Early kinetics of *T. gondii* dissemination.

Infection is initiated upon ingestion of oocysts or tissue cysts. Cysts release sporozoites or bradyzoites in the stomach, which enter the intestinal lumen and from there invade the lamina propria. Parasites are initially detected in the apical end of intestinal enterocytes but rapidly transition to primarily being located in the lamina propria. 2 hpi = 2 hours post infection, 6 hpi = 6 hours post infection.

Chapter 2: *Toxoplasma* actin is required for efficient host cell invasion

Preface

LLD designed and performed all experiments and drafted the manuscript. LDS supervised the studies and contributed to experimental conception. LLD and LDS collaboratively revised the manuscript.

This chapter has been previously published:

Drewry, L.L. & Sibley, L.D. Toxoplasma Actin Is Required for Efficient Host Cell Invasion. *mBio* 6, e00557 (2015).

Summary

Apicomplexan parasites actively invade host cells using a mechanism predicted to be powered by a parasite actin-dependent myosin motor. In the model apicomplexan *Toxoplasma gondii*, inducible knockout of actin, *ACT1*, was recently demonstrated to limit, but not completely abolish invasion. This observation has led to the provocative suggestion that *T. gondii* possesses alternative, ACT1-independent invasion pathways. Here we dissected the residual invasive ability of Δ*act1* parasites. Surprisingly, we were able to detect residual ACT1 protein in inducible Δ*act1* parasites as long as 5 days after *ACT1* deletion. We further found that the longer Δ*act1* parasites were propagated after *ACT1* deletion, the more severe of an invasion defect was observed. Both findings are consistent with the quantity of residual ACT1 retained in Δ*act1* parasites being responsible for their invasive ability. Furthermore, invasion by the Δ*act1* parasites was also sensitive to the actin polymerization inhibitor cytochalasin D. Finally, there was no clear defect in attachment to host cells or moving junction formation by Δ*act1* parasites. However, Δ*act1* parasites often exhibited delayed entry into host cells, suggesting a defect specific to the penetration stage of invasion. Overall, our results support a model where residual ACT1 protein retained in inducible Δ*act1* parasites facilitates their limited invasive ability, and confirm that parasite actin is essential for efficient penetration into host cells during invasion.

Introduction

Toxoplasma gondii is a model for studying the gliding motility and active host cell invasion characteristic of many members of the Apicomplexa phylum of eukaryotic parasites. During gliding, T. *gondii* tachyzoites secrete transmembrane adhesins at their apical (anterior) end (32). Rearward trafficking of these adhesins is predicted to generate the force that propels the parasite forwards (32). A parasite actin-dependent myosin motor is thought to power this process (17,56). Under the currently prevailing model for gliding and invasion, the force generated by gliding motility can be exploited to power movement along a surface substrate, invasion into a host cell or across biological barriers, or egress out of a host cell (32).

When used for invasion, gliding motility is coupled to secure apical attachment to a host cell. Once apically attached, parasites squeeze through a tight constriction referred to as the moving junction (MJ) and penetrate into the host cell (58,63). Invasion is rapid, typically completing in less than a minute (57), but contains several distinct stages (140). The first committed step is apical attachment to a host cell, with contact mediated by sequential secretion of proteins from the microneme and rhoptry organelles (62). Penetration though a MJ containing a complex of micronemal and rhoptry neck proteins (141,142) leads to invagination of the host cell plasma membrane. Ultimately, pinching off of the host membrane results in internalization (32,140).

A role for parasite actin in invasion was first suggested by studies demonstrating the ability of the actin polymerization inhibitor cytochalasin D (CytD) to block invasion (143). *T. gondii* encodes only one actin gene, *ACT1 (67).* Subsequent studies showed CytD sensitivity is abolished in parasites bearing a CytD-resistance conferring *act1*^{A136G} allele, but unaffected by the introduction of a CytD-resistant actin allele in host cells (17). In concert, these results were

interpreted to indicate that CytD acts primarily and specifically on *T. gondii* ACT1, and support a role for ACT1 polymerization as necessary for invasion.

Although CytD mutant analysis suggests parasite ACT1 is the predominant actin required for invasion, host cell actin may also contribute to invasion. In support of this idea, several recent studies have highlighted rearrangements of host cell cortical actin during invasion, and proposed a possible secondary role for host actin during invasion (59,60). In addition, the development of a Cre-Lox based inducible knockout system for *T. gondii* facilitated the generation of inducible *ACT1* knockout parasites *(68)*. Studies using these inducible Δ*act1* parasites have demonstrated that low levels of invasion are observed as many as 4 days following *ACT1*^{f} excision (68,69). This result has been suggested as evidence for the presence of an alternative, ACT1-independent invasion pathway in *T. gondii* (68,69). Under this model, it was suggested that the essential function of ACT1 is to enable segregation of the apicoplast organelle among daughter cells (68), rather than participate in invasion. Additionally, based on noted defects in MJ formation by these inducible Δ*act1* parasites, it was proposed that any role for ACT1 in invasion occurs during early attachment stages (69), rather than powering penetration as was previously theorized (17).

Additional studies used the same Cre-Lox technology to generate stable parasite lines deleted for the myosin *MYOA* (68,69) and micronemal MJ component *AMA1* (70). As *T. gondii* is an obligate intracellular parasite, the viability of these knockouts clearly demonstrates that *MYOA* and *AMA1* are not essential for invasion, as had been previously theorized (56,144). Further work has demonstrated that paralogs can functionally compensate for *MYOA* and *AMA1* loss (72,73). A similar scenario is unlikely to apply to *ACT1*, as the *T. gondii* genome does not encode any clear ACT1 paralogs. However, all studies so far agree that, unlike *MYOA* and *AMA1*, *ACT1* appears to be an essential gene in *T. gondii*, in that no viable null clones are able to

grow as stable lines (68,69). Accordingly, ACT1 function can only be analyzed in parasites that are depleted for ACT1, rather than in true phenotypic nulls. Notably, *T. gondii* ACT1 polymerizes isodesmically, with no apparent critical concentration required to support polymerization (74,75). It thus is possible that even very low amounts of ACT1 retained in inducible Δ*act1* parasites could be sufficient to support ACT1 polymerization. Unfortunately, to date studies using inducible Δ*act1* parasites have only cursorily examined these mutants for residual ACT1 (68,69), and failed to rigorously quantify the residual ACT1 present in these mutants. It thus remains uncertain how closely inducible Δ*act1* parasites approximate true phenotypic nulls, or whether ACT1 polymerization is likely to be entirely ablated in such mutants.

Here we sought to analyze in more detail the invasion of inducible Δ*act1* parasites. In particular, we focused on evaluating: 1) how severely and consistently ACT1 is depleted in Δ*act1* parasites; 2) how robustly invasion and other forms of gliding motility are able to continue in Δ*act1* parasites; and, 3) how ACT1 depletion impacts specific stages of invasion. In total, our results highlight the importance of residual ACT1 in evaluating the phenotype of inducible Δ*act1* parasites, and confirm that ACT1 is specifically required at the penetration stage of invasion.

Results

Impact of ACT1 knockout on parasite motility

To investigate the relationship between ACT1 protein abundance and function, we assayed actin-dependent motility using an inducible knockout strain, *ACT1*^{f}, described previously (68). We compared the ability of parasites to invade host cells, egress from host cells, and to glide on serum-coated glass 2 days after *ACT1* disruption. As rapamycin induction achieves only low rates of *ACT1*^{f} excision in this strain, we analyzed the invasion competence of Δ*act1* parasites by tracking their abundance in a mixed population of *ACT1*^{f} intact and Δ*act1* parasites (YFP positive), before and after invasion of host cells. To do this, we modified a standard immunofluorescence-based invasion assay (145) to stain parasites based on whether they were YFP positive or negative, in addition to determining if they were intracellular or extracellular. This modification allows for the classification of every parasite as intracellular or extracellular based on permeabilization-selective staining, and Δ*act1* or *ACT1*^{f} intact based on YFP expression. When invasion was analyzed in this manner, Δ*act1* parasites were consistently under-represented among intracellular parasites relative to their abundance in the input population, indicating a strong invasion defect (Figure 2.1A). Similarly, when A23187-induced egress was observed by time-lapse video microscopy, Δ*act1* vacuoles overwhelmingly failed to egress from host cells, indicating a strong egress defect compared to *ACT1*^{f} intact parasites (Figure 2.1B). Δ*act1* parasites were also observed to glide less frequently on serum-coated coverslips than *ACT1*^{f} intact parasites, and although less efficient, knockouts were capable of all three motility patterns (Figure 2.1C).

Generation of a new inducible ACT1 knockout

The low excision rate of the *ACT1*^{f} strain hinders rigorous quantification of these mutants' phenotypes. Accordingly, to facilitate further work with inducible Δ*act1* parasites, we used the same strategy employed previously (68) to generate additional *ACT1*^{f} clones. Briefly, in this strategy the native *ACT1* allele was replaced by double homologous recombination with an exogenous copy where the *ACT1* coding sequence is immediately flanked 5' and 3' by LoxP sites, and followed downstream by a YFP reporter and selectable HXPGRT marker (Figure S1). The native *ACT1* promoter was retained so that Cre-mediated recombination at the LoxP sites creates a locus where *ACT1* is deleted, and YFP is instead expressed from the *ACT1* promoter. We isolated a clone, *ACT1*^{f}-2, with reliably high excision (>75% rapamycin-induced excision as indicated by YFP expression), that was used for the remainder of our studies.

Residual ACT1 in inducible knockouts

To correlate knockout phenotypes with the extent of ACT1 depletion, we developed a semi-quantitative approach that uses ACT1 immunofluorescence staining intensity in single parasites as a proxy for ACT1 protein abundance (Figure 2.2A). Consistent with a previous report (69), we observed that a large portion of the Δ*act1* parasites retained substantial residual ACT1 at 2 days after the induction of gene excision (Figure 2.2B-C). When assayed 3 days or more following induction of gene excision, Δ*act1* parasites were much more uniformly depleted for ACT1 relative to *ACT1*^{f} intact controls (Figure 2.2B-C). Importantly, at all time-points considered, the mean ACT1 staining intensity of Δ*act1* parasites never fell below the low end of ACT1 staining observed in *ACT1*^{f} intact parasites (Figure 2.2B-C). Similar low level ACT1 staining was also observed in parasites of the parental *diCre* strain bearing a native *ACT1* locus (Figure 2.2B-C), suggesting these results are unlikely to be an artifact of misclassifying Δ*act1*

parasites as *ACT1*^{f} intact due to low YFP expression. In addition, in every biological replicate and every time-point, even 5 days after inducing gene disruption, a small number of knockout parasites still stained moderately for ACT1 (Figure 2.2B-C).

We then asked whether any of the detected residual ACT1 staining in Δ*act1* parasites might actually represent bleed through from the YFP channel, or cross-reactivity of the actin antibody. To test for bleed through, we altered our immunostaining protocol to exclude the primary or secondary antibodies used to detect ACT1. These alterations strongly reduced the signal observed in the ACT1 channel, suggesting that the original signal detected using TgACT1 antibody was only minimally influenced by channel bleed through (Figure S2). Replacing our TgACT1 antibody with rabbit IgG sera as an isotype control also significantly reduced the observed signal, although not as strongly as exclusion of primary or secondary antibodies (Figure S2). Unlike the TgACT1 staining in Δ*act1* parasites, the mean signal observed using this isotype control was below the range of TgACT1 staining observed in *ACT1*^{f} intact parasites. Thus, portion, but not all, of the residual staining with TgACT1 in Δ*act1* parasites may derive from a low level of reactivity of rabbit sera against parasites. Because of the low reactivity of rabbit sera against parasites, we further tested specificity of the residual ACT1 staining by using a monoclonal mouse antibody raised against *Dictyostelium* actin. Using this monoclonal antibody, we again observed substantial residual ACT1 staining in Δ*act1* parasites (Figure 2.2B), again suggested the observed signal does indeed reflect residual ACT1 in Δ*act1* parasites.

The consistent presence of residual ACT1 in some portion of Δ*act1* parasites, combined with the prior observation that *Toxoplasma* ACT1 polymerizes isodesmically with no detectable critical concentration (74), led us to hypothesize that trace ACT1 retained by Δ*act1* parasites may suffice to support the limited invasion observed after gene disruption. Under this model, we

would predict that the longer parasites are maintained after *ACT1* disruption, the more strongly depleted of protein they would be, and the more severe defects in invasion would become. To test this, we used our modified invasion assay to determine the severity of the invasion defect in parasites maintained for 2-5 days after rapamycin-induction of *ACT1*^{f} excision. As predicted, the strength of Δ*act1* parasites' invasion defect positively correlated with the length of time parasites were maintained after inducing gene excision (Figure 2.3A).

If residual ACT1 is responsible for the continued ability of some Δ*act1* parasites to invade host cells, we would expect that ACT1 would still be detectable in Δ*act1* parasites following invasion. To test this, we quantified ACT1 immunofluorescence staining intensity in confocal images of parasites that were allowed to newly invade fibroblasts 4 days after rapamycin induction of *ACT1*^{f} excision. In this experiment, we observed no significant differences in the ACT1 content of intracellular or extracellular parasites, although Δ*act1* parasites were again on average depleted for ACT1 relative to *ACT1*^{f} intact parasites (Figure 2.3B). Importantly, there was substantial overlap in the ACT1 staining intensity observed in individual Δ*act1* and *ACT1*^{f} parasites, again consistent with a model of residual ACT1 facilitating Δ*act1* parasite invasion (Figure 2.3B).

Sensitivity of invasion to actin polymerization inhibitors

Parasite invasion is known to be sensitive to the actin polymerization inhibitor cytochalasin D (CytD) (17). If Δ*act1* parasites rely on residual ACT1 for invasion, we reasoned these Δ*act1* invasions would retain CytD sensitivity. To test this, we used our modified invasion assay to track parasite invasion into both HFF cells and a CytD-resistant epithelial cell line, Cyt-1 (146). Four days after the induction of gene excision, we observed dose-dependent CytD inhibition of invasion into HFFs by both *ACT1*^{f} intact and Δ*act1* parasites, confirming invasion

by Δ*act1* parasites is indeed actin-dependent (Figure 2.4A). CytD is a reversible inhibitor of actin polymerization. Because Δ*act1* parasites contain less ACT than *ACT1*^{f} intact parasites, we accordingly predicted that Δ*act1* parasites would be inhibited at lower CytD concentrations than *ACT1*^{f} intact parasites. Consistent with this prediction, when invading HFFs, Δ*act1* parasites were inhibited by 200 nM CytD in 3 independent experiments, while *ACT1*^{f} intact parasites never showed significant sensitivity below 500 nM CytD (Figure 2.4A).

We then asked if in the case of Δ*act1* parasite invasion, CytD sensitivity might reflect inhibition of an actin-dependent pathway in the host. This possibility was tested by analyzing invasion into the CytD-resistant epithelial cell line, Cyt-1 (146). For all parasites, invasion into Cyt-1 cells was slightly more CytD sensitive than in HFF cells. This may stem from differing quantities of actin in the host cells altering the effective CytD concentration experienced by the parasites, or the drug impacting host processes that may contribute to invasion. Importantly, however invasion by both Δ*act1* and *ACT1*^{f} intact parasites into Cyt-1 cells was inhibited by CytD (Figure 2.4). Furthermore, parallel invasions by parasites with a CytD-resistant *act1*^{A136G} allele (17), into both HFF and Cyt-1 cells was not affected at these concentrations of CytD, supporting the ability of our assay to detect a CytD-resistant phenotype. In combination, these results suggest that the major invasion-inhibiting target of CytD is parasite actin, rather than host actin, for both Δ*act1* and *ACT1*^{f} intact parasites.

Impact of ACT1 knockout on invasion stages

We finally asked if it was possible to delineate roles for ACT1 in specific stages of invasion. We first considered the attachment of parasites to HFFs rendered too rigid to invade by glutaraldehyde fixation. When a mixed population of *ACT1*^{f} intact and Δ*act1* parasites were allowed to attach to glutaraldehyde-fixed HFF, Δ*act1* parasites were similarly abundant among

the input parasite population and attached parasites, indicating that *ACT1* disruption does not inhibit the initial attachment stages of invasion (Figure 2.5A). We then used a short (90 sec) invasion pulse and staining for the MJ marker RON4 to consider whether Δ*act1* parasites could effectively secrete rhoptry contents and establish a MJ. In these experiments, Δ*act1* parasites were significantly less likely to have completed penetration in comparison to *ACT1*^{f} intact parasites (Figure 2.5B). Importantly, however, about half of the Δ*act1* parasites detected were apically-attached at a focus of RON4 secretion, or in the process of actively penetrating a host cell (Figure 2.5B), suggesting the failure of Δ*act1* parasites to invade does not reflect an inability to establish a functional MJ.

Relatively few Δ*act1* parasites were detected as intracellular in comparison to the number captured in the process of penetration in our MJ assays (Figure 2.5B). We hypothesized that this may reflect that Δ*act1* parasites may either penetrate more slowly than *ACT1*^{f} intact parasites, or fail to complete invasion attempts at all. To test this possibility, we used time-lapse video microscopy to observe invasions by *ACT1*^{f} intact and Δ*act1* parasites. About half of the Δ*act1* parasite invasions detected were completed in a similar time frame as *ACT1*^{f} intact parasite invasions (Figure 2.5C). The detection of some Δ*act1* invasions with normal kinetics are consistent with a model where a portion of the Δ*act1* parasites are not strongly depleted for ACT1 and thus are not true phenotypic nulls. However, while nearly all *ACT1*^{f} intact parasite invasions were complete within a minute, almost a third of the Δ*act1* parasite invasions failed to complete within 4 minutes (Figure 2.5C), suggesting that Δ*act1* parasites have a specific defect in the penetration stage of invasion.

Discussion

Here we sought to evaluate if limited invasion by inducible Δ*act1* parasites supports a need for revising the current model that invasion requires a parasite actin-dependent myosin motor. Our analysis of invasion, gliding motility, and egress all indicated that gliding motility-dependent behaviors are inhibited, but not completely abolished, in Δ*act1* parasites 2 days following *ACT1*^{f} excision (Figure 2.1). By quantifying ACT1 abundance in individual parasites, we found that residual ACT1 is detectable in Δ*act1* parasites as many as 5 days after inducing *ACT1*^{f} excision (Figure 2.2). Supporting functional relevance of this residual ACT1, we observed a positive correlation between the length of time Δ*act1* parasites are propagated after *ACT1*^{f} excision and the severity of the invasion defect observed in Δ*act1* parasites. Consistent with a model where residual ACT1 enables Δ*act1* parasite invasion, both *ACT1*^{f} and Δ*act1* parasites were sensitive to the actin polymerization inhibitor CytD (Figure 2.4). We were unable to detect a defect in host cell attachment for Δ*act1* parasites (Figure 2.5A). We further found that Δ*act1* parasites were capable of secreting rhoptries and forming functional MJs (Figure 2.5B). However, the frequent failure of Δ*act1* parasites to complete invasion attempts within the time period typical for wild-type parasites (Figure 2.5C) suggests a requirement for *ACT1*^{f} specific to the penetration stage of invasion.

Initial studies using inducible Δ*act1* parasites observed low levels of parasite motility and invasion as many as 4 days after *ACT1*^{f} excision, and interpreted the ability of some parasites to still invade as evidence in support of an ACT1-independent invasion pathway in *T. gondii* (68,69). In these studies, the conclusion that ACT1 polymerization was ablated in inducible Δ*act1* parasites relied on qualitative estimation of residual ACT1 by immunofluorescence staining, and Western blots of pooled parasite extracts, although the sensitivity of this method

was not determined (68,69). In contrast, our quantification of ACT1 content in individual parasites revealed that there is considerable overlap in the ACT1 content of individual Δ*act1* and *ACT1*^{f} intact parasites, even 5 days after *ACT1*^{f} excision (Figure 2.2). We were surprised to detect Δ*act1* parasites with moderate levels of ACT1 so long after rapamycin-induction of *ACT1*^{f} excision. We speculate that these cases represent either parasites that spontaneously excised *ACT1*^{f} after rapamycin induction, or parasites that inherited an unusually large portion of the ACT1 mRNA or protein present at the time of *ACT1*^{f} excision. Both scenarios are likely rare. However, the fitness defects associated with substantial ACT1 depletion could easily impose a strong selection in favor of any rare Δ*act1* parasites with significant residual ACT1 and thus increase their prevalence in the population.

Our subsequent finding that extended propagation of Δ*act1* parasites is correlated with increased severity of the invasion defect supports the role of actin in this process. Accordingly, the isodesmic polymerization of ACT1 (74) should allow low amounts of residual ACT1 to form filaments and power invasion. We note that the increasing severity in invasion defect was moderate relative to the expected rapid dilution of ACT1 protein among dividing Δ*act1* parasites. However, quantification of ACT1 levels in Δ*act1* parasites by IFA also did not show Δ*act1* parasites becoming dramatically more depleted for ACT1 beyond day 3. We hypothesize that upon falling below some required threshold for ACT1 content, Δ*act1* parasites perish and are thus removed from the population.

Further support for the residual ACT1 model is provided by the finding that invasion by inducible Δ*act1* parasites retained sensitivity to the actin polymerization inhibitor, CytD. The inability of CytD-resistant host cells to rescue invasion by Δ*act1* parasites demonstrates that CytD is not inhibiting invasion by acting on a host actin-dependent pathway. Rather, CytD

inhibits the invasion of Δ*act1* parasites by acting on a parasite target, presumably ACT1, which exhibits CytD-sensitive filament assembly *in vitro* (75). We cannot, however, exclude the possibility that CytD might target some other protein in Δ*act1* parasites, such as the previously-described actin-like proteins encoded by *T. gondii* (147).

When considering the invasion stages that ACT1 depletion may impact, we did not detect a defect in the attachment of Δ*act1* parasites to glutaraldehyde-fixed host cells. After attaching to host cells, invading parasites go on to secrete rhoptry proteins and penetrate through a MJ (58). A previous study reported that Δ*act1* parasites overwhelmingly fail to secrete rhoptries or form MJs, and hypothesized this MJ formation defect is primarily responsible for the failure of Δ*act1* parasites to invade host cells (69). When we analyzed MJ formation, we also found that Δ*act1* parasites were less efficient at invasion. However, we observed that nearly half of the Δ*act1* parasites attached to host cells had already secreted rhoptries, or even begun penetrating into the host cell (Figure 2.5B). Our results suggest that many Δ*act1* parasites are able to form functional MJs, but are inhibited at a later step in the invasion process. The discrepancy in these results may stem from methodological differences between the studies. Specifically, our assay used a much shorter invasion pulse (90 sec vs. 5 min), designed to capture a greater number of parasites still in the process of invading (~2-fold more). However, given the discrepancy between these results and their respective interpretations, we wished to further probe the potential defect of Δ*act1* parasites in invasion stages following attachment and MJ formation. Our subsequent finding that Δ*act1* parasites often fail to complete invasion within the time period typical for *ACT1*^{f} intact parasites, as determined by video microscopy, serves as further evidence that Δ*act1* parasites have a defect specific to the penetration stage of invasion.

In concert, our results are consistent with a model where ACT1 is essential for efficient penetration of *T. gondii* into host cells. Under this model, inducible knockout of *ACT1* leads to depletion of ACT1 protein and corresponding defects in invasion and other gliding motility-dependent processes. However, because *ACT1* deletion is ultimately lethal to *T. gondii*, generating populations of Δ*act1* parasites that are true phenotypic nulls is not feasible. Instead, Δ*act1* parasite populations generated by Cre-mediated excision of *ACT1*^{f} contain parasites, that although Δ*act1* by genotype, still retain functionally-relevant quantities of ACT1. Because these parasites with residual ACT1 are present in Δ*act1* parasite populations, invasion is able to continue, albeit at a reduced level. Notably, our results do not exclude the possible existence of additional pathways that could contribute to *T. gondii* invasion. However, the existence of such alternative pathways is not necessary to explain the phenotype of Δ*act1* parasites. Moreover, any such alternative pathways seem unlikely to be major contributors to *T. gondii* invasion, as they are not able to offer a robust or efficient alternative to ACT1-dependent invasion, as evidenced by the major invasion defects of Δ*act1* parasites.

The development of inducible Cre-Lox genetic tools for *T. gondii* (68) offers an exciting opportunity to dissect essential processes. In particular, inducible Cre-Lox technology has facilitated the deletion of several genes thought to encode essential components of the invasion machinery (68-70). For some of these genes, residual invasive ability can be explained by functional redundancies built in the *T. gondii* genome (72,73). For other truly essential genes such as actin, our results highlight the importance of considering the functional implications of residual protein retained in mutants after inducible gene knockout.

Materials and methods

Parasite strains and growth conditions.

Parasites were passaged as tachyzoites in human foreskin fibroblast (HFF) monolayers as previously described (57). An RH *Δku80::diCre* strain (68), here referred to as *diCre*, was used as a wild-type control strain, and to generate the new inducible *ACT1* knockout. Initial experiments used a previously described inducible *ACT1* knockout, diCre-Act1 (68), here referred to as *ACT1*^{f}-1. Subsequent experiments used a new inducible *ACT1* knockout, *ACT1*^{f}-2, created as described below. In both *ACT1*^{f} strains, excision was induced by treating partially lysed (50-75%) parasite cultures with 50 nM rapamycin for 4 hr. Induced parasites were isolated by filtration through 3.0 micron filters (Nucleopore), washed twice by dilution in HHE (Hank's Balanced Salt Solution supplemented with 1M HEPES and 0.1M EGTA) and centrifugation at 400 x *g* to remove any residual rapamycin, and then used to infect fresh HFF monolayers. Mixed populations of *ACT1*^{f} intact and Δ*act1* parasites were isolated by mechanical lysis of partially lysed cultures, typically 40-48 hours after inoculation. To culture Δ*act1* parasites for 4-5 days, cultures were mechanically lysed 2 days after induction and re-infected into HFFs at high doses to compensate for low invasion.

Generation of new inducible ACT1 knockout strain

Plasmids and oligonucleotides used in this study are listed in Table 2.1. To generate the high-excising *ACT1*^{f}-2 strain, a plasmid (pLD-03) was constructed with the *ACT1* CDS immediately flanked 5' by a *Toxoplasma*-specific Kozak sequence (GGCAAA) and LoxP site, and 3' by a LoxP site followed by a YFP reporter and the HXPGRT selectable marker. To this end, the LoxP-flanked 3'UTR of *ACT1* was amplified from RH genomic DNA and ligated into the plasmid pG265, generating the plasmid pLD-02. Gibson assembly of the *ACT1* 3'UTR

preceded by YFP and HXPGRT, isolated from pLD-02 by *PacI* and *ApaI* digestion, and *ACT1* 5'UTR and CDS fragments amplified from genomic DNA was then used to generate pLD-03. The resulting ACT1-floxing cassette was then released from pLD-03 by *PvuII* digestion to expose the 5' and 3' ends of the construct for homologous recombination, and electroporated into the *diCre* strain. After selection with 25 µg/mL mycophenolic acid and 50 µg/mL xanthine (Sigma-Aldrich, St. Louis, MO), parasite clones were isolated by limiting dilution in 96-well plates containing HFF monolayers. Clones were screened with both diagnostic PCR (Figure S1) and dual ACT1/YFP immunostaining after rapamycin treatment to obtain *ACT1*^{f}-2, a reliably high-excising inducible knockout strain.

Invasion assay

A previously developed differential staining method was adapted to identify parasites as intracellular or extracellular, and *ACT1*^{f} intact or Δ*act1* (148). In this assay, parasites harvested by mechanical lysis were allowed to invade sub-confluent HFF monolayers on coverslips for 30 min. After thorough rinsing, coverslips were first stained with mAb DG52 to SAG1 to mark extracellular parasites. Cell were then permeabilized with 0.05% saponin. After permeabilization, rabbit anti-TgACT1 (67) and rat anti-GFP (Santa Cruz Biotechnology) were used to identify Δ*act1* parasites by YFP expression. All primary antibodies were recognized by fluorophore-conjugated secondary antibodies (DG52: Alexa594; TgACT1: Alexa647; GFP: Oregon Green 488). Slides were imaged on a Cytation3 cell imaging multimode reader, using Gen5 software for analysis (BioTek, Winooski, VT). All experiments were performed at least 3 independent times, each with 3-5 technical replicates.

To determine the abundance of Δ*act1* parasites in input populations, aliquots of the parasites used for invasion were adhered to poly-L-lysine-coated coverslips, and then stained

with mouse anti-GFP and rabbit anti-TgACT1, followed by fluorophore-conjugated secondary antibodies (GFP: Alexa594; TgACT1: Alexa488). Slides were visualized on a Zeiss Axioskop 2 MOT Plus microscope with an AxioCam MRm monochrome camera and Axiovision software (Carl Zeiss, Inc., Thornwood, NJ).

To test the effect of cytochalasin D (CytD) on invasion, parasites were allowed to invade both CytD-sensitive HFF host cells, and CytD-resistant Cyt-1 (24) host cells. HFF cells were seeded onto 96-well plates, and Cyt-1 cells on 0.1% gelatin-coated coverslips. Prior to invasion, cells were pre-treated for 10 min at room temperature with either CytD or 0.02% DMSO. In experiments testing invasion into HFF cells, only parasites were pre-treated with CytD; when testing invasion into the resistant Cyt-1 cells, both parasites and the Cyt-1 cells were pre-treated with CytD. After CytD pre-treatment parasites were briefly settled onto host cells by centrifugation at 400 *g* and 18°C for 2 min, and then allowed to invade for 12 min at 37°C. The same differential staining approach described above was used, except that Cyt-1 cells were permeabilized with 0.25% Triton X-100.

Time-lapse microscopy of egress, gliding, and invasion

To observe egress, parasites were infected onto HFF monolayers on glass-bottom culture dishes (MatTek, Ashland, MA), and cultured for 2 days. Immediately prior to the experiment, monolayers were rinsed twice into Ringer's media (155 mM NaCl, 3 mM KCl, 2 mM $CaCl_2$, 1 mM $MgCl_2$, 3 mM $NaPO_4$, 10 mM HEPES, 10 mM D-glucose, pH 7.4). To induce egress, 2 µM A23187 was added 30 sec into 10 min total acquisition periods, during which alternating brightfield and FITC fluorescence images were captured at ~2 frame/5 sec, using the Zeiss Axio Observer Z1 imaging system and Zen software as previously described (149).

Gliding motility was observed with video microscopy as previously described (50), expect that dishes were pre-coated with 50% fetal bovine serum. Alternating brightfield and FITC fluorescence images were acquired at ~1 frame/3 sec. Data from multiple videos taken on the same day were pooled so that 25 -60 Δ*act1* parasites were analyzed for every experiment, with *ACT1*^{f} intact parasites from the same videos serving as control.

Invasion was monitored with video microscopy as previously described (149), expect that cells were imaged in dishes containing indicator-free DMEM (Sigma D5030) supplemented with 1g/L glucose, 25 mM HEPES, and 3% FBS (pH 7.4). Alternating brightfield and FITC fluorescence images were acquired for 10 min periods at ~3 frame/ sec. Invasion duration was defined as the length of times parasites displayed visible moving junctions. To analyze the rare Δ*act1* invasion events, data from 16 independent experiments were pooled, and randomly selected invasions by *ACT1*^{f} intact parasites from the same days used as control.

Quantification of ACT1 abundance by IFA

ACT1 staining intensity was used as a semi-quantitative proxy for ACT1 protein abundance. Parasite-infected HFF monolayers were fixed with 4% formaldehyde, and subjected to permeabilization with 0.05% Saponin and immunostaining. When considering only ACT1 and YFP expression, ACT1 was stained with rabbit anti-TgACT1 and YFP with mouse anti-GFP, followed by fluorophore conjugated secondary antibodies (TgACT1: Alexa594; YFP: Alexa488). For these experiments, 0.25 micron Z-series of images were acquired on a Zeiss Axioskop 2MOT Plus microscope, and deconvolved with a nearest-neighbor algorithm in AxioVision software. When distinguishing intracellular and extracellular parasites in addition to ACT1 and YFP expression, cells were stained with the GFP/TgACT1/DG52 antibody combinations used in the modified invasion assay. For these experiments, images were acquired

on a Zeiss LSM 510 META Confocal Laser Scanning Microscope and LSM Image Examiner software. In all experiments, at least 20 parasites for every reported category were measured. To quantify ACT1 staining in images generated by either method, individual parasites were manually traced and fluorescent signals were quantified using Volocity software (Perkin Elmer, Waltham, MA). The mean signal of 5 host cytosol regions within the same field of view was used for background subtraction.

Attachment assay

Confluent HFF monolayers in 96-well plates were fixed for 10 min in 2% glutareldehyde to generate rigid, impenetrable host cells. Once fixed, HFF were rinsed in PBS and quenched overnight in 1M glycine. The day of the assay, the fixed HFF were rinsed in D3 (DMEM supplemented with 3% FBS, 2 mM glutamine, 10 µg/mL gentamicin, 44 mM sodium bicarbonate, and 10 mM HEPES), and then equilibrated at least 1 hour in D3 at 37°C, and transferred to Invasion Media (DMEM supplemented with 3% FBS and 25 mM HEPES) immediately before the assay. After briefly settling parasites into each well with 2 min of centrifugation at 400 *g*, attachment was carried out for 15 min at 37°C. Unattached parasites were then removed by rinsing wells 10 times with room temperature PBS. Live parasites attached to the glutareldehyde-fixed HFF were immediately imaged, using the Zeiss Axio Observer Z1 imaging system with Zen software (Carl Zeiss, Inc., Thornwood, NY) and an ORCA-ER digital camera (Hamamatsu Photonics, Japan) to generate brightfield and FITC images. 80-200 parasites, split among at least 2 separate fields of view were analyzed for each well. Brightfield and FITC images of control aliquots of parasites spun directly into HFF-free wells were used to determine the abundance of YFP-expressing Δ*act1* parasites in the input population.

Moving junction assay

After harvesting by mechanical lysis, parasites were transferred to intracellular buffer (5 mM NaCl, 142 mM KCl, 1 mM $MgCl_2$, 2 mM EGTA, 5.6 mM D-glucose, 25 mM HEPES, pH 7.4), and allowed to invade sub-confluent HFF monolayers on coverslips in 24-well plates for 90 sec. The 24-well plates were then immediately transferred to an ice water bath. Coverslips were rinsed, then fixed with 4% formaldehyde, and processed for immunofluorescence. To mark extracellular parasites, cells were stained with mAb DG52 prior to permeabilization with 0.05% Saponin. After permeabilization, anti-GFP was used to mark Δ*act1* parasites, a rabbit polyclonal antibody to RON4 provided by John Boothroyd used to mark the moving junction, and fluorophore-conjugated secondary antibodies (DG52: Alexa350; GFP: Alexa488; RON4: Alexa594) were used for visualization. Images were acquired on a Zeiss Axioskop 2MOT Plus microscope, using an AxioCam MRm monochrome camera and Axiovision software (Carl Zeiss, Inc., Thornwood, NY).

Statistics

All statistical tests were performed in Prism (Graph-Pad Software, Inc., La Jolla, CA). Unless otherwise noted, data sets were assumed to be normally distributed and analyzed with repeated measures one-way ANOVA if considering only a single independent variable (e.g. genotype alone), and two-way ANOVA if considering two independent variables (e.g. genotype and CytD). To compare individual means within an ANOVA, Dunnett's multiple comparisons test was used if comparing all means against a single control, and Sidak's multiple comparisons test if comparing selected pairs of means. ACT1 staining intensity data sets were not normally distributed and accordingly analyzed using a non-parametric Kruskal-Wallis test, and Dunn's multiple comparisons test for selected groups. To accommodate non-complete invasion events,

invasion duration data was treated as ordinal and analyzed with a Mann-Whitney test. All post tests used corrections for multiple comparisons. In all cases two-tailed *P* –values were calculated, and $P \leq 0.05$ was considered significant.

Acknowledgements

We thank Markus Meissner for sharing the *ACT1*^{f}-1 strain and plasmids for inducible diCre, Wandy Beatty for assistance with imaging, Jennifer Barks for excellent technical support, and members of the Sibley lab for helpful discussions. This work was supported by a grant from the NIH (A1034036). L.D. is supported by a NSF GRFP fellowship.

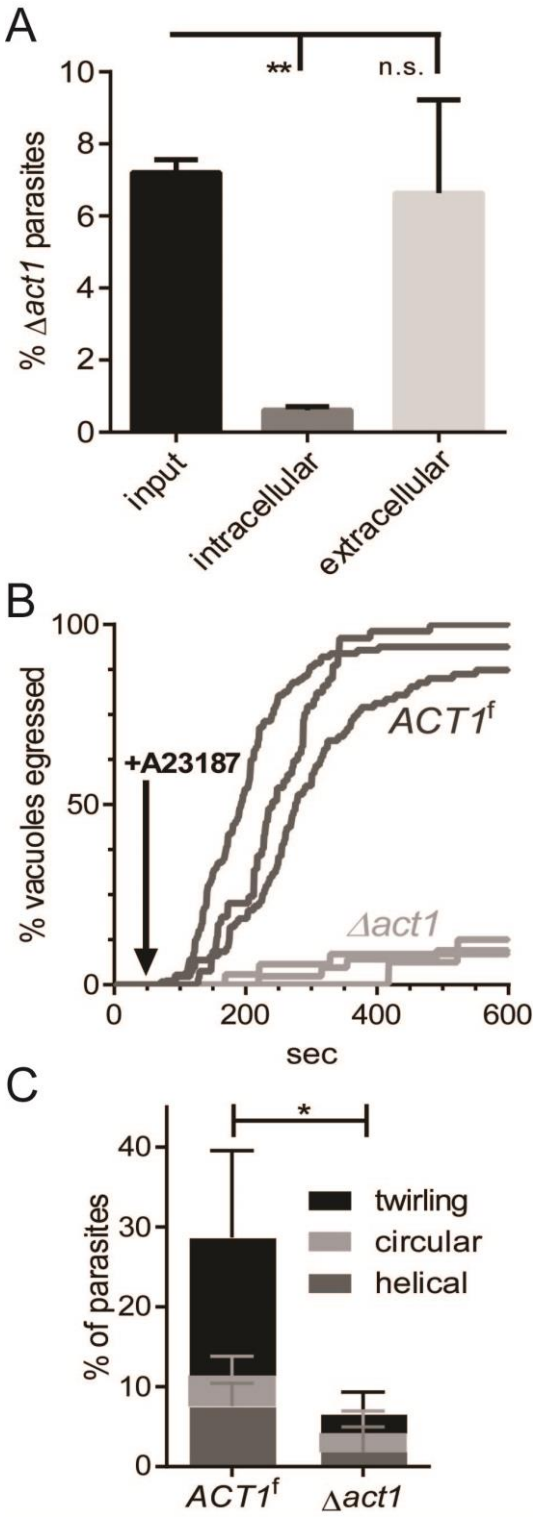

Figure 2.1: Analysis of actin-dependent motility after deletion of *ACT1*^{f}.

(A) Invasion efficiency determined with a differential staining protocol that detects intracellular or extracellular parasites based on protection from SAG1 (mAb DG52) staining prior to permeabilization, and differentiates between *ACT1*^{f} intact and Δ*act1* based on YFP expression. Percentage of knockouts in the input parasite population, intracellular, or extracellular parasites after a 30 min invasion period is shown as mean +/- SD (N=3). **, $P \leq 0.01$, one-way ANOVA with Dunnett's multiple comparisons test. Data shows 1 of 3 independent experiments, in all of which Δ*act1* parasites were significantly under-represented among intracellular parasites relative to the input. (B) Egress induced by A23187 and tracked with time-lapse video microscopy. Δ*act1* parasites were identified by YFP expression. Traces show cumulative percent egression of $N \geq 16$ vacuoles; each individual trace represents an independent experiment. (C) Parasite gliding on serum-coated coverslips as observed by time-lapse video microscopy; Δ*act1* determined by YFP expression. Columns show mean percentages of parasites +/- SD, from 3 independent experiments, each with 25-60 Δ*act1* parasites scored. *, $P \leq 0.05$, one-way ANOVA. All experiments were performed 2 days after rapamycin induced excision of *ACT1*^{f} in a previously described strain (15), *ACT1*^{f}-1.

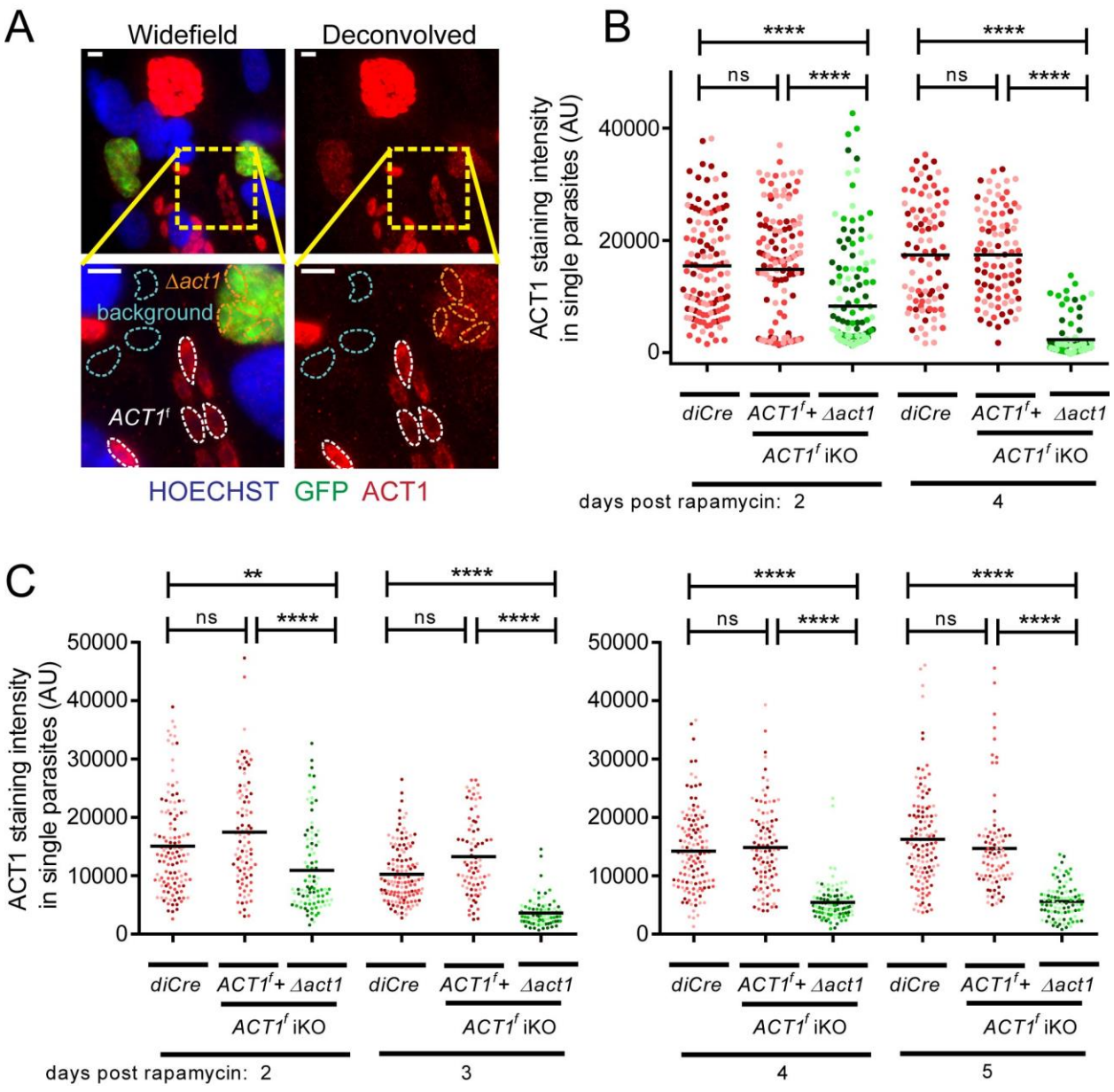

Figure 2.2: Estimating ACT1 abundance after gene excision.

(A) ACT1 abundance was estimated by immunofluorescence staining intensity. Individual parasites were traced in de-convolved Z-series images to quantify anti-TgACT1 staining intensity. Δ*act1* parasites were identified by YFP expression, as indicated by anti-GFP staining. The mean signal from 5 host cytosol regions within the same field of view was used for background subtraction. Images depict an example field containing both *ACT1*^{f} and Δ*act1*

parasites, 4 days after inducing gene excision. Scale bar = 5 microns. (B-C) Quantification of ACT1 staining intensity in *ACT1*^{f}-2, and the parental *diCre* strain, 2-5 days after rapamycin induction of *ACT1*^{f} excision. ACT1 was stained with either monoclonal anti-*Dictyostelium* actin (B), or polyclonal anti-TgACT1 (C). Three separate cultures were induced in parallel, different color intensities denote parasites from different biological replicates. Markers indicate background-subtracted fluorescence intensities from single parasites, expressed in arbitrary units (AU). Lines show mean intensity. **, $P \leq 0.01$, ****, $P \leq 0.0001$, Kruskal Wallis test with Dunn's multiple comparisons test. All experiments were performed with a newly-derived inducible *ACT1* knockout, *ACT1*^{f}-2.

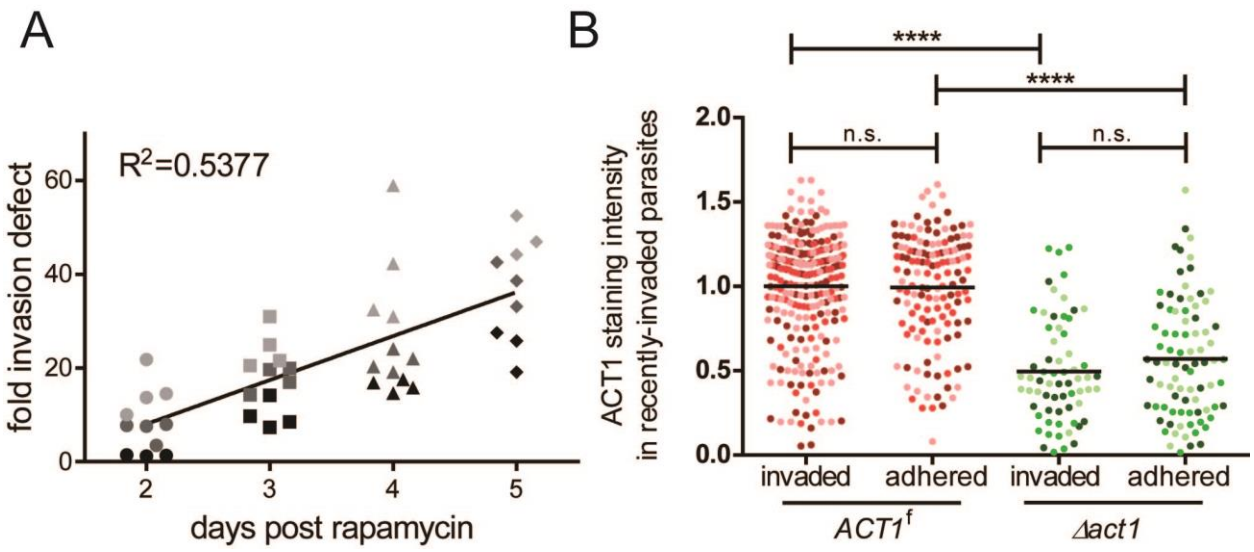

Figure 2.3: Residual ACT1 levels and invasion by Δ*act1* parasites.

(A) Magnitude of the invasion defect of Δ*act1* parasites was determined at different time points after rapamycin-induced *ACT1* excision. Invasion defect was quantified by comparing the frequency of Δ*act1* parasites among intracellular parasites after a 30 min invasion, to abundance in the initial parasite population. Fold invasion defect = (%Δ*act1* in input) / (%Δ*act1* in intracellular parasites). Δ*act1* parasite frequency was determined using the differential staining protocol described in Figure 1. Data shows 3 independent experiments, each with 3-4 technical replicates. Matched color shades denote technical replicates from the same experiment. Linear regression (R^2= 0.5377, $P < 0.0001$ different from slope = 0). (B) At 4 days after inducing gene excision, ACT1 abundance in recently-invaded parasites was estimated by staining intensity. Parasites were classified as intracellular or extracellular, and *ACT1*^{f} intact or Δ*act1* using the differential staining protocol described in Figure 2.1. Lines show mean intensity for each category. Because invading Δ*act1* parasites are relatively rare, data from 3 independent experiments were combined to generate the graph. Intensities from each data set were

normalized to the mean intensity of *ACT1*^{f} intact intracellular parasites. Matched color shading indicates data from the same experiment. At least 20 parasites are shown for every category in each experiment. ****, $P \leq 0.0001$, Kruskal Wallis test with Dunn's multiple comparisons test. All experiments were performed with *ACT1*^{f}-2.

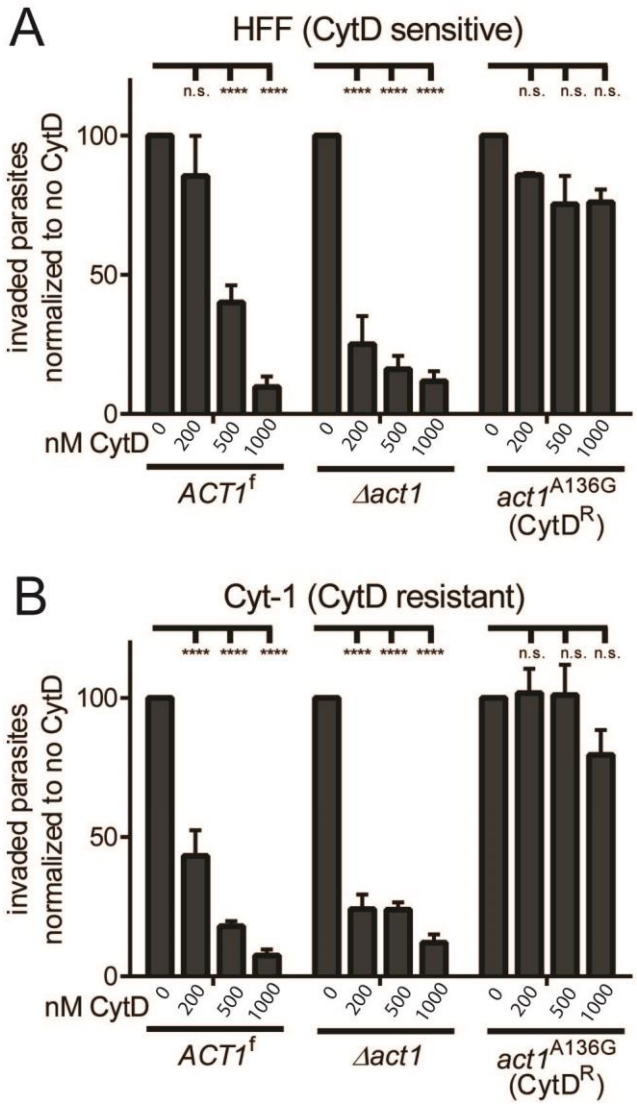

Figure 2.4: Testing sensitivity of invasion to actin inhibitor cytochalasin D.

(A-B) Parasites were classified as intracellular or extracellular, and *ACT1*^{f} intact or Δ*act1* using the differential staining protocol described in Figure 1. The invasion rates of *ACT1*^{f} intact and Δ*act1* parasites, and Cytochalasin D (CytD)- resistant *act1*^{A136} parasites were compared in CytD-sensitive HFF cells (A), and Cyt-D resistant Cyt-1 cells (B). Data shows mean values, +/- SEM, from 3 independent experiments with the *ACT1*^{f} parasites and 2 independent experiments with the *act1*^{A136} parasites, each with 3-5 technical replicates. For each group, the number of

intracellular parasites was normalized to the mean invasion rate of that group with no CytD. ****, $P \leq 0.0001$, Two-way ANOVA with Dunnett's multiple comparisons test. All experiments were performed with *ACT1*^{f}-2, 4 days after rapamycin induction of gene excision.

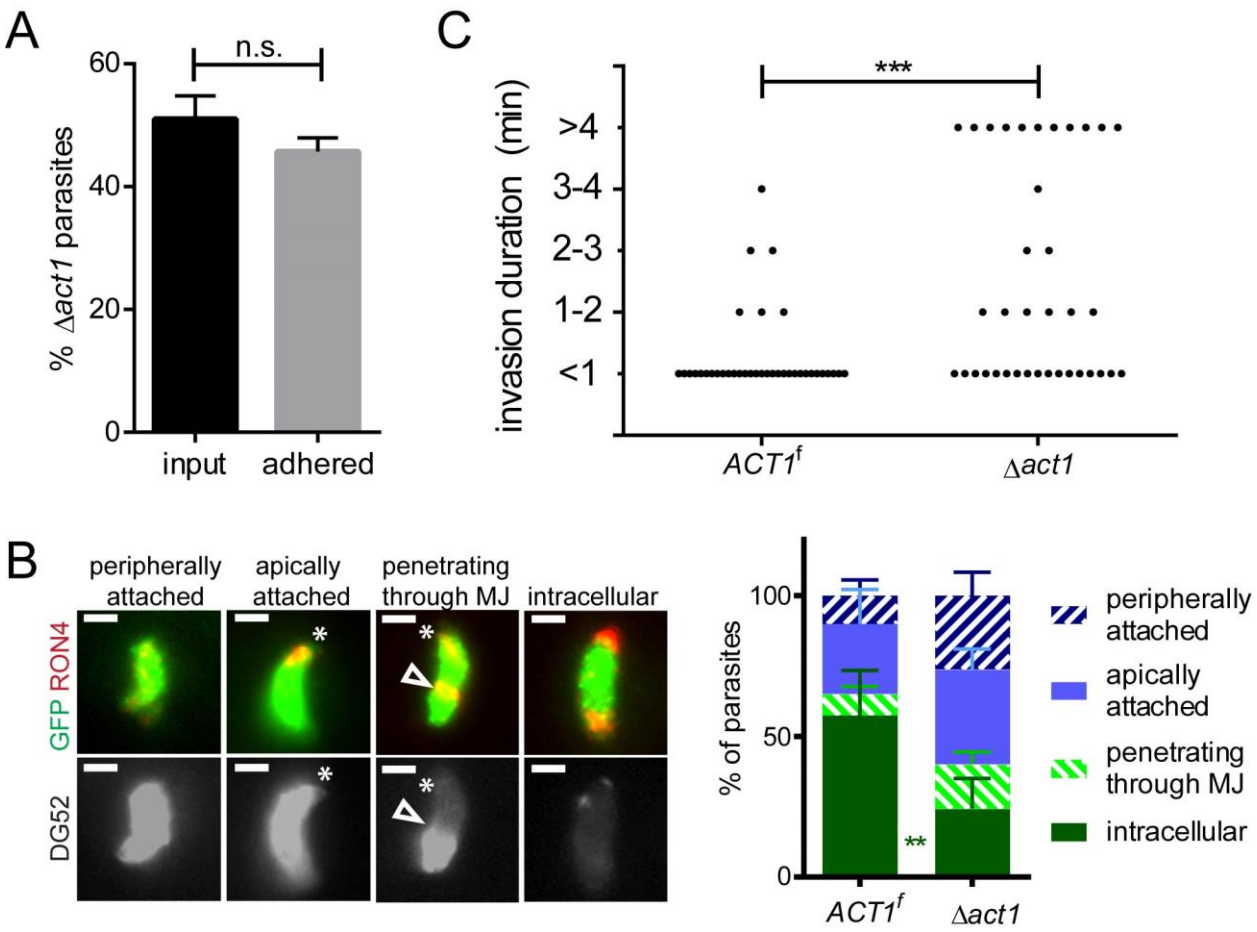

Figure 2.5: Impact of *ACT1* deletion on adhesion and invasion efficiency.

(A) Efficiency of attachment to glutareldehyde-fixed HFF cells by Δ*act1* parasites relative to *ACT1*^{f} intact parasites was determined 4 days after rapamycin-induced *ACT1* excision. Δ*act1* parasites were identified by YFP expression, and an aliquot of the input parasites used to determine Δ*act1* parasite abundance prior to attachment. n.s., $P > 0.05$, unpaired T-test. Data from one of 3 independent experiments, each with 3-4 technical replicates, is shown. In all 3 experiments no significant differences in Δ*act1* frequency between input and adhered parasites were observed. (B) Moving junction (MJ) formation was analyzed by immunostaining after a 90 sec invasion pulse. Parasites were classified as: "peripherally attached" or "apically attached" based on detection of secreted RON4; "penetrating" based on partial SAG1 (mAb DG52)

protection and presence of RON4 rings; and “intracellular” based on protection from SAG1 (mAbDG52) staining preceding permeabilization. Images show representative Δ*act1* parasites from each category. White asterisks indicate apical end. White arrowhead indicates the MJ. Scale bars = 2 micron. Data shows means +/- SEM from 3 independent experiments, each with 3 technical replicates. **, $P \leq 0.01$, two-way ANOVA with Sidak’s multiple comparisons test. (C) Speed of invasion was determined with time-lapse video microscopy 4 days after *ACT1* excision, using YFP expression to classify parasites as Δ*act1*. Each marker represents a single invasion event. Data from 16 independent experiments were pooled. ***, $P \leq 0.001$, Mann-Whitney test. All experiments were performed with *ACT1*^{f}-2, 4 days after rapamycin induction of gene excision.

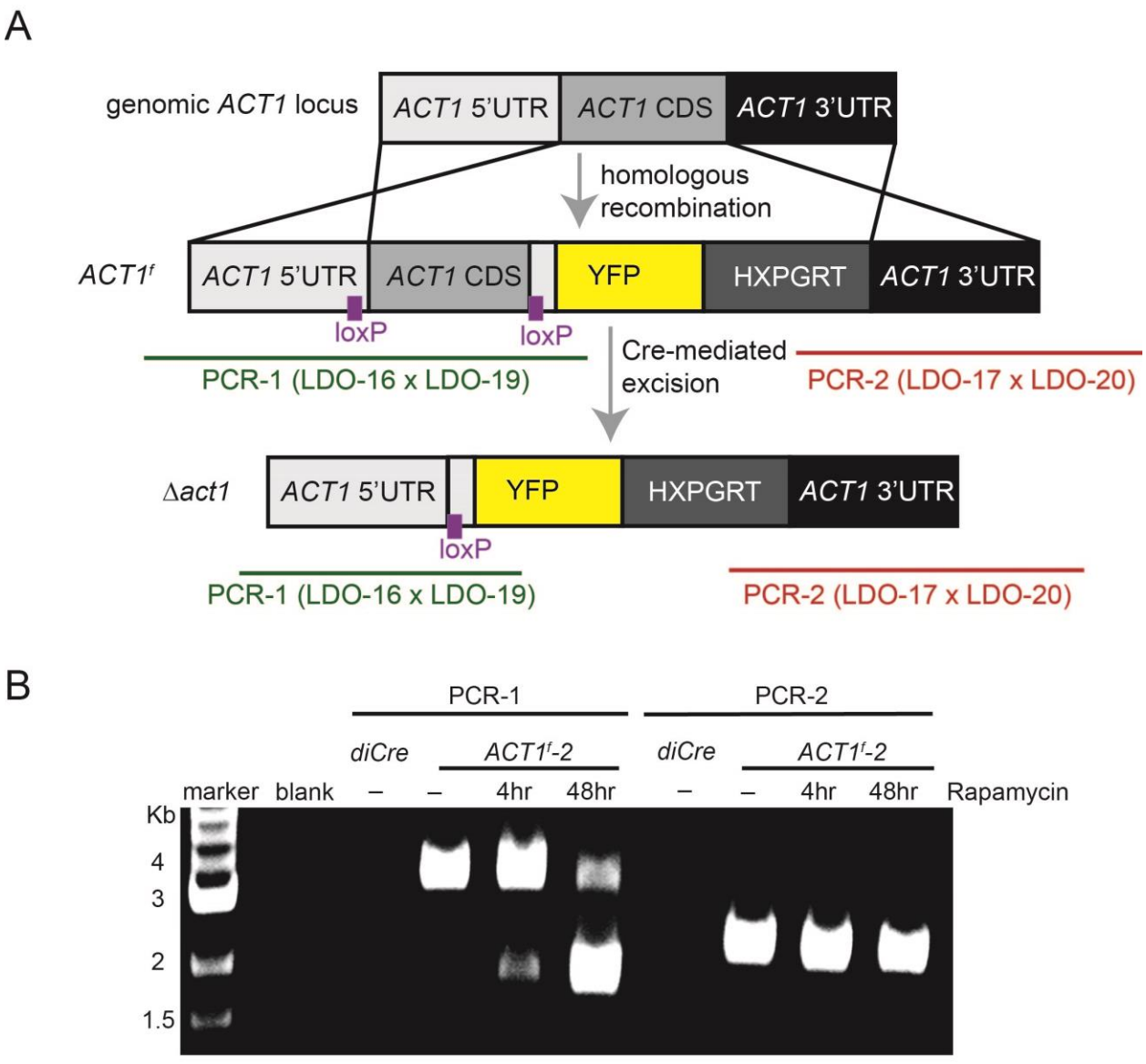

Figure S1: Generation of an inducible *ACT1* knockout with increased excision efficiency. (A) Schematic of the strategy used to generate a floxed *ACT1*^{f} inducible knockout. (B) Diagnostic PCR of *ACT1* locus in the *diCre* background used for mutant generation, and the *ACT1*^{f}-2 mutant prior to, and 4 and 48 hours following induction of gene excision with rapamycin. PCR-1 analyzes 5' integration of the floxing construct, and also detects Cre-mediated excision. PCR-2 analyzes 3' integration of the floxing construct.

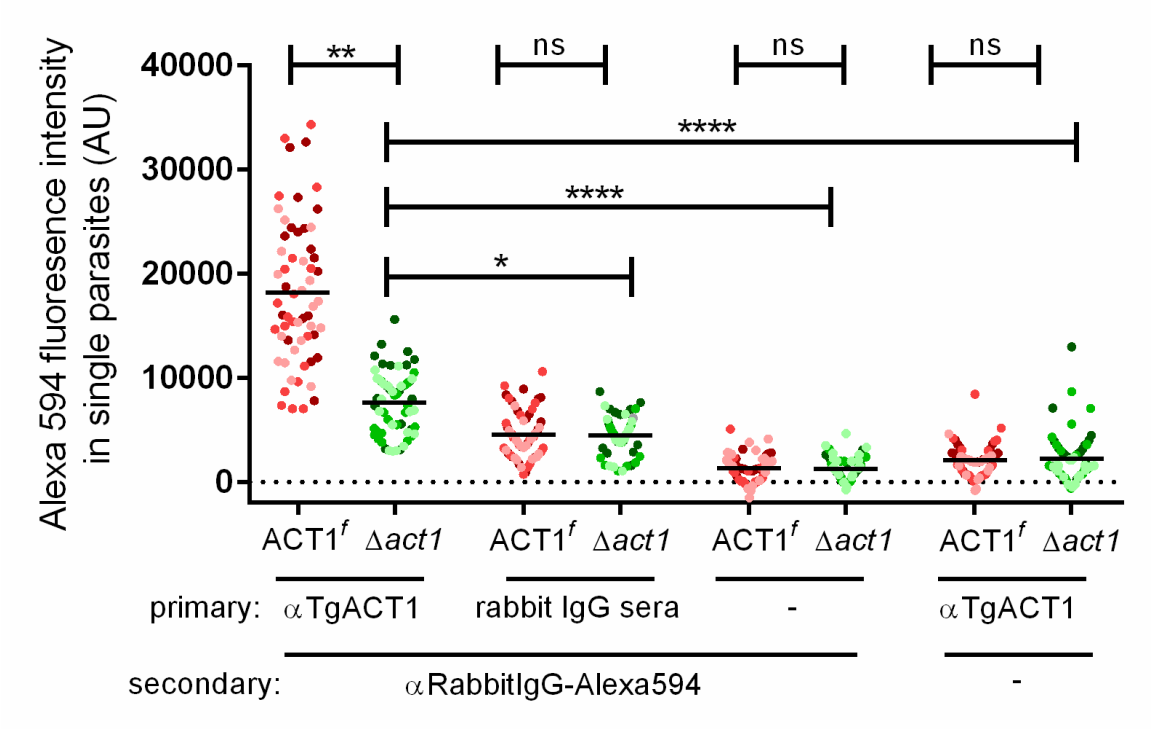

Figure S2: Specificity of ACT1 staining.

ACT1^{f}-2 parasites were stained with the indicated antibody combinations 4 days after inducing *ACT1* excision with rapamycin. Rabbit IgG sera (*Santa Cruz Biotechnology)* was used as an isotype control. Δ*act1* parasites were identified by YFP expression, and staining was quantified as in Fig. 2. Three separate cultures were induced in parallel, different colors denote parasites from different replicates. Markers indicate background-subtracted fluorescence intensities from single parasites, expressed in arbitrary units (AU). Lines show mean intensity. *, $P \leq 0.05$, **, $P \leq 0.01$, ****, $P \leq 0.0001$, Kruskal Wallis test with Dunn's multiple comparisons test.

Table 2.1: Primers and oligonucleotides used in this study.

Primer	**Sequence**	**Purpose**
LDO-003	TCACCgagctcGCAGTTTGTGGTGTTTTATCGA	Clone 3'UTR of *TgACT1* with SacI site
LDO-004	TCACCgagctcCATACCTGACCTCGCTGAAA	
LDO-013	ACTCACTATAGGGCGAATTGGGTACCGCTGCAGTTCGTGAACGAT	Clone 5'UTR of *TgACT1* with LoxP, Kozak, and overlap for Gibson assembly
LDO-006	tttgccataacttcgtataatgtatgctatacgaagttatCTTACCTATGAAAAAGTGGA	
LDO-007	gtatagcatacattatacgaagttatggcaaaATGGCGGATGAAGAAGTGC	Clone CDS of *TgACT1* with LoxP, Kozak, and overlap for Gibson assembly
LDO-012	TTTATAACTTCGTATAATGTATGCTATACGAAGTTATTAATTTAGAAGCACTTGCGGTGG	
LDO-016	AGAAGATGGTGCGCTCCTG	Diagnostic PCR-1 (5' integration of ACT1 floxing cassette and Cre-mediated excision)
LDO-019	GTACCTACGAATCGGCAATACA	
LDO-017	TCGTTGGTTGCTGCTACGAC	Diagnostic PCR-2 (3' integration of ACT1 floxing cassette)
LDO-020	GTGCAAAGCTTCTCGTACAGTG	
Plasmid	**Construction**	**Purpose**
pLD-02	pG265-ACT3'UTR: 3'UTR of Tg*ACT1* cloned upstream of YFP-HXPGRT cassettes in pG265	Intermediate cloning plasmid to generate *ACT1* floxing construct
pLD-03	pACT1iKO: 5'UTR and CDS of Tg*ACT1* with LoxP sites inserted upstream of Tg*ACT1* 3'UTR in pLD-02 by Gibson assembly	Floxing Tg*ACT1*

Chapter 3: The secreted kinase ROP17 promotes *Toxoplasma gondii* dissemination by hijacking monocyte tissue migration

Preface

L.L.D. designed and performed all experiments and drafted the manuscript. N.G.J. generated fluorescent *T. gondii* strains critical for time-lapse microscopy. M.J.M. collaborated on the design, execution and analysis of two-photon imaging studies. L.D.S. supervised the studies and assisted with experimental design and analysis. L.L.D. and L.D.S. collaboratively revised the manuscript with input from all authors.

This chapter is currently under review for publication:

Drewry L.L., Jones N.G., Miller M.J., Sibley L.D. The secreted kinase ROP17 promotes *Toxoplasma gondii* dissemination by hijacking monocyte tissue migration.

Summary

The protozoan parasite *Toxoplasma gondii* is thought to exploit extravasation of infected monocytes to facilitate dissemination across endothelial barriers such as the blood-brain barrier. Here we analyzed the migration of parasitized monocytes in models of vascular and tissue environments. We report that infection enhanced monocyte locomotion on the surface of endothelial cells, but profoundly inhibited monocyte transmigration across endothelial barriers. In contrast, infection robustly increased monocyte migration through collagen-rich tissues in a Rho/ROCK-dependent manner consistent with integrin-independent interstitial migration. We further demonstrated that the secreted *T. gondii* kinase ROP17 was required for enhanced monocyte tissue migration. *In vivo*, ROP17-deficient parasites failed to upregulate monocyte tissue migration and exhibited an early dissemination delay, leading to prolonged mouse survival. Our findings indicate that parasitized monocytes are ill-suited for delivering parasites across the blood-brain barrier as previously predicted, but instead function to shuttle *T. gondii* through tissues and thereby promote systemic dissemination.

Introduction

The protozoan parasite *Toxoplasma gondii* causes severe disease in immunocompromised humans (7). *T. gondii* is among the few pathogens that can cross endothelial barriers to reach deep tissues such as the central nervous system (CNS). The parasite is theorized to hijack leukocytes as shuttles to enable extravasation across the blood-brain barrier (BBB) (33,150). Infected leukocytes could potentially aid dissemination at several different stages of infection. Following oral ingestion, parasites traverse intestinal epithelium and enter the intestinal lamina propria (15,151). Here, parasites encounter resident macrophages and dendritic cells (DCs) (28,150,152) and trigger an influx of inflammatory monocytes (112). From this infection nidus, parasites disseminate to draining lymph nodes, the blood, spleen, and eventually, all organs including the brain (15,30,151). Infected leukocytes could potentially promote dissemination by carrying parasites out of the intestinal lamina propria, through the lymphatic vasculature and into the circulation. Circulating leukocytes could also deliver parasites across endothelial barriers and into new tissues though the process of extravasation, a sequential cascade that is initiated by selectin-mediated capture of rolling leukocytes, then progresses to stable integrin-based adhesion and vascular crawling, and finally commences with endothelial traversal (110).

One of the most severe complications of toxoplasmosis is encephalitis (7). Hence, the potential for extravasating leukocytes to ferry parasites across the BBB has been keenly investigated (29,30). Studies aimed at mimicking this process *in vitro* reveal that *T. gondii* infection enhanced crawling of primary human monocytes on human umbilical endothelial cells (HUVEC), without significantly altering transendothelial migration (TEM) (108,111). These findings led to the proposal that infected monocytes are poised to deliver *T. gondii* across the BBB (87,150). However, infection diminished integrin-mediated endothelial adherence

(106,107), a step generally considered a prerequisite to endothelial crawling and transmigration (110). Although *T. gondii* infection has been shown to induce a hypermigratory state in DCs (96,97,153,154), previous studies found that nearly all parasitized leukocytes present in the blood of infected monocytes are $CD11b^{+}$ monocytes (29). Consistent with a role for monocytes in dissemination, adoptive transfer of infected monocytes hastens dissemination to the CNS in mice (29). A different conclusion was reached by a recent study probing the potential for extracellular parasites present in the blood of infected mice to seed brain infections, which noted that adoptively transferred infected monocytes were readily detected in brain vasculature but not the parenchyma (30). In total, current data is inconsistent with a simple model where infected monocytes are the primary vehicle for parasites to cross the BBB.

Here we examine how infected monocytes migrate using *in vitro* models that mimic vascular *vs.* tissue environments. We found that infection inhibited monocyte transmigration across the BBB and peripheral endothelium, processes that require integrin-dependent adhesion. In contrast, infection enhanced monocyte migration through collagen-rich tissues, a distinct environment that also supports integrin-independent motility. The tissue migration of parasitized monocytes relied upon host Rho/ROCK signaling, and the secreted parasite kinase ROP17, which was required for efficient dissemination *in vivo*. Our findings suggest that *T. gondii* is unlikely to cross the BBB within monocytes serving as Trojan horses, but instead rapidly spreads within tissues to achieve systemic dissemination through activation of Rho-dependent interstitial tissue migration in infected monocytes.

Results

T. gondii infection impaired monocyte endothelial adherence and transmigration

We used hCMEC/D3 brain endothelial cells cultured on collagen-coated transwell inserts (155) to model transendothelial migration (TEM) across the BBB. Uninfected THP-1 monocytes exhibited time-dependent TEM across hCMEC/D3 monolayers, as well as enhanced migration in response to a chemotactic gradient of MCP-1 (Figure 3.1a). Strikingly, *T. gondii* pre-infection inhibited spontaneous and chemotaxis-driven TEM through hCMEC/D3 monolayers (Figure 3.1a). We extended these studies to primary monocytes from healthy human platelet donors. TEM of primary monocytes was inhibited by prior infection with *T. gondii*, at different time points (1 vs 4 h) and infection densities (MOI 1.5 vs 4) (Figure 3.1b). We further established that *T. gondii*-inhibition of TEM was observed with primary and immortalized endothelial cells derived from multiple tissue types, a hCMEC/D3-astrocyte co-culture BBB model, and parasite strains representing all major North American *T. gondii* lineages and a highly genetically divergent South American isolate (Supplementary Figure 3.1). Notably, the very low basal migration of monocytes through human umbilical vein endothelial cells (Supplementary Figure 3.1a) likely explains the failure of an earlier study to detect significant *T. gondii*-induced inhibition of TEM (108).

We hypothesized that the failure of parasitized monocytes to transmigrate may stem from defects in integrin-mediated adherence. To test this, we measured monocyte adherence to hCMEC/D3 monolayers. As expected, we found that pre-activation of the hCMEC/D3 with the inflammatory cytokines TNFα and IFNγ enhanced THP-1 monocyte adherence (Figure 3.1c). In contrast, infection with *T. gondii* markedly inhibited THP-1 monocyte adherence to both the resting and cytokine-activated hCMEC/D3 model BBB (Figure 3.1c). We next asked whether

this inhibition derived from defects in integrin-mediated adherence, through either affinity- or avidity-enhancing processes (156). We used total internal reflection fluorescence (TIRF) immunofluorescence microscopy to assess avidity-enhancing integrin mobilization in THP-1 monocytes adhering to fibronectin ligands. TIRF imaging revealed that *T. gondii*-infected monocytes fail to spread on fibronectin surfaces, forming both significantly smaller surface footprints and fewer detectable foci of the integrins LFA-1 and VLA-4 than mock-infected control monocytes (Figure 3.1d-h). We further used flow cytometry to establish that *T. gondii* infection did not alter surface expression of the integrins LFA-1 and VLA-4 in THP-1 monocytes or $MnCl_2$-induced integrin unfolding into high affinity conformations (Supplementary Figure 3.2). Collectively, these results suggest that defects in avidity-enhancing integrin mobilization likely lead to inefficient adherence of *T. gondii*-infected monocytes to our model BBB resulting in their subsequent failure to transmigrate through the endothelium.

Parasitized monocytes locomoted over BBB endothelium with an amoeboid morphology

We next asked if, despite their defects in integrin-mediated adherence, infected monocytes could effectively crawl on model BBB, as has been reported with HUVEC (108). To analyze migration, we cultured hCMEC/D3 cells on a soft polyacrylamide substrate previously demonstrated to enhance endothelial maturation (157), and observed the locomotion of THP-1 monocytes expressing the actin polymerization reporter F-tractin-eGFP with video microscopy (158). We found that infection with *T. gondii* enhanced THP-1 migration velocity and displacement across hCMEC/D3 cells (Figure 3.2a). Intriguingly, careful inspection of the videos revealed that the morphology of *T. gondii*-infected monocytes migrating on hCMEC/D3 cell monolayers markedly differed from mock-infected cells (Figure 3.2b-d, Supplementary Figure 3.3, Supplementary Videos 1-3). As expected for cells crawling on endothelium, mock-infected

monocytes moved by forming pointed pseudopodial structures at their leading edge that were enriched in F-actin (Figure 3.2b-d, red arrows). In contrast, *T. gondii*-infected monocytes rarely formed pseudopodial extensions. Instead, infected monocytes moved in an amoeboid manner, typified by a rounded and flowing morphology, and frequently produced spherical membrane protrusions (Supplementary Figure 3.2b, yellow arrows). A pronounced F-actin-rich leading edge was typically absent in migrating infected monocytes, and their membrane protrusions instead appeared to be stabilized by subsequent F-actin recruitment into membrane protrusions (Figure 3.2b,d), consistent with the established dynamics of bleb-based motility (159). To quantify these differences, we scored the number of structures consistent with pseudopodia (defined by pointed morphology) and blebs (defined by rounded morphology and delayed F-actin recruitment) formed by monocytes (Figure 3.2c-d). *T. gondii*-infected monocytes formed significantly fewer pseudopodia and more blebs than mock-infected control monocytes (Figure 3.2c-d).

In summary, although *T. gondii*-infected monocytes migrated efficiently over hCMEC/D3 endothelial cells, their morphology was strikingly inconsistent with canonical adhesion-based vascular crawling and instead reminiscent of reports of amoeboid or bleb-driven motility (122,159).

T. gondii infection enhanced monocyte migration through collagen-rich tissues

The amoeboid morphology of migrating parasitized monocytes led us to hypothesize that the parasite may be activating a mode of motility similar to that of integrin-independent leukocyte migration through tissue interstitium (122). To test this possibility, we used a simple migration assay (123) where cells are allowed to migrate through 3-D matrices of polymerized collagen I, the primary component of tissue interstitial space (160). We generated 3-D renderings

from Z-stack images of fluorescently-labeled THP-1 monocytes captured after migration into collagen I matrices (Figure 3.3a-b, top), and used automated cell identification to quantify the number of monocytes that penetrated into the matrix, and their relative vertical positions (Figure 3.3a-b, bottom). Infection increased the number of THP-1 monocytes that penetrated into collagen matrices and the distance they migrated (Figure 3.3a-d). Enhanced migration of infected THP-1 cells was observed whether 3-D migration was spontaneous or chemokinetically stimulated with MCP-1 chemokine (Figure 3.3c-d). Infection also enhanced the migration of primary human monocytes, RAW 264.7 macrophages, and murine bone marrow-derived macrophages in collagen I matrices (Supplementary Figure 3.4), confirming the robustness of this phenotype.

To better reflect the complex composition and architecture of tissue interstitial space, we next adapted a method previously used to analyze DC interstitial migration through *ex vivo* dermal ear sheets (122,161). Briefly, we labeled the vessels in the interstitial space of *ex vivo* murine ear dermis by laminin staining, and then collected time-lapse microscopy images of RAW 264.7 macrophages crawling within the dermis (Figure 3.3e-f). As in the collagen I matrices, infection stimulated macrophage migration within ear dermis, significantly increasing both the distanced traveled and velocity of migrating RAW macrophages (Figure 3.3g-h). Taken together, our results show that *T. gondii* infection enhances macrophage migration in collagen-rich tissue substrates.

Migration of infected cells relies upon host Rho/ROCK and parasite ROP17

Having determined that *T. gondii*-infected monocytes overwhelmingly fail to traverse endothelial barriers yet robustly migrate through collagen-rich tissues, we next sought to determine the mechanism by which infection specifically enhances tissue migration.

Monocytes and macrophages can migrate through 3-D substrates via amoeboid and mesenchymal modes with differing integrin-dependencies (121,138,139), and these different modes can be separated based on their sensitivity to specific inhibitors of actin-based motility. We used the compounds ML-141, NSC-23766, and Rhosin to respectively disrupt Cdc42, Rac, and Rho signaling (162) (Figure 3.4a), and found that only inhibition of Rho was disruptive to 3-D migration of parasitized THP-1 monocytes (Figure 3.4b). Consistent with a key role for Rho signaling, we further found that inhibition of the Rho effector ROCK by the compound Y-27632 significantly decreased the distance traveled by parasitized monocytes (Figure 3.4b). In contrast, we found that inhibition of the Rho effector PKC-α with the compound Gö 6976 (163) had a minimal effect on 3-D migration (Figure 3.4b). Rho/ROCK signaling often lead to motility via formin-mediated actin polymerization. Further supporting the relevance of Rho and ROCK in our system, we found that SMIFH2 inhibition of formins (164) had a significantly larger dampening effect on the migration of infected monocytes than CK-666 (165) inhibition of the actin-nucleator Arp2/3 (Figure 3.4b). The migration of infected RAW 264.7 macrophages was also blocked by Y-27632 inhibition of ROCK (Supplementary Figure 3.4e), suggesting a shared mechanism of enhanced migration in human monocytes and murine macrophages. Consistent with their inefficient endothelial adherence, infected cells migrate via an integrin-independent amoeboid mode that is highly reliant on Rho/ROCK signaling.

The ability of Rho inhibition to block migration of infected monocytes implies that *T. gondii* enhances motility by acting at or upstream of Rho. *T. gondii* secretes an array of effector proteins into host cells, several of which interfere with innate immunity(120,166). None of these effectors have been shown to target the host cytoskeleton, and the *T. gondii* genome does not encode any obvious analogs to Rho GEFs or GAPs (http://toxodb.org). However, the *T. gondii* kinases ROP17 and ROP18 phosphorylate the SWI region of immunity-related GTPases (IRGs) (167). As Rho GTPases also contain SWI regions (168), we hypothesized that perhaps they could also be targeted by ROP18 or ROP17 (167).

By infecting RAW 264.7 macrophages with *Δrop5*, *Δrop17*, and *Δrop18 T. gondii*, we determined that *rop17* is required for parasites to enhance penetration into and travel through collagen matrices (Figure 3.4c-d). Only *ROP17* was required for parasites to enhance macrophage migration, with *Δrop5 and Δrop18* parasites enhancing migration as effectively as wild-type parasites (Figure 3.4c-d). No synergy with ROP18 was evident, as *Δrop17Δrop18* parasites blocked migration no more effectively than *Δrop17* parasites (Figure 3.4c-d). ROP17 has been previously shown to perform kinase activity *in vitro* (167), but the necessity of its kinase activity for any of its proposed functions remains untested. The catalytic triad of ROP17 is conserved and easily identifiable (Figure 3.4e) (169). We generated parasites where *Δrop17* is complemented with either a cMYC-tagged wild-type *ROP17* allele, or one of two mutant alleles where disruption of the catalytic triad residues (K312A, D436A) should ablate kinase activity. $ROP17^{WT}$-cMYC, $ROP17^{K312A}$-cMYC, and $ROP17^{D436A}$-cMYC are all expressed at similar levels and accumulate as immature pro-proteins and a mature processed variant (Figure 3.4f). Complementation of *Δrop17* with *$ROP17^{WT}$-cMYC* restored collagen migration, while both

catalytic triad mutants phenocopied *Δrop17* (Figure 3.4g), demonstrating the necessity of ROP17 kinase activity for enhancing macrophage migration,

If ROP17 functions by activating Rho signaling, this could also lead to inhibition of Rac-dependent process such as endothelial adherence and transmigration via Rho-Rac crosstalk (170). Accordingly, we next tested if ROP17 is involved in parasite inhibition of monocyte adherence to our hCMEC/D3 model BBB. Parasites lacking *rop17* inhibited the adherence of THP-1 monocytes, although the observed decrease was significantly less dramatic than that caused by infection with wild-type *T. gondii (*Figure 3.4h). This result suggests that ROP17 contributes to the inhibition of monocyte endothelial adherence, but another parasite effector likely required for more complete suppression. In contrast, ROP17 appears essential for *T. gondii* to enhance migration through collagen-rich 3-D substrates.

ROP17 ablation slows parasite dissemination and eliminates enhanced tissue migration of infected monocytes in vivo

We then asked if ROP17-dependent enhancement of monocyte tissue migration alters parasite dissemination in an *in vivo* murine model. Mice were infected subcutaneously with luciferase-expressing *T. gondii* and intravital bioluminescence imaging was performed to assess parasite dissemination. In mice infected with knockout (i.e. *Δrop17::cLUC*) *vs*. complemented (i.e. *Δrop17::cLUC/ROP17-cMYC*) parasites, we found that ROP17-deficient parasites robustly amplified at the injection site but spread more slowly, resulting in a lower parasite burden compared to the complemented line as reflected by luminescence signal (Figure 3.5a-b). Although subtle, the reduced tissue dissemination seen with the *Δrop17* knockout led to a significant enhancement in mouse survival (Figure 3.5c).

ROP17 has been previously implicated as a minor partner in ROP18/ROP5-mediated defense of the parasitophorous vacuole from host IRGs (167). We accordingly asked whether the deficient spread and amplification of knockout *Δrop17::luc* parasites could derive from enhanced clearance of these mutants in macrophages. To test this, we infected mice intraperitoneally so that parasite dissemination would be aided by peritoneal flow into the systemic circulation, but a robust immune response including macrophage defense would still be encountered. In this system, we observed no consistent difference between knockout and complemented parasites, as assessed by either intravital imaging or mouse lethality (Figure 3.5d-f). We further established that *Δrop17::cLUC* parasites establish normal parasitophorous vacuoles and do not exhibit impaired growth in IFNγ/LPS-activated RAW 264.7 murine macrophages (Supplementary Figure 3.4). Collectively, these findings imply that the attenuation of *Δrop17::luc* parasites derives primarily from deficiencies in dissemination.

Finally, we used intravital two-photon imaging to examine whether ROP17 is critical for *T. gondii* to enhance monocyte tissue dissemination *in vivo*. We focused on the spleen as it is the major tissue reservoir of monocytes (171) and it is readily infected by *T. gondii* during natural infections (29). We found that wild-type *T. gondii* infection increased the migration of CX3CR1$^{GFP/+}$ monocytes significantly, enhancing their median track speed, mean square displacement, and median track straightness (Figure 3.6a-c, left). In contrast, *Δrop17* infection had no statistically significant effect on measured monocyte motility parameters (Figure 3.6a-c, right). Consistent with our observations of motility in the BBB model (Figure 3.2), infected monocytes migrated *in vivo* with a flowing amoeboid morphology suggestive of integrin-independent interstitial migration (Figure 3.6e-f). Our intravital imaging data strongly support

the model that ROP17-dependent enhancement of monocyte tissue migration promotes parasite dissemination through tissues *in vivo*.

Discussion

T. gondii parasites have been proposed to exploit the migration of leukocyte Trojan horses to gain access to the CNS, although compelling supporting data for this model is lacking. Here we show that *T. gondii* infection profoundly impaired monocyte transmigration across a model BBB *in vitro* and integrin-dependent adherence to endothelial ligands. In contrast, infection enhanced monocyte locomotion over endothelial surfaces and interstitial migration through 3-D tissues, both *in vitro* and *in vivo*. Enhanced tissue migration was driven by activation of a Rho/ROCK-mediated pathway typically associated with integrin-independent amoeboid interstitial migration. We further identified the secreted *T. gondii* kinase ROP17 as essential for *T. gondii* to activate monocyte tissue migration. By infecting mice with *rop17*-deficient *T. gondii*, we show that loss of parasite-enhanced monocyte tissue migration leads to slower parasite dissemination kinetics and prolonged mouse survival. In summary, we show that *T. gondii* dissemination is promoted by ROP17-dependent activation of interstitial tissue migration in infected monocytes, while integrin-dependent processes that lead to endothelial traversal are strongly inhibited.

Although integrins were once thought to be pivotal players in all forms of leukocyte migration, elegant genetic work in mice has established that integrin-independent migration is possible within tissues (122). When leukocytes interact with vasculature, integrins function as both adhesins that enable stable leukocyte adherence to endothelial ligands and as critical force-transducers that convert retrograde actin polymerization into forward movement (172). However, the 3-D environments of tissue interstitial space de-emphasize the importance of adhesion. In such tissue environments, low affinity interactions with the surrounding matrix and Rho/ROCK-driven actin-based contractility can propel leukocytes forward in the absence of any

contributions from integrins (122,172). Here we report that *T. gondii* infection of monocytes simultaneously inhibits integrin-dependent processes and activates Rho-dependent tissue motility. The overwhelming failure of infected monocytes to perform integrin-mediated adherence to or transmigration through endothelium suggests that infected monocytes are ill-suited to act as Trojan horses that deliver parasites across the BBB and into the CNS. Instead, we speculate that enhanced tissue migration could carry infected monocytes via lymphatic drainage into the circulation. Once in the circulation, parasites may egress from infected monocytes and directly invade brain endothelium (30), a process that could perhaps be aided by infected monocytes embolizing in small capillaries of the brain.

Our studies demonstrate that *T. gondii* programs monocytes to preferentially migrate through tissues in an amoeboid manner by using the secreted kinase ROP17 to activate Rho/ROCK- and formin-dependent processes. During natural infections, *T. gondii* first encounters and infects leukocytes in the intestinal lamina propria (28). Our findings predict that the parasite may activate the tissue migration of infected lamina propria monocytes in order to rapidly escape this compartment. We focused on monocyte and macrophage motility due to the abundance of infected monocytes in the blood (29). However, *T. gondii* can also alter DC motility (96,97,153,154), and DCs are infected in the lamina propria, although again to a lesser extent than monocytes and macrophages (28). The specific subsets of leukocytes that are the primary target(s) of ROP17-mediated enhanced tissue migration *in vivo* remains a question for further study. Consistent with a role in dissemination, we showed that *T. gondii* infection enhanced *in vivo* migration of CX_3CR1^+ monocytes in the spleen, and that loss of ROP17-dependent enhanced monocyte tissue migration delayed the dissemination of hypervirulent type I *T. gondii* parasites. Similarly, *ROP17* ablation was reported to cause a near complete loss of

brain cyst formation in a cyst-competent type II *T. gondii* lineage (173), likely as a consequence of reduced dissemination.

Our findings establish that catalytic activity of the secreted serine/threonine kinase ROP17 is required for *T. gondii* to enhance monocyte tissue migration. Prior work theorized that ROP17 forms a complex with the kinase ROP18 and regulatory pseudokinase ROP5, and synergizes with these partners to ensure parasite survival within activated macrophages by phosphorylating IRGs (167). In stark contrast to this IRG defense system, we found that when enhancing monocyte migration, ROP17 functions completely independently of ROP5 and ROP18. We presume that ROP17 enhances tissue migration by phosphorylating an unknown, non-IRG target. We previously showed that ROP17 exhibits a strong preference for threonine phosphorylation and slight preference for surrounding hydrophobic residues (167). Although kinase targets cannot be easily predicted from substrate preference motifs, RhoA GTPase, Rho GEFs VAV and GEF-H1, Rho GAP DLC1, and Rho GDI1 can all be phosphoregulated (174), and are thus candidate substrates through which ROP17 could activate Rho-driven amoeboid migration. Future elucidation of ROP17 substrates may provide exciting insights into both *T. gondii* dissemination and the currently completely unknown mechanisms that prompt leukocytes to adopt integrin-independent migratory strategies *in vivo*.

Materials and methods

Parasite culture

T. gondii parasites were propagated in human foreskin fibroblasts (HFF) obtained from the laboratory of John Boothroyd at Stanford University. Type II ME49 mCherry parasites were used throughout Figures 1-3 unless otherwise indicated. All studies with ROP17 were performed in a Type I RH *Δku80 Δhxpgrt* background. Source and generation details for all *T. gondii* strains used are described in Supplementary Table 3.1.

Primary human monocytes

Primary human monocytes were obtained by flushing human peripheral blood from leukoreduction (LRS) chambers provided by the Washington University School of Medicine apheresis center, and then isolating monocytes via negative immunodensity selection with a RosetteSep Human Monocyte Enrichment Cocktail (Stem Cell Tech) and Ficoll-Paque sedimentation. To confirm successful isolation of monocytes, cells were analyzed for CD33 and CD14 positivity by flow cytometry. Monocytes were cryopreserved immediately after harvest in 7.5% DMSO and 10% human serum. Upon thaw, primary monocytes were cultured in RPMI supplemented with 10% human serum, 1% non-essential amino acids, 10 mM HEPES, and 100U/mL penicillin-1 µg/mL streptomycin.

Culture of primary human cells

Primary human aortic endothelial cells (HAEC) at passage 3 were obtained from Lonza and cultured in fully-supplemented EGM-2 media (Lonza). HAEC from passages five to seven were used in experiments. Primary human astrocytes were acquired from ScienCell and cultured in Astrocyte Media (ScienCell) in flasks coated with 2 µg/cm^2 collagen. Upon receipt, astrocytes were cryopreserved at passage 1. Thawed aliquots at passage 3 or 4 were used for experiments.

Bone marrow-derived macrophages

Bone marrow-derived macrophages (BMDM) were harvested from the femurs of C57/BL6 mice with standard protocols, matured in BMDM Harvest Media (DMEM, 10% FBS, 5% horse serum, 40 µM L-glutamine, 100 µg/mL gentamicin, 20% L929-conditioned media), and maintained in BMDM Maintenance Media (DMEM, 10% FBS, 5% horse serum, 40 µM L-glutamine, 100 µg/mL gentamicin, 10% L929-conditioned media).

Culture of cell lines

The human brain endothelial cell line hCMEC/D3(175) was obtained from the laboratory of Robyn Klein at Washington University and grown as previously described(155) from passages 28 to 34. THP-1 monocytes were cultured in RPMI media supplemented with 10% FBS. RAW 264.7 macrophages were cultured in DMEM media supplemented with 10% FBS. HUVEC EA.hy926 cells were obtained from ATCC and cultured in DMEM supplemented with 10% FBS.

All lines were confirmed as mycoplasma-negative with the e-Myco plus mycoplasma PCR detection kit (Boca Scientific) upon acquisition.

Growth of hCMEC/D3 on polyacrylamide pads

To provide a soft substrate for cell growth, 0.4% polyacrylamide pads were prepared in glass-bottom dishes as previously described(157), and then coated with 150 µg/mL rat collagen I. Dishes were each seeded with $5x10^4$ hCMEC/D3 and grown until confluence.

Microscopy

In vitro imaging studies were performed on a Axio Observer Z1 inverted microscope (Zeiss) that features modules for conventional fluorescence, spinning disk confocal, and total internal reflection fluoresecence (TIRF) microscopy. Conventional fluorescence images were acquired with illumination from a Colibri LED light source (Zeiss) and ORCA-ER digital

camera (Hammamatsu Photonics, Japan). Spinning disk and TIRF images were acquired using illumination from 488 nm and 561 nm solid state lasers (Zeiss) and Evolve 512 Delta EMCCD cameras (Photometrics). For all modules, Zen software (Zeiss) was used for image acquisition.

Time-lapse imaging of monocyte crawling on hCMEC/D3 endothelium

To quantify crawling, THP-1 monocytes were labeled with CellTrace Oregon Green 488 Carboxy-DFFDA (ThermoFisher), resuspended in Migration RPMI [phenol-red free RPMI supplemented with 3% FBS, 1% non-essential amino acids (Gibco), and 10 mM HEPES] and then infected with freshly-harvested *T. gondii* at an MOI of ~ 4.5 for 3-6 h. Just prior to imaging, the hCMEC/D3 dishes were changed to Migration RPMI and then equilibrated for ten min at 37°C in the incubation chamber of an inverted microscope. Alternating conventional bright-field and fluorescent images were captured at 1 min intervals over a 45-min period, using the above-described spinning disk microscopy system with a 40x C-Apochromat water immersion objective (N.A. 1.20). Automated tracking of individual monocytes' centroids was performed using *Volocity* software (PerkinElmer). To follow actin polymerization dynamics, cells were transfected with F-Tractin-eGFP one day prior to imaging crawling on soft substrate-supported hCMEC/D3. Actin polymerization videos were collected with the above spinning disc imaging system, using five-sec intervals over 5-min periods. Structures consistent with pseudopodia or blebs were manually counted**.**

Animals

All protocols requiring animals were approved by the Institutional Animal Care and Use Committee at the Washington University in St Louis School of Medicine. Mice were housed in Association for Assessment and Accreditation of Laboratory Animal Care International-approved facilities at Washington University. CX3CR1$^{GFP/+}$ mice were obtained from Jackson

Laboratory or as generous gifts from Gwen Randolph (Washington University). CD1 mice were purchased from Charles River Lab.

Intravital Two-Photon Imaging

Heterozygous CX3CR1$^{GFP/+}$ mice were infected with 2-4x10^{7} Cell Tracker Red CMPTX-labeled *T. gondii* via tail vein injection. Time-lapse imaging was performed with a custom built 2P microscope(176,177) equipped with a Chameleon Vision II Ti:Sapphire laser (Coherent) and a 1.0 NA 20x water dipping objective (Olympus). SlideBook software (Intelligent Imaging Solutions) was used to control laser scanning, image acquisition and z-step movements. *In vivo* imaging of the spleen used a custom imaging chamber built in house(176). Mice were anesthetized with 1.5% isoflurane in carbogen carrier gas and body temperature was maintained with a warming plate. The skin was cut away over the spleen and a small incision made in the peritoneal membrane to access the spleen. The spleen was lifted gently with forceps and a small portion secured to thin plastic support with VetBond adhesive. The upper chamber plate was lowered on to the tissue until contact was made with the coverslip and then the upper chamber filled with water for imaging. The plastic support was then clipped to the upper chamber plate with a hair pin to dampen movement artifacts. Small electrical heaters (resisters) attached to both the upper and lower chamber plates were used to prevent the mouse from becoming hypothermic. After the imaging preparation was completed and prior to imaging, the spleen was examined under the microscope to confirm that blood flow was robust in sinuses and blood vessels. CX3CR1-GFP cell migration was analyzed using 3D time-lapse imaging for up to 30min. Florescence was excited at 980nm and fluorescence emission detected by PMTs simultaneously using 495nm and 560nm dichroic filters: Blue (<495nm, SHG collagen), green (495-560nm, eGFP) and red (>560nm, CMTPX-Toxo). Auto fluorescence appears as mix of

color (495-600nm) and thus can be discriminated from eGFP, and CMTPX. For time-lapse imaging, we acquired a 500x500x60µm volume as 31 sequential 2 µm z-steps with a time resolution of approximately 25s per time point and a X,Y resolution of 0.585 µm /pixel. Intravital imaging focused on the red pulp at <100 µm below the surface. Multi-dimensional data sets were exported as TIFFs and rendered in 3D using Imaris (Bitplane). Cell tracking and data analysis were performed using Imaris (Bitplane) and Motility Lab (2ptrack.net). CX3CR1+ cells were identified by GFP signal and tracked in 3-D with an automated Imaris protocol. Macrophages were manually excluded on the basis of morphology, and infected monocytes manually identified by signal from the Cell Tracker Red dye. To assess track speed and mean square displacement, infected monocytes were compared to all unambiguously uninfected monocytes with verified accurate tracks from the same videos (RH-infected, N=34; *Δrop17*-infected, N=41; uninfected, N>200). Straightness was assessed in only subsets of each population chosen to have similar track durations (RH-infected monocytes, 74%, RH-uninfected monocytes-42%, *Δrop17*-infected monocytes-95%, *Δrop17*-uninfected monocytes-66%).

In vivo infections and intravital luminescence imaging

8-10 week-old female CD1 mice were challenged intraperitoneally or subcutaneously in the right rear flank with 200 parasites. Luminescence imaging was performed on mice anesthetized with 2% isoflurane and injected intraperitoneally with D-luciferin (Biosynth AG) (150mg/kg) with a Xenogen IVIS200 machine. Luminescence data was analyzed with Xenogen Living Image software (Caliper Life Sciences).

Generation of transgenic monocytes and macrophages

THP-1 monocytes were transfected using the Amaxa 4D Nucleofection system (Lonza) and cell line SG kit. For each transfection, 1 µg of plasmid DNA prepared with a PureLink

HiPure Plasmid Midiprep Kit (Invitrogen) was used with $2x10^6$ THP-1 monocytes. RAW 264.7 macrophages were transfected using Lipofectamine LTX with PLUS Reagent (Thermofisher) and 7 µg DNA per plasmid, prepared with a NucleoBond Xtra Midi EF kit (Macherey-Nagel). To generate a stable GFP-expressing line of RAW 264.7 macrophages, we introduced the plasmids pSB-100 and pSB-Bi-GP, followed by selection with 5 µg/mL puromycin and maintenance in 2.5 µg/mL puromycin (178).

Static adherence of monocytes to hCMEC/D3

Optical grade black 96-well plates were seeded with $1x10^5$ hCMEC/D3 cells per well and grown to confluence. The day prior to the adherence assay, hCMEC/D3 were activated overnight with IFNγ (200 U/mL) and TNFα (200 U/mL) as indicated. THP-1 monocytes were labeled with Cell Trace CFSE (Invitrogen), and then infected with *T. gondii* at an MOI of ~4.5. After four h of infection, $10x10^5$ monocytes per well were transferred to the pre-activated hCMEC/D3 and allowed to adhere for 30 min at 37°C. Non-adherent monocytes were then removed by vigorous rinsing, and the remaining adherent monocytes were fixed with 4% formaldehyde. Samples were imaged with a Cytation 3 imager (Biotek), using automated cell finding from CFSE fluorescence to locate focal planes. Approximately 80% of the well bottom was imaged, and Gen5 software (Biotek) then used to quantify the number of adherent monocytes. Three independent experiments were performed; each with 5-6 technical replicates per condition.

Integrin staining and TIRF microscopy

THP-1 monocytes were pre-infected *T. gondii* for 4 h (MOI=4) and then allowed to adhere onto 50 µg/mL fibronectin-coated glass coverslip dishes (MatTek) for 30 min. Samples were then gently rinsed with PBS and fixed for 10 min with ice-cold 4% formaldehyde in PBS. Cells were permeabilized with 0.05% saponin and stained with monoclonal antibodies to LFA-1

(TS2/4) or VLA-4 (9F10), followed by Alexa fluorophore-conjugated secondary antibodies. Samples were imaged in PBS with the earlier-described TIRF microscopy system and a 100x oil Plan-Apochromat (N.A. 1.46) objective. Tandem Z-stack series of the same cells were captured with the earlier-described spinning disc system to visualize cells as infected or uninfected. TIRF images were analyzed in *Volocity* software. Cell outlines were manually traced, and integrin foci were identified using the *Volocity* Spot Finder function.

Transendothelial migration assays

Transendothelial migration (TEM) was quantified by allowing CFSE-labeled monocytes to cross *in vitro* barriers of endothelial cells grown on 24-well format Falcon transwell permeable supports with PET membranes and 8-micron pores. To create a flat surface for automated imaging, 15 mm coverslips coated with 0.1% gelatin were placed in the basal chambers. After allowing for transmigration, transwell inserts were removed and basal chambers were fixed with 0.4% formaldehyde. Rectangular grids covering about 90% of the basal chambers were then imaged in medium-throughput format using a Cytation 3 (Biotek) plate imager with 10x objective. Gen5 software (Biotek) was used to quantify the number of monocytes in each basal chamber, as defined by size and fluorescence signal. Where indicated, chemotactic gradients were generated by adding 100 ng/mL MCP-1 chemokine (Peprotech) to basal transwell chambers. The hCMEC/D3 cell line was seeded onto transwell membranes pre-coated with 150 µg/mL rat collagen I, using 4-5x10^5 cells/cm^2 and grown 5-7 days prior to TEM assays. Barrier integrity was confirmed by measuring TEER with an EVOM2 Voltohmmeter (World Precision Instruments). At the time of TEM assays, hCMEC/D3 cells typically achieved a TEER of 50-70 ohms/cm^2.

HAEC and HUVEC EA.hy926 were seeded 10 µg/mL fibronectin-coated transwell membranes using 0.5-1x10^5 cells/cm^2 and cultured for two days to generate a robust barrier. Barrier integrity was confirmed by measuring transendothelial electrical resistance (TEER) with an EVOM2 Voltohmmeter (World Precision Instruments). At the time of TEM assays, HAEC cells typically achieved a TEER pf 40-50 ohms/cm^2 and HUVEC a TEER of 80-120 ohms/cm^2.

Three-dimensional collagen migration assays

Collagen matrices were prepared from Nutragen Type I Bovine Collagen (Advanced BioMatrix) in 1X MEM Eagle supplemented with 7.5% sodium bicarbonate (pH 9) in optical-grade black 96-well plates. Matrices were allowed to polymerize at 37°C for 60 min to overnight, and then equilibrated ≥ 60 min in monocyte growth media supplemented with 3% serum. In each well, 5x10^4 monocytes or macrophages pre-labeled with Cell Trace CFSE (Invitrogen) and pre-infected with *T. gondii* (THP-1: MOI 4.5 with ME49 mCherry, 4 h; RAW 264.7: MOI 3 with ME49 mCherry) were allowed to migrate into the matrix. After overnight migration at 37°C and 5% CO_2, the samples were rinsed with PBS and fixed with 4% formaldehyde. Z-stack image series of the monocytes captured within the collagen matrices were captured with the above-described spinning disk microscopy system and an EC Plan-Neofluar 10x (N.A. 0.30) objective. *Volocity* software was used to generate 3-D renderings of the Z-stacks and locate each monocyte using an automated Object Finding protocol based on fluorescence intensity and cell size. Vertical distance migrated was calculated as the distance between the centroid of the cell with the highest Z-position and every other cell.

Harvest of ex vivo dermal ear tissue and video microscopy of macrophage migration

Ventral ear sheets were harvested from 7-8 week old female BALB/C mice (Charles River Lab) and stained for laminin (Sigma Aldrich) with AlexaFluor555-conjugated secondary

antibody as previously described(161). GFP-expressing RAW macrophages were pre-infected for 3-5 h with ME49 mCherry parasites or IC buffer control, and then harvested by gentle scraping. Infected and uninfected macrophages were mixed together and given 20 min to crawl into the dorsal side of an ear sheet. Ear sheets were then rinsed and imaged dorsal side-down in a temperature (37°C) and CO_2 (5%)-controlled chamber and the inverted spinning disc microscope with a 20x EC Plan-Neofluar objective (N.A. 0.50). Videos were collected for 2 h at 3 min intervals, each with Z-stacks spanning 50-80 micron in 5-micron increments. *Zen* (Zeiss) software was used to correct drift with the Time Alignment function and deconvolve images with a regularized inverse filter. A *Volocity* automated protocol was used to track all macrophages. Every macrophage track was manually examined to confirm track accuracy and infection status.

Flow cytometry analysis of integrin expression and activation

THP-1 monocytes were infected with *T. gondii* at an MOI of ~4.5 for 3 h, or IC buffer in equivalent volume. Monocytes were then pelleted and resuspended in Integrin Activation Buffer (IAB) (Hanks's Balanced Salt Solution, 1 mM Ca^{2+}, 1 mM Mg^{2+}, 20 mM HEPES, 0.5% FBS pH 7.4) and equilibrated at 37°C for 60 min. To activate integrins, monocytes were treated with 9 mM $MnCl_2$ for 5 min at 37°C, then immediately transferred to ice. Live cells were stained for integrin expression with primary monoclonal antibodies: activated LFA-1, mAb24 (Abcam); activated VLA-4, mAb 12G10 (Abcam); LFA-1, mAb TS2/4 (Biolegend); VLA-4, mAb 9F10 (Biolegend), and Alexa-488-conjugated anti-mouse-IgG secondary antibody for detection. After staining, cells were fixed with ice-cold 4% formaldehyde and stored at 4°C in PBS prior to analysis with a BD-FacsCanto. Forward and side scatter gating was used to separate monocytes from debris and extracellular parasites.

Parasite growth in activated macrophages

RAW 264.7 macrophages were activated for 18 h with mouse IFNγ (10 U/mL) and LPS (1 ng/mL), then infected with *T. gondii*. After 24 h, cells were fixed and parasites stained with anti-DG52 antibody. The number of parasitophorous vacuoles present in five fields per technical replicate was counted.

Parasitophorous vacuole staining

RAW 264.7 macrophages were infected with *T. gondii*. After fixation and permeabilization with 0.05% saponin, cells were stained with anti-GRA7 (179).

Statistical Analysis

Data-sets were analyzed in *Prism 7* (Graphpad). Normally distributed data were analyzed with one-way ANOVA and Holm-Sidak's multiple comparison's test. Non-normally distributed data were analyzed with Kruskal-Wallis Test and Dunn's multiple comparison's test. Whenever applicable, two-tailed *P*-values were calculated and corrected for multiple comparisons. Two-photon data was analyzed in Motility Lab (http://2ptrack.net/) using two-tailed Wilcoxon's tests to assess significance.

Acknowledgements

Thanks to Mike Onken and John Cooper for constructive comments, Robyn Klein and Tamara Doering for sharing hCMEC/D3 cells, Todd Fehniger for facilitating the acquisition of primary human monocytes, Felipe Santiago and Hamid Salimi for advice regarding the BBB model, Quiling Wang for assistance with mouse infections, Seonyoung Kim, Lihua Yang and the Washington University School of Medicine In vivo Imaging Core for technical support and fluorescent reporter mice for the intravital imaging experiments and Gwen Randolph for generously sharing CX3CR1$^{GFP/+}$ mice. Work was supported in part by grants from the National Science Foundation to LLD (DGE-1143954), and National Institute of Health to MJM (R01AI077600) and LDS (AI034036). The authors declare no competing financial interests.

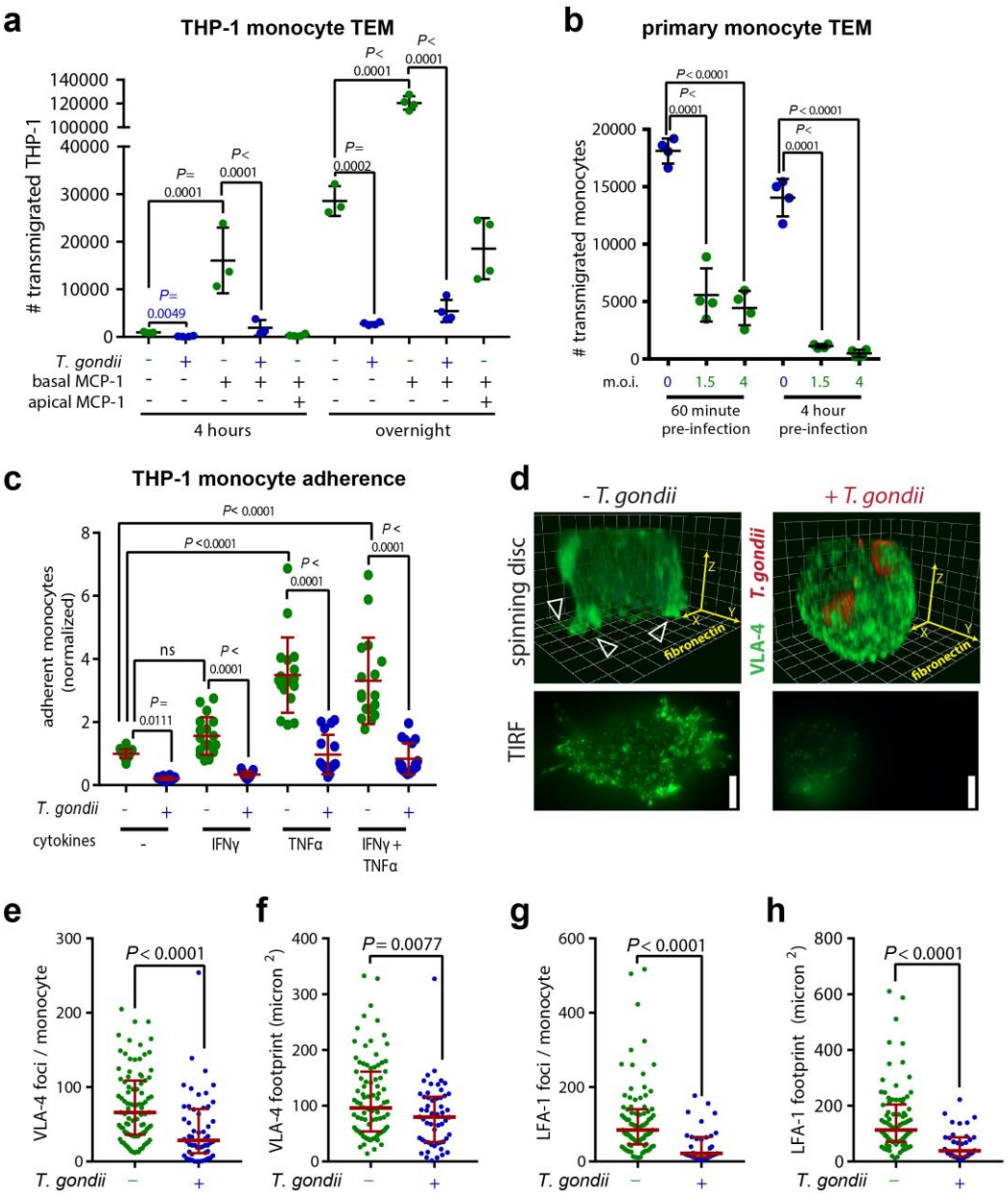

Figure 3.1: Transendothelial migration and adherence of infected monocytes.

(a-b) Transmigration of THP-1 (a) and primary human monocytes (b) through a hCMEC/D3 blood-brain barrier model. MCP-1 chemokine was added at 100 ng/mL to transwell chambers as indicated. Prior to transmigration, monocytes were pre-infected with ME49-mCherry *T. gondii*. Data is shown from one experiment representative of three independent experiments with the

same outcome. Each symbol indicates an individual technical replicate (N=3-4/experiment). Lines and error bars denote mean ± SD. Multiplicity-adjusted *P* -values from one-way ANOVA and Holm-Sidak's multiple comparison tests are shown in black (NS, $P > 0.05$); *P* -values from unpaired t-tests are shown in blue. **(c)** Number of THP-1 monocytes adhered to hCMEC/D3 endothelial cell monolayers. Data derived from three independent experiments, each with 5-6 technical replicates. All quantities were normalized to the mean number of uninfected monocytes adhering to non-activated hCMEC/D3. Error bars indicate mean ± SEM. Multiplicity-adjusted *P*-values from Holm-Sidak's multiple comparisons tests are shown (NS, $P > 0.05$). **(d-h)** Monocytes adhering to fibronectin-coated glass were stained with antibodies to VLA-4 (mAb 9F10) and LFA-1 (mAb TS2/4). (**d**) (top) Three-dimensional renderings from spinning disc confocal imaging (top) of VLA-4-stained mock- (left) and *T. gondii*-infected (right) THP-1 monocytes, and (bottom) sample TIRF microscopy images of the same cells. White arrowheads indicate spreading protrusions on the fibronectin surface. Scale bars = 5 micron. (**e-h**) Quantification of the number of TIRF-detectable integrin foci (**e,g**) per monocyte, and total integrin-contact-containing surface area occupied by individual monocytes (**f,h**). Each data point shows an individual monocyte. Data were pooled from three independent experiments. Two-tailed *P* -values from unpaired Mann-Whitney tests are shown.

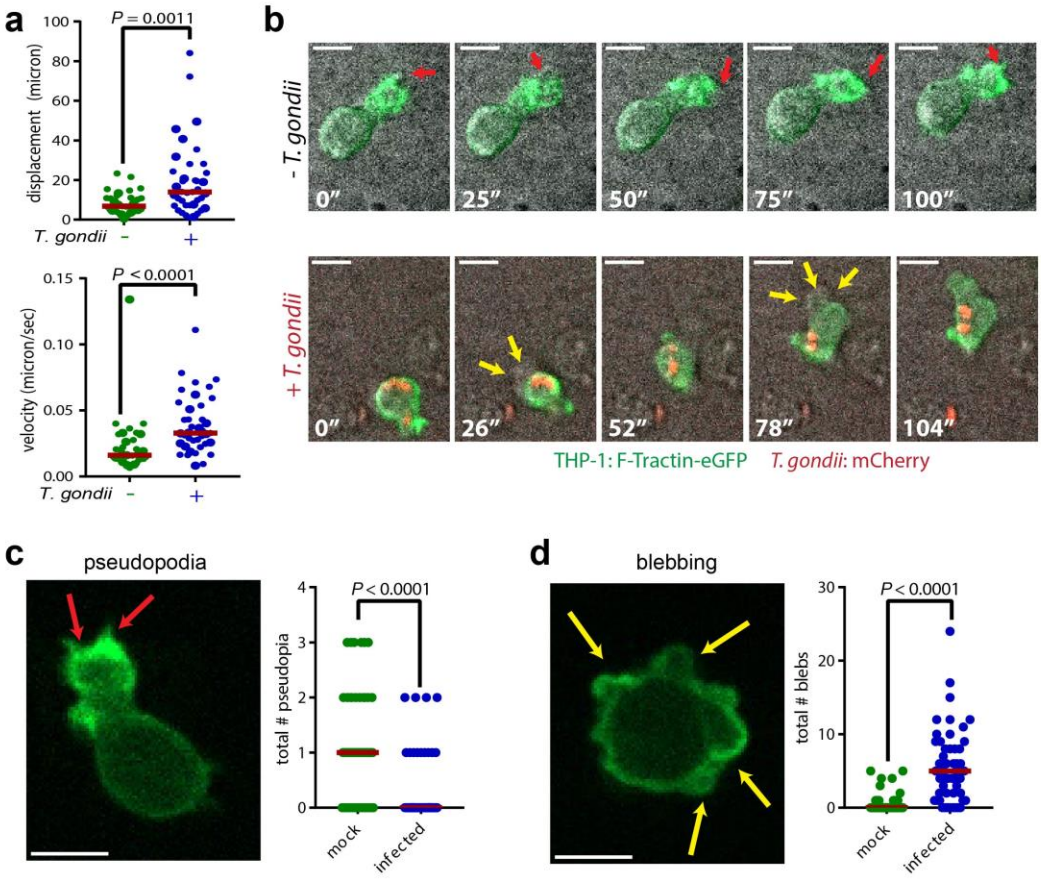

Figure 3.2: Locomotion of infected monocytes on model BBB.

(a) Displacement (top) and mean velocity (bottom) of THP-1 monocytes moving over hCMEC/D3 endothelial monolayers, as quantified from 45 min time-lapse microscopy videos. Data from three independent experiments were pooled (N= 8, 10, and 15 examples for mock-infected THP-1 monocytes; N= 12, 12, and 15 examples for infected). (b) Time lapse images of crawling mock- (top) and T. gondii-infected (bottom) THP-1 monocytes expressing F-Tractin-eGFP. Red arrows indicate F-actin-rich pseudopodia. Yellow arrows indicate membrane swellings not enriched for F-actin. Images correspond to Supplementary Videos 1-2. (c-d) The number of structures consistent with pseudopodia (c) and blebs (d) formed by THP-1 monocytes during five min periods on hCMEC/D3. Images show representative pseudopodia (red arrows)

and blebs (yellow arrows) and correspond to Supplemental Videos 1 and 3. Data from three independent experiments were pooled. (a-d) Data points denote individual monocytes, and lines median values. Two-tailed P-values from unpaired Mann Whitney tests are shown. All images show 10-micron scale bars and time in sec.

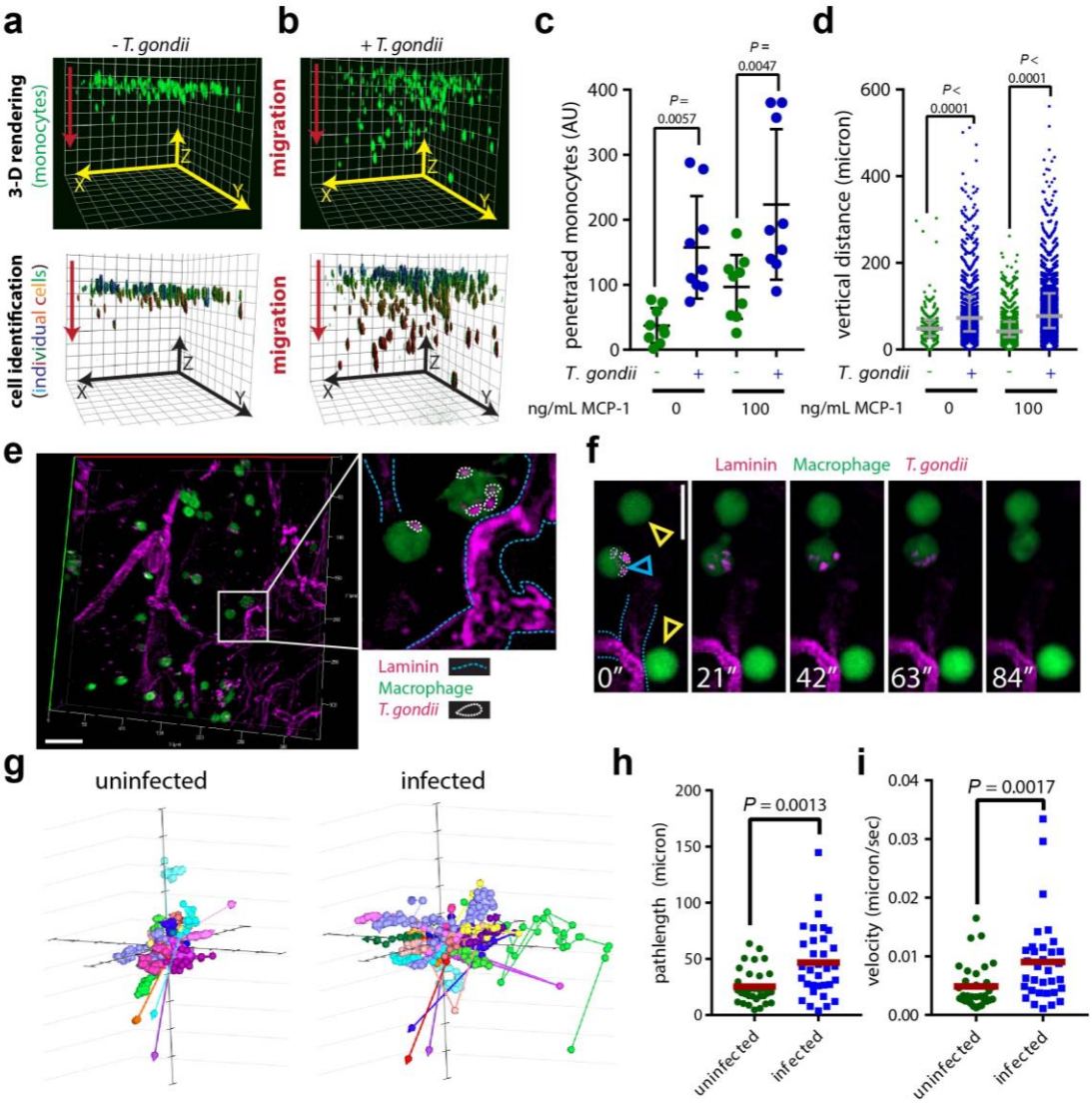

Figure 3.3: Migration of infected monocytes through 3D collagen-matrices and skin tissue. **(a-b)** Schematic of collagen matrix assay with mock- (a) and infected (b) THP-1 monocytes. Top images show three-dimensional renderings created from spinning disk confocal images of fluorescently-labeled monocytes captured within collagen matrices. Red arrows indicate the direction of migration. Bottom images show individual monocytes located with an automated protocol. **(c-d)** After overnight migration, the absolute number of penetrant monocytes (**c**) and vertical distance from each monocyte relative to the matrix top (**d**) was quantified for a single Z-stack running through the center of each matrix. Plots show pooled data from three independent

experiments, each with three technical replicates. The number of penetrant monocytes was analyzed with one-way ANOVA and Holm-Sidak's multiple comparison post-test and plotted as means ± SD. Distance migrated was not normally distributed and accordingly analyzed with a Kruskal-Wallis test and Dunn's multiple comparison post-test and plotted with medians and interquartile ranges. Multiplicity-adjusted *P* -values are shown. **(e)** 3-D rendering of dermal ear sheet. Vessels (red) were stained for laminin. Macrophages were visualized by GFP, and *T. gondii* by mCherry. Scale bar = 50 micron. Inset shows vessels traced in blue and intracellular parasites in white. **(f)** Time-lapse series showing an infected macrophage migrating through ear dermis, with vessels traced in blue and intracellular parasites in white on first image. Blue arrowhead indicates infected macrophage. Yellow arrowheads indicate uninfected macrophages. Scale bar 20 micron. **(g-h)** The trajectories of individual macrophages through ear dermis tracked over a 2 h period. Displacement plots of uninfected (left) and infected (right) macrophages **(g)**. The total pathlength traveled (**h**) and average velocity (**i**) for each monocyte in the displacement plots, with lines indicating mean values. Data was pooled from three independent experiments (N=33 for both uninfected and infected monocytes) and analyzed using Mann-Whitney tests.

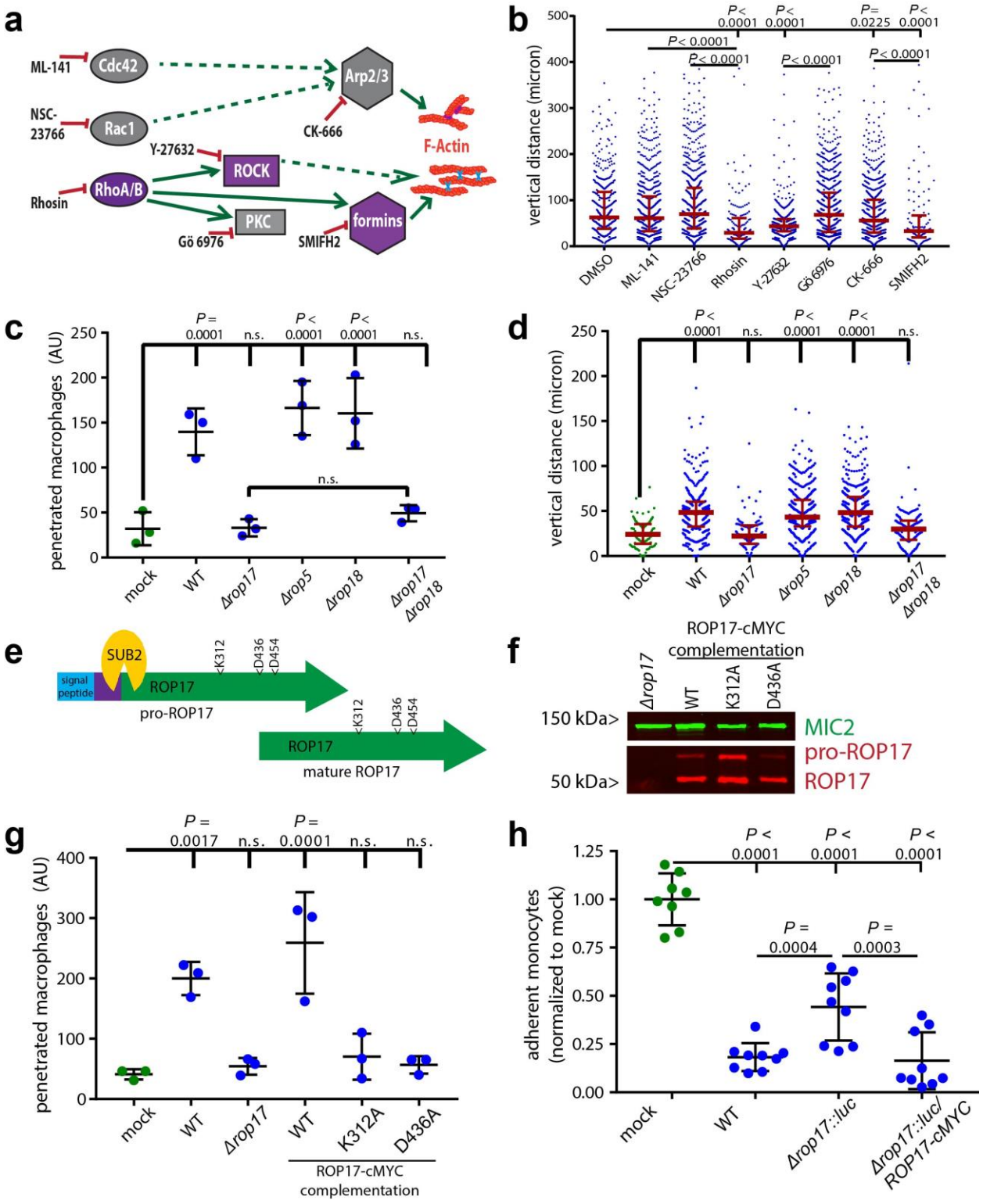

Figure 3.4: Role of Rho/ROCK and ROP17 in enhanced tissue migration.

(a) Schematic of Rho GTPase signaling and inhibitors **(b)** Vertical distance migrated by *T. gondii*-infected THP-1 monocytes into a 0.8 mg/mL collagen I matrix loaded with 100 ng/mL MCP-1 chemokine, during treatment with inhibitors schematized in (a) (10 µM ML-141, 100 µM NSC-23766, 100 µM Rhosin, 30 µM Y-27632, 1 µM Gö 6976, 100 µM CK-666, 30 µM SMIFH2). Plot shows data from one experiment that is representative of three independent experiments with the same outcome, each with three technical replicates. Median values and interquartile ranges are indicated in red. **(c-d)** Migration of RAW 264.7 macrophages in 2 mg/mL collagen matrices after pre-infection with *T. gondii* of indicated genotype (**c**- number penetrated macrophages, **d**- distance traveled). Plots show data from one experiment representative of three independent assays, each with the same outcome and three technical replicates. Black lines and error bars indicate mean ± SD (c), and red median and interquartile ranges (d) **(e)** Schematic of ROP17 protein with catalytic triad residues and putative SUB2 processing site indicated. **(f)** Western blot of *Δrop17* parasites expressing complementation constructs *ROP17*^{WT}*-cMYC*, *ROP17*^{D436A}*-cMYC*, and *ROP17*^{K312A}*-cMYC*, probed with antibodies against cMYC and *T. gondii* MIC2. **(g)** Number of RAW macrophages migrated into a 2 mg/mL collagen matrix after pre-infection with *T. gondii* of indicated genotype. Data is shown from one experiment representative of three independent assays all with the same outcome. Lines indicate mean, and errors bars SD. **(h)** Adherence of THP-1 monocytes to IFNγ/TNFα- (200U/mL) stimulated hCMEC/D3 endothelial monolayers following pre-infection with *T. gondii* of indicated genotype. Pooled data from three independent assays is shown, with figures normalized to the mean number of adherent mock-infected monocytes in each experiment. Lines indicate mean, and errors bars SD. Statistical significance was assessed with one-way ANOVA and Holm-Sidak's multiple comparison test for normally-distributed data (**c**, **g**, **h**), and Kruskal-

Wallis test and Dunn's multiple comparisons test for non-normal distributions (**b**,**d**).

Multiplicity-adjusted *P* values are shown (n.s., $P > 0.05$).

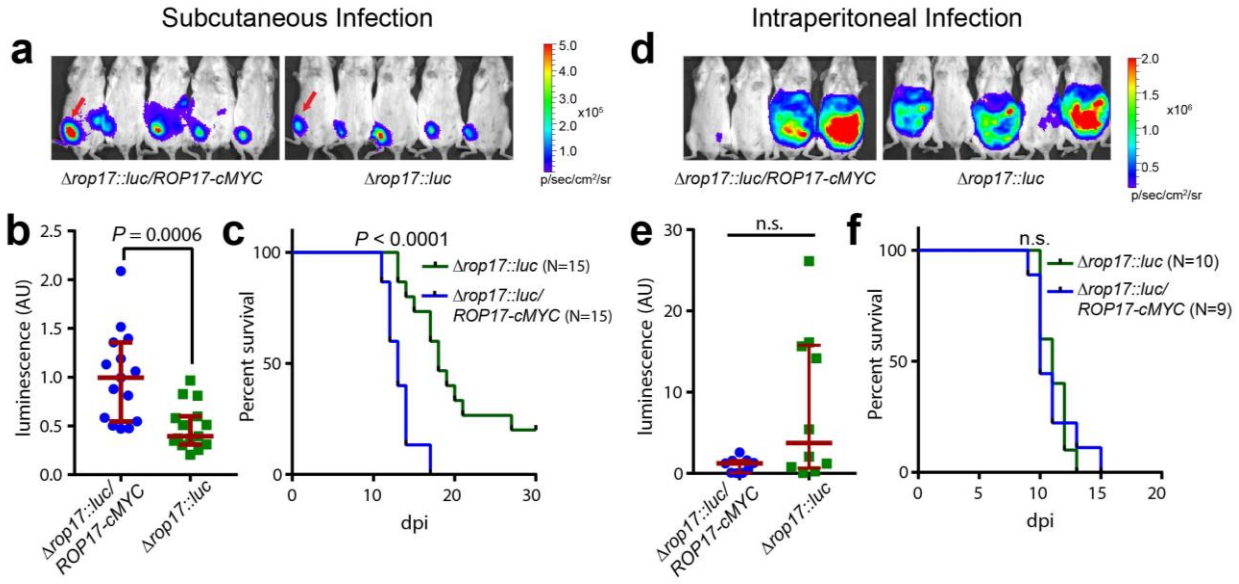

Figure 3.5: Role of ROP17 during *in vivo* infection.

(a-f) Female CD1 mice were infected subcutaneously (**a-c**) or intraperitoneally (**d-f**) with 200 *T. gondii* of indicated genotype. Parasite burden and spread were monitored by intravital luminescence imaging prior to fatality (**a-b**, subcutaneous- 8 days post-infection (dpi); **d-e**, intraperitoneal- 6 dpi), and survival monitored daily (**c,f**). Pooled data from three independent subcutaneous infections (5 mice/group) and two independent intraperitoneal infections (4-5 mice/group) are shown as total normalized luminescence signal in individual mice (**b,e**) and survival curves (**c,f**). Luminescence data was analyzed by Mann-Whitney test, and mouse survival by Gehan-Breslow-Wilcoxon test (n.s., $P > 0.05$).

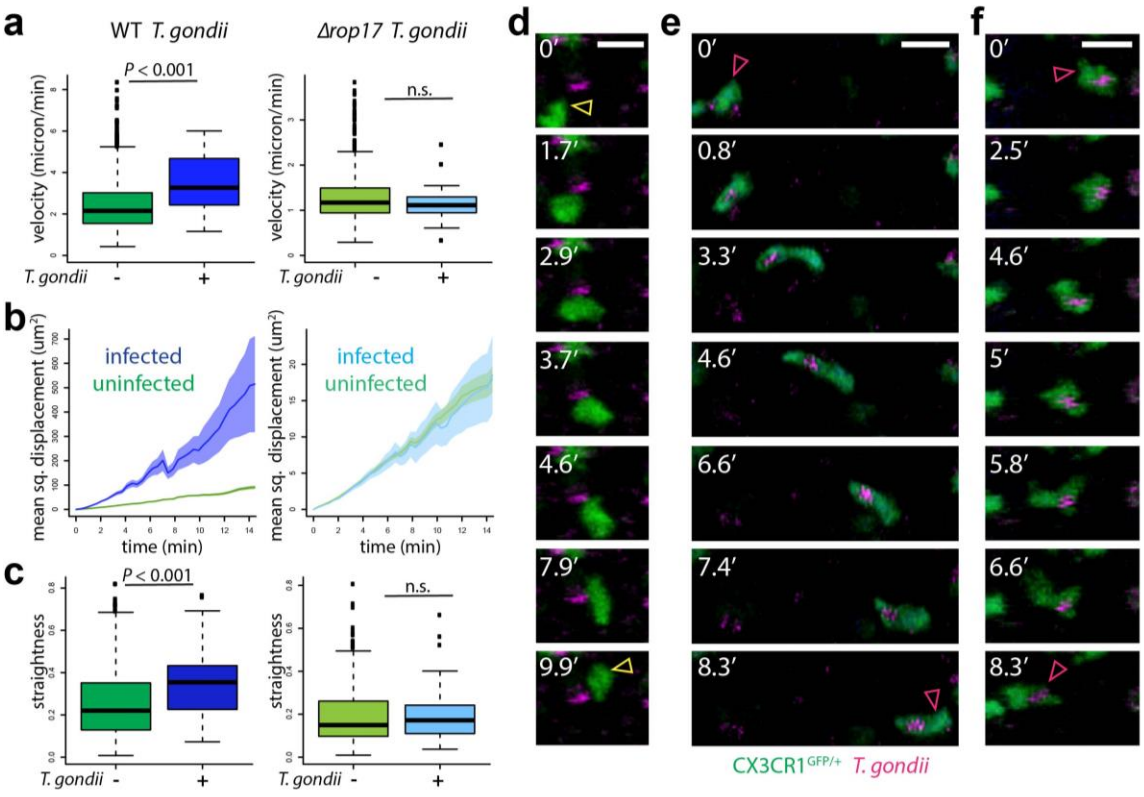

Figure 3.6: *In vivo* motility of splenic monocytes infected with WT and *Δrop17* parasites. **(a-f)** Intravital two-photon spleen imaging was performed 2-4 h after CX3CR1$^{GFP/+}$ mice were infected i.v. with 2-4x10^{7} wild-type or *Δrop17 T. gondii* labeled with Cell Tracker Red CMPTX. **(a-c)** Median track speed (**a**), mean square displacement (**b**) of all tracked CX3CR1$^{GFP/+}$ monocytes, and median track straightness of the motile subset (**c**) is plotted (left: wild type (WT) *T. gondii* infections; right: *Δrop17* infections). Shaded areas indicate SEM for mean square displacement (**b**). Medians and interquartile ranges are shown in colored bars, with min/max values indicated by black lines for track speed (**a**) and straightness (**c**) plots. Pooled data from three mouse infections per parasite genotype is shown (N=34, WT-infected monocytes; N=41, *Δrop17*-infected monocytes, N>200, uninfected monocytes). Data were analyzed by two-tailed Wilcoxon tests (n.s., $P > 0.05$). **(d-f)** Still frame images show migration of individual monocytes

displaying typical morphology. Start and end positions of migrating monocytes are indicated by yellow arrowheads (uninfected, **d**) and pink arrowheads (infected, **e-f**). Scale bars: 10 microns. Time shown in min. Images correspond to Supplementary Videos 4-6.

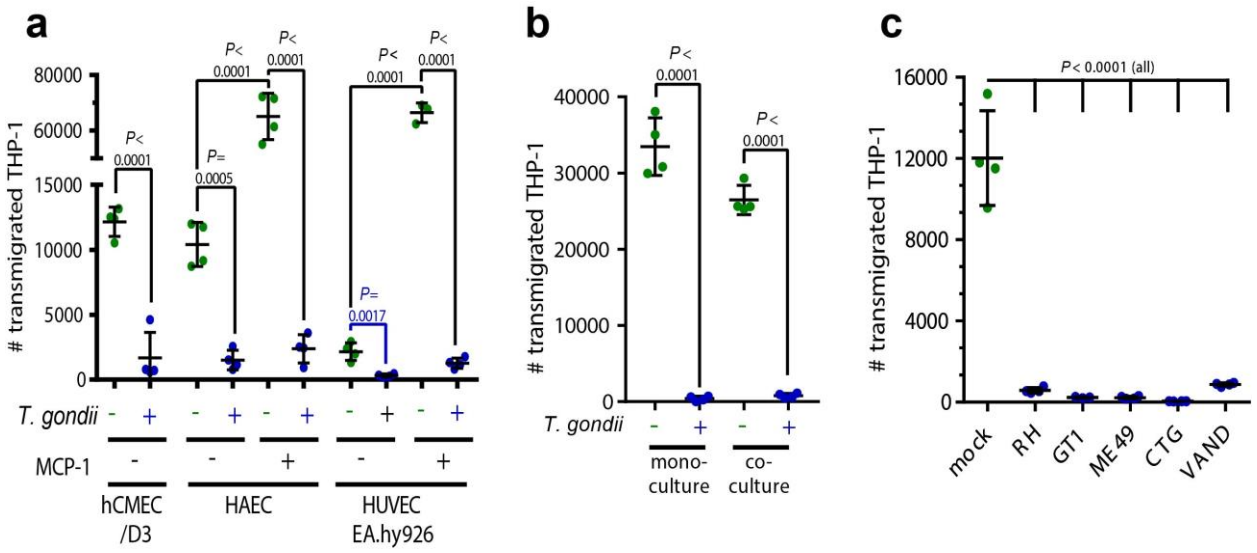

Supplementary Figure 3.1: Transendothelial migration.

(a) Number of THP-1 monocytes transmigrated through barriers composed of immortalized hCMEC/D3, primary human aortic endothelial cells (HAEC), or immortalized EA.hy926 human umbilical vein endothelial cells (HUVEC). **(b)** Number of THP-1 monocytes transmigrated through hCMEC/D3 barrier following astrocyte co-culture as indicated. **(c)** Number of THP-1 monocytes transmigrated through hCMEC/D3 barrier following pre-infection with indicated *T. gondii* strains. All panels show data from either two (**a**, HAEC cells, **c**, CTG parasites) or three independent experiments with the same outcome. Each marker indicates an individual technical replicate (N=3-4 / experiment). Lines and error bars denote mean ± SD. Multiplicity-adjusted *P* -values from one-way ANOVA and Holm-Sidak's multiple comparisons tests are shown in black (NS, $P > 0.05$); *P* -values from unpaired t-tests are shown in blue. All indicated differences between means were statistically significant in all independent experiments.

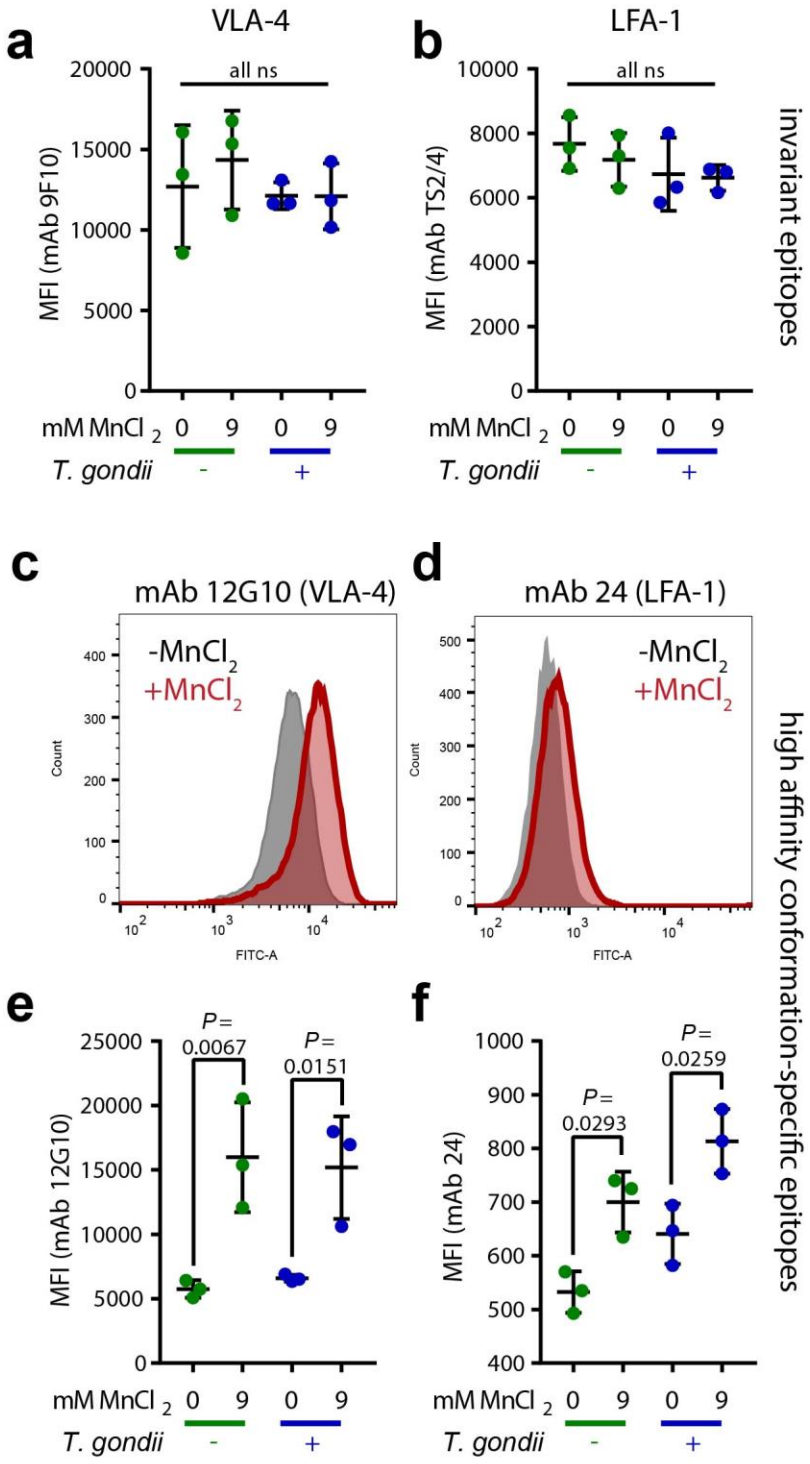

Supplementary Figure 3.2: Integrin expression and conformation.

(a-f) Monoclonal antibodies were used to stain invariant VLA-4 (mAb 9F10) (**a**), invariant LFA-1 (mAb TS2/4) (**b**), activated VLA-4 (mAb12G10) (**c,e**), and activated LFA-1 (mAb 24) (**d,f**).

(c-d) Histograms of THP-1 monocytes activated by $MnCl_2$ and stained with antibodies specific to activated VLA-4 (**c**) and LFA-1 (**d**). **(a-b, e-f)** Data points show median fluorescence intensities (MFI) calculated from each of three independent experiments. Lines and error bars indicate mean and SD. Multiplicity-adjusted *P* -values from all calculated Sidak's multiple comparisons tests are shown (ns, $P > 0.05$).

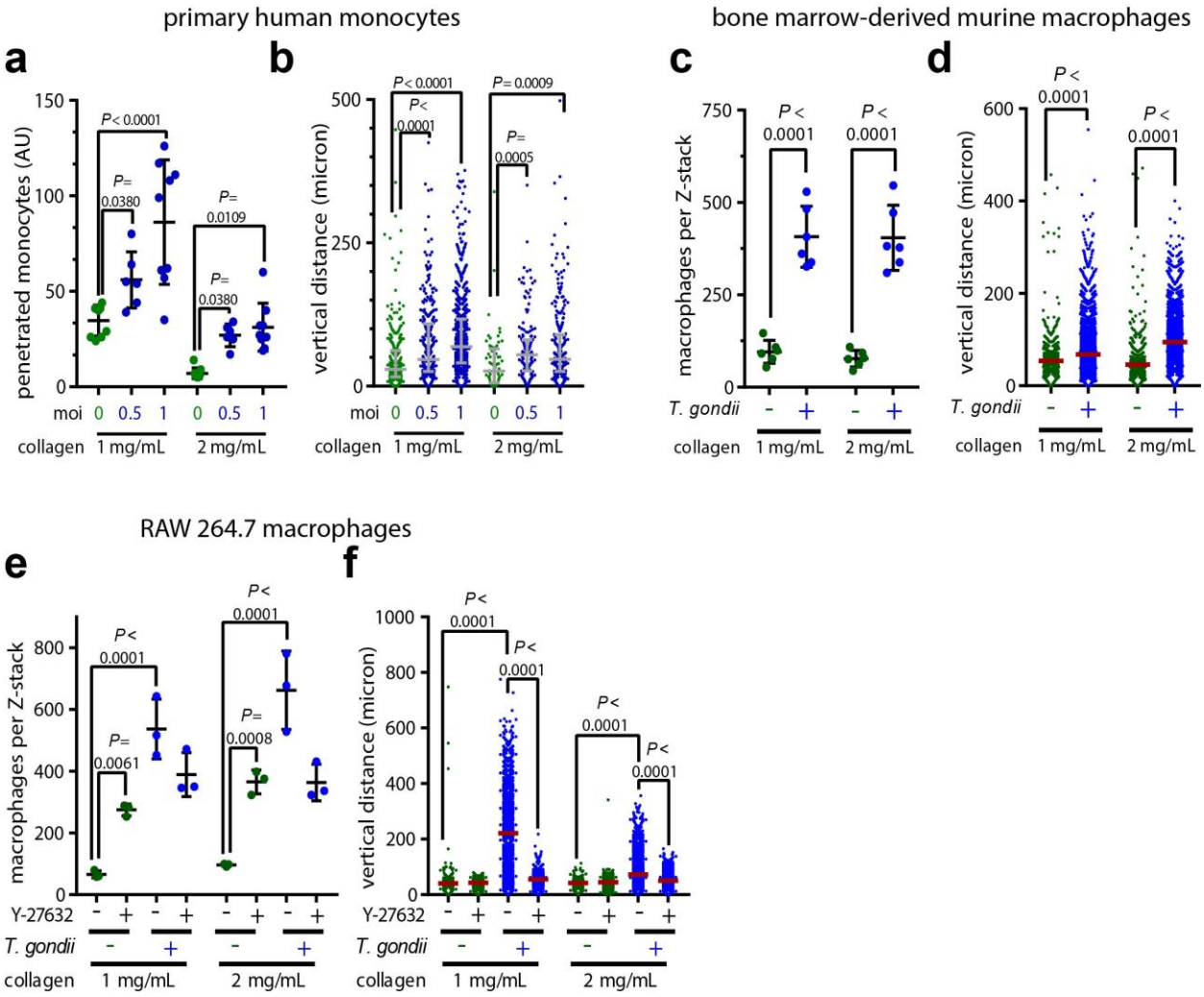

Supplementary Figure 3.3: Migration through collagen I matrix.

(a-f) Migration of primary human monocytes (**a-b**), RAW 264.7 macrophages (**c-d**), and murine bone marrow-derived macrophages (**e,f**) into and through matrices of indicated collagen density, following pre-infection with ME49-mCherry *T. gondii* or a buffer control. Pooled data from three independent experiments, each with three technical replicates, is shown. The number of penetrant monocytes was analyzed with one way ANOVA and Holm-Sidak's multiple comparisons post-test and plotted with means and standard deviations (**a,c,e**). The distance migrated by monocytes was not normally distributed and accordingly analyzed with a Kruskal

Wallis Test and Dunn's multiple comparisons post-test, and plotted with medians and interquartile ranges (**b,d,f**). For both analyses, multiplicity-adjusted *P* -values are shown.

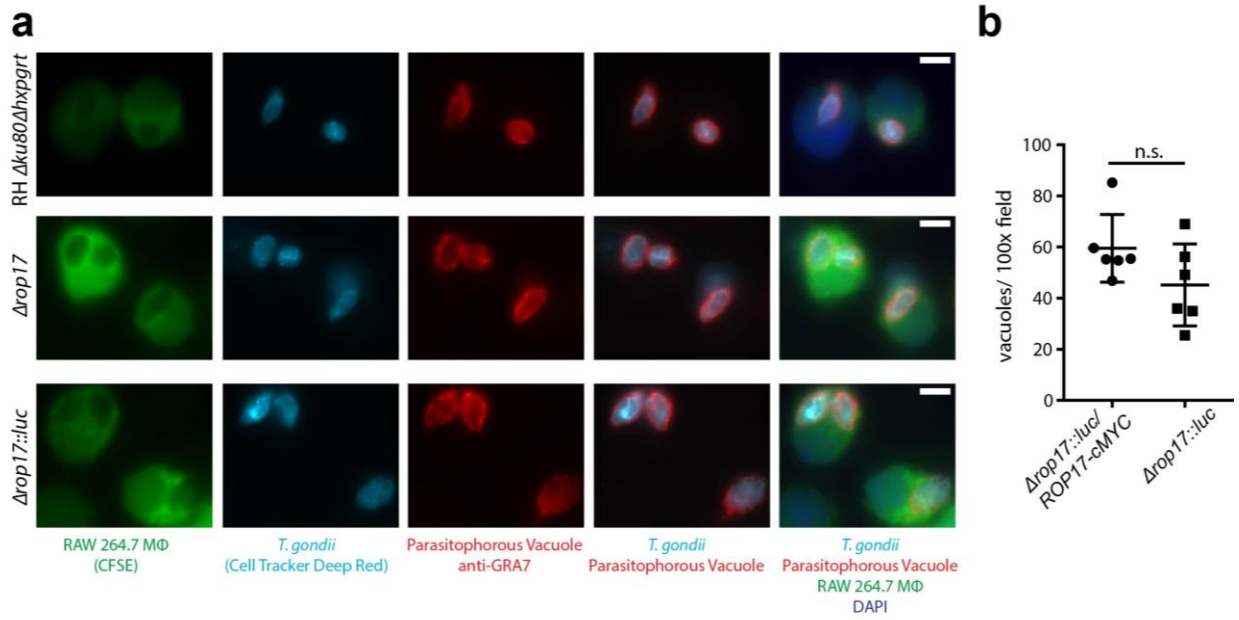

Supplementary Figure 3.4: Growth of *Δrop17* parasites in RAW 264.7 macrophages.

(a) RAW 264.7 macrophages were labeled with CellTrace CFSE and infected overnight with *T. gondii* of indicated genotype labeled with Cell Tracker Deep Red. Parasitophorous vacuoles were stained with anti-GRA7 Scale bars: 5 micron. **(b)** Number of *T. gondii* vacuoles present after 24 h of growth in IFNγ/LPS-stimulated RAW 264.7 macrophages. Plot shows pooled data from two independent experiments, each with three technical replicates. (n.s., $P > 0.05$, unpaired t-test).

Table 3.1: *T. gondii* strains used in this study.

Name	Genotype	Source	Details
CTG		(180)	
GT1		(181)	
ME49	ME49 Δ*hxpgrt*::*FLUC*	(182)	
ME49 mCherry	ME49 Δ*hxpgrt*::*FLUC GRA1:MCHERRY, DHFR:HXPGRT*	This study	Random integration of *GRA1:MCHERRY, DHFR:HXPGRT*
RH	RH *Δku80Δhxpgrt*	(183)	
VAND		(184)	
Δrop17	RH *Δku80 Δrop17::HXPGRT*	(167)	
Δrop17::luc	RH *Δku80 Δrop17::cLUC*	(167)	
Δrop17 ROP17^{WT} -cMYC	RH *Δku80 Δrop17::HXPGRT/ROP17^{WT}-cMYC*	This study	*Δrop17* complemented with wild-type ROP17 (pLD-14, pCAS9sg-UPRT)
Δrop17 ROP17^{K312A} -cMYC	RH *Δku80 Δrop17::HXPGRT/rop17^{K312A}-cMYC*	This study	*Δrop17* complemented with ROP17^{K312A} (pLD-17, pCAS9sg-UPRT)
Δrop17 ROP17^{D436A} -cMYC	RH *Δku80 Δrop17::HXPGRT/rop17^{D436A}-cMYC*	This study	*Δrop17* complemented with ROP17^{D436A} (pLD-16, pCAS9sg-UPRT)
Δrop17::luc ROP17 -cMYC	RH *Δku80 Δrop17::cLUC/ROP17-cMYC*	This study	*Δrop17::luc* complemented wild wild-type ROP17 (pLD-14, pCAS9sg-UPRT)
Δrop5	RH *Δku80 Δrop5::HXPGRT*	(185)	
Δrop18	RH *Δku80 Δrop18::HXPGRT*	(186)	
Δrop17Δrop18	RH *Δku80 Δrop17::cLUC Δrop18::HXPGRT*	(167)	

Table 3.2: Plasmids used in this study.

Stock Name	Short Name	Construction	Purpose
pSAG1:CAS9-GFP,U6:sgUPRT	pCAS9-sgUPRT	(187)	Induce double-stranded break at UPRT locus
pUPRT-FloxedDHFR-TS*		Kevin Brown, Addgene 100606	
pLD-08	pROP17	Gibson assembly of: vector backbone amplified from pUPRT-FloxedDHFR-TS with LDO-73 and LDO-74 and *ROP17* amplified from RH genomic DNA with LDO-61 and LDO-62	Construct for ROP17 expression in *T. gondii* under native promoter
pLD-14	pROP17-cMYC	Q5 mutagenesis of pLD-08 using LDO-65 and LD0-66	Construct for ROP17-cMYC expression in *T. gondii* under native promoter
pLD-16	pROP17-D436A-cMYC	Q5 mutagenesis of pLD-14 using LDO-75 and LDO-76	Construct for ROP17^{K312A}-cMYC expression in *T. gondii* under native promoter
pLD-17	pROP17-K312A-cMYC	Q5 mutagenesis of pLD-14 using LDO-77 and LDO-78	Construct for ROP17^{D436A}-cMYC expression in *T. gondii* under native promoter

Table 3.3: Oligonucleotides used in this study.

Stock Name	Sequence	Purpose
LDO-61	TGTTGAGAAAGCGGTTCGGC tgtgctcactggtggtagtg	Sense oligo to amplify ROP17 5'UTR with homology to pUPRT-FloxedDHFR-TS
LDO-62	TCTCCCGCATGTCACGTGGC ctgtaagtccgcgaagctg	Antisense oligo to amplify ROP17 3'UTR with homology to pUPRT-FloxedDHFR-TS
LDO-65	ctccttctgtaataaagccgc	Antisense oligo to amplify ROP17 CDS starting before stop
LDO-66	GAACAAAAACTCATCTCAGAAGAGGATCTG taatctgatgcggtcaatgc	Sense oligo to introduce cMYC tag before ROP17 stop codon via Q5 mutagenesis
LDO-75	TGTTCATGGCgctGTGAAACTGC	Sense oligo to introduce D436A SNP in *ROP17* via Q5 mutagenesis
LDO-76	AGTCCGAACGCGTGGAAT	Antisense oligo to introduce D436A SNP in *ROP17* via Q5 mutagenesis
LDO-77	ATTCGCGCTGgcgATATTTGTTCAACGGGTG	Sense oligo to introduce K312A SNP in *ROP17* via Q5 mutagenesis
LDO-78	GGTTGCCCTGTGGTGGGA	Antisense oligo to introduce K312A SNP in *ROP17* via Q5 mutagenesis

Chapter 4: Conclusion and future directions

This chapter was composed by LLD. Comments from LDS were incorporated into the final version.

Conclusions

Toxoplasma gondii is an apicomplexan parasite capable of infecting a diverse array of host cells and tissues. Infections are orally acquired upon the ingestion of parasite cysts within undercooked meat or oocysts within contaminated food or water, and accordingly are initially concentrated in the intestinal lamina propria. However, *T. gondii* systemically disseminates during acute infections and the most severe manifestations of acute toxoplasmosis derive from the parasite's ability to access protected host compartments such as the central nervous system and placenta.

Parasite spread relies on the intrinsic gliding motility of *T. gondii*, which allows extracellular parasites to locomote within tissues to new host cells and invade diverse host cells including migratory leukocytes. Gliding motility and host cell invasion have long been theorized to be powered by a parasite actin-myosin motor (32). The development of improved tools for inducible ablation of *T. gondii* genes had suggested the possible existence of invasion processes that function independently of parasite actin (68,69). However, the essential and pleiotropic nature of the *T. gondii* actin *ACT1* complicated the assessment of whether *ACT1* was specifically required for parasite invasion of host cells.

Infected migratory leukocytes can also promote dissemination by shuttling intracellular parasites to new host compartments as they traffic throughout the host. Monocytes have been widely theorized as potential Trojan horses that could deliver intracellular *T. gondii* across the blood-brain barrier and into the CNS (29,87,108). However, limited *in vivo* data supported this model and *in vitro* approaches had not established whether infected monocytes could efficiently traverse blood-brain barrier endothelium or tissue environments. The role that infected monocytes were likely to play in advancing *in vivo* dissemination thus remained unclear.

Parasite actin is critical for gliding motility and invasion

ACT1 depletion is not uniform in individual parasites and correlates with invasion defects

Previous studies developed a dimerized Cre-Lox system in which rapamycin induces Cre-mediated excision ablates a floxed *ACT1*^{f} allele and replaces it with a YFP cassette that functions as a reporter for knockout parasites (68,69). During short term propagation, low levels of residual gliding and cell invasion in *Δact1* parasites were proposed to comprise evidence for an ACT1-independent invasion pathway in *T. gondii*. However, because these studies did not quantitatively assess the extent of ACT1 depletion in recently induced *Δact1* parasites, the degree to which these parasites resembled phenotypic nulls was uncertain.

The findings of my thesis confirm that inducible *Δact1* parasites exhibited marked impairment but not a complete block in all forms *T. gondii* motility: extracellular gliding, egress, and host cell invasion (188). Importantly, the data presented here also show that ACT1 protein content widely varied in individual parasites after inducible *ACT1*^{f} excision (188). Inducible *Δact1* parasites identified by YFP expression contained significantly less ACT1 than control parasites, but residual ACT1 was detectable up to five days following rapamycin induction of excision. As parasites were cultured for longer time periods following rapamycin-induced *ACT1*^{f} excision, increasingly severe depletion for ACT1 and defects in invasion were observed. The correlation between ACT1 depletion and invasiveness suggests that the residual ACT1 could be functioning in invasion. Consistent with this interpretation, inducible *Δact1* parasite invasion was further blocked by the actin polymerization inhibitor cytochalasin D.

The wide variety in ACT1 protein content among both wild-type and *Δact1* parasites was surprising. The observation that individual *Δact1* parasites retained detectable ACT1 protein so

long after rapamycin-induced gene excision could be explained by two mechanisms. First, some of the inducible knockouts staining strongly for ACT1 may represent parasites that spontaneously excised *ACT1*^{f} after the rapamycin induction period. Consistent with this hypothesis, rare YFP-expressing parasites were observed in uninduced *ACT1*^{f} parasites cultured *in vitro*. Second, some portion of parasites may inherit unusually large subsets of ACT1 mRNA or protein present before gene excision. These mechanisms would both be expected to occur very infrequently. However, a requirement for ACT1 for both parasite division and host cell invasion would also cause truly ACT1-ablated parasites to rapidly drop out of the population during *in vitro* propagation. The resulting selection in favor of the rare *Δact1* parasites with meaningful residual ACT1 protein would increase their apparent prevalence in pools of *Δact1* parasites. Importantly, a portion of *ACT1*^{f}-intact parasites that stained for ACT1 protein levels as low as the mean content of induced *Δact1* parasites was consistently detected, even as long as five days after induction of *ACT1*^{f} excision. This finding suggests that *T. gondii* parasites naturally express a range of ACT1 protein levels, and that most parasites contain far more ACT1 protein than is necessary to power invasion. Accordingly, the ACT1 depletion in *Δact1* parasites must be extremely severe to truly approximate functional knockout.

A later study used a similar quantitative immunostaining approach to estimate ACT1 protein content in inducible *Δact1* parasites and consistent with my findings, reported detectable ACT1 staining above background up to four days post rapamycin-induced gene excision (189). Surprisingly, this report failed to detect overlap in the ACT1 content of individual *ACT1*^{f}-intact and *Δact1* parasites at any time-points later than 36 hours past rapamycin induction of gene excision (189). However, this study used an automated approach to staining quantification that relied solely on YFP expression to identify parasites (189). This approach would not detect

recently-excised knockouts expressing only low levels of YFP, such as spontaneous late excisers. The methods that were used in this later study to ensure that a representative range of YFP-negative *ACT1*^{f}-intact parasites were identified for quantification in this system were not specified, but a range of ACT1 staining intensity was detected in control parasites (189), as in my studies. The discrepancy between my studies and this report might derive from the use of different antibodies or independently-generated *ACT1*^{f} inducible excision lines. However, the most likely explanation is that the automated approach employed in this later study failed to identify all parasites in the analyzed populations, with the result of excluding low-YFP-expressing *Δact1* parasites and low-staining *ACT1*^{f}-intact parasites from analysis. Relatedly, the automated subtraction of putative background signal in the later paper may have also inadvertently eliminated true signal from the analysis.

Actin is specifically involved in the penetration step of host cell invasion

Initial reports of inducible *Δact1* parasites proposed that a defect in moving junction formation by these mutants implied that ACT1 promotes invasion by mediating attachment (69) rather than providing motive force during host cell penetration as was initially theorized by the glideosome model (17). My thesis work found that *Δact1* parasites exhibited no defect in adherence to fibroblasts rendered resistant to parasite invasion via glutaraldehyde fixation (188). However, a subsequent study reported that *Δact1* parasites exhibited profound defects in adherence to collagen under shear stress conditions (189). It thus appears possible that under some conditions, ACT1 helps promote parasite adherence to substrates. However, my work also used a rapid invasion pulse to capture many parasites in the process of invasion, and thereby demonstrated that *Δact1* parasites are able to form moving junctions (188). Moreover, video microscopy showed that inducible *Δact1* parasites invading fibroblasts initiated the invasion

process but were significantly delayed in host cell entry, with a subset failing to complete invasion at all (188). Importantly, video analysis of invasion also showed that about half of the Δ*act1* parasites invaded fibroblasts with normal kinetics, consistent with a model where a portion of these mutants are not strongly depleted for ACT1 and thus not functionally knockouts (188). The ability of *Δact1* parasites to form moving junctions and initiate invasion suggests that they stably adhere under standard culture conditions, and in such conditions exhibit defects specific to the penetration stage of invasion, presumably by working with myosin to generate force.

My thesis establishes that ACT1 plays a specific role in the penetration step of *T. gondii* invasion, and that *ACT1*-independent invasion pathways are unlikely to robustly function in *T. gondii* parasites. The possible existence of a very low efficiency ACT1-independent invasion pathway in *T. gondii* cannot be formally excluded. However, such a pathway appears unlikely to be an important contributor to host cell invasion given its negligible ability to compensate for the loss of ACT1-dependent invasion. The variable levels of ACT1 expression in single parasites and inconsistency of inducible Cre-Lox-mediated excision efficiency suggest that a more decisive answer to this question would require different technology, for example the auxin-inducible rapid protein degradation system recently adapted to *T. gondii* (190).

T. gondii activates monocyte tissue migration, but inhibits integrin-dependent adherence and transendothelial migration

Because they are the most abundantly infected circulating leukocyte in murine models of toxoplasmosis (29), monocytes have been proposed as Trojan horses that could deliver intracellular *T. gondii* parasites across the blood-brain barrier and into the brain (87,108). Several studies supported this theory by showing that *T. gondii* infection can manipulate monocyte

motility, specifically leading to decreased integrin-mediated adherence (106,107), enhanced velocity and pathlength of crawling (108), and a net neutral impact of transendothelial migration (108), all observed in an *in vitro* model based upon human umbilical vein endothelial cells (HUVEC). However, no previous reports had considered the ability of infected monocytes to traverse the highly specialized endothelium that comprises the blood-brain barrier, or tissue environments representative of the intestinal lamina propria where *T. gondii* first encounters monocytes.

Infection inhibited integrin-dependent processes

My thesis work used transwell systems to assess the ability of infected monocytes traverse barriers composed of the human brain endothelial cell line, hCMEC/D3 (175). Contrary to the prediction of a simple Trojan horse model of *T. gondii* CNS invasion, I found that *T. gondii* infection severely inhibited the ability of monocytes to traverse this model blood-brain barrier. This result was generalizable across many *T. gondii* strains, the monocytic cell line THP-1 and primary human monocytes, and endothelial barriers composed of primary and immortalized cells from CNS and peripheral tissues. Notably, I observed very limited spontaneous transmigration of monocytes across HUVEC, which likely accounts for the failure of a previous study to detect significant parasite inhibition of monocyte transmigration in an analogous system (108). Integrins are well-established as key players in the transendothelial migration cascade, functioning as both adhesins and force transducers (110). The failure of infected monocytes to transmigrate through endothelial barriers likely stems from a failure to successfully perform the processes that enhance avidity during integrin-mediated adherence, as I observed that infected monocytes ineffectively adhered to endothelial substrates and failed to mobilize integrins to ligand-contacting poles.

In vivo, the blood-brain barrier is a complex system composed of many cell types and subjected to mechanical stress from blood flow. To better reflect this complexity, I further tested our phenotype in a hCMEC/D3-astrocyte co-culture system that more faithfully models the blood-brain barrier (155), and still observed *T. gondii* inhibition of monocyte transendothelial migration. Physiological transendothelial migration also occurs under conditions of shear stress, which promotes selectin engagement preceding integrin activation (110,125) and might somehow relieve defects in the integrin-mediated adherence and subsequent transendothelial migration. However, a separate study does confirm my findings of faulty integrin-mediated adherence in infected monocytes under shear stress conditions (107). Admittedly, my *in vitro* model likely does not recapitulate several further features of the blood-brain barrier relevant to toxoplasmosis *in vivo*, for example, the inflammatory state induced by infection, presence of pericytes and extracellular matrix in addition to endothelial cells and astrocytes, and formation of a more robust barrier. Accordingly, if infected monocytes have a specific preference for traversing blood-brain barrier endothelium, this may not be triggered by my *in vitro* model.

Infected monocytes use an amoeboid migratory mode suited to tissue migration

I consistently observed that although very ineffective at transendothelial migration, infected monocytes were very active cells. When monocytes migrated on top of endothelial substrates, *T. gondii* infection led to enhancements in velocity and pathlength traveled. This enhanced motility is consistent with previous reports analyzing migration over HUVEC under shear stress conditions (108). However, because integrins are theorized to be critical force transducers during vascular crawling (128,129), this observation seemed inconsistent with infection blocking integrin-mediated adherence. Close examination of videos of the motility of

migrating infected monocytes revealed dramatic amoeboid morphological changes markedly inconsistent with typical monocyte vascular crawling.

Leukocytes have been previously shown to migrate through tissue interstitium in an integrin-independent mode characterized by amoeboid morphology and reliance on Rho-driven contractility for negotiation of small pores (121,122). I found that infected monocyte efficiently migrated through an *in vitro* collagen matrix model of tissue interstitium. Consistent with an integrin-independent mode that relies on Rho/ROCK signaling to formin-mediated actin polymerization, the migration of infected monocytes was potently blocked by inhibitors of Rho, ROCK, and formins. Physiological tissues are composed of many substrates arranged in complex geometries not approximated by simple collagen I matrices (121). Accordingly, I further established that infected monocytes migrate with enhanced efficiency through *ex vivo* murine dermal sheets and *in vivo* splenic tissue.

T. gondii ROP17 is required for enhanced monocyte tissue migration and effective in vivo dissemination

The critical role of monocytes in controlling acute toxoplasmosis (112,113) renders monocyte ablation ill-suited to assessing whether monocytes also serve a specific role in advancing *T. gondii* dissemination. To circumvent this limitation, I sought to identify parasite factors required for the enhancement of monocyte tissue migration. My thesis work implicated the secreted *T. gondii* kinase ROP17 in parasite-enhanced monocyte tissue migration. The data presented in this dissertation show that *Δrop17* parasites fail to enhance monocyte migration through *in vitro* collagen matrix models of tissue, and splenic tissue *in vivo*. I further showed that *Δrop17* parasites disseminate more slowly in murine infection models when parasites are introduced subcutaneously.

ROP17 has been previously theorized to synergize with the kinase ROP18 and pseudokinase ROP5 in defending the *T. gondii* parasitophorous vacuole from attack by host immunity-related GTPases in activated macrophages (167). This model raises the possibility that the attenuation of *Δrop17* parasites could derive from a failure to survive clearance within macrophages, rather than deficiencies in spread. However, ROP17 on its own appears to play a very minor role in this defense, with single *Δrop17* deletion parasites exhibiting negligible defects in macrophage survival (167,173), a finding that I confirmed. I further showed that the attenuation of *Δrop17* parasites is linked to an infection route that emphasizes the role of tissue dissemination. Mice infected subcutaneously with *Δrop17* parasites exhibited delayed *T. gondii* spread and enhanced infection survival. In contrast, intraperitoneal infections that featured passive *T. gondii* spread via lymphatic drainage exhibited no significant change in either *T. gondii* spread or mouse survival for *Δrop17* parasites. Overall, my results suggest that *Δrop17* parasites are specifically attenuated due to decreased dissemination efficiency. This conclusion implies that ROP17-dependent enhancement of monocyte tissue migration likely promotes parasite dissemination during *in vivo* infections. Consistent with this model, another study found that *ROP17* deletion in a moderately virulent *T. gondii* lineage used to study chronic infections led to a complete loss of brain cyst formation, presumably caused by a failure of *Δrop17* parasites to systemically disseminate (173).

Mechanism of ROP17 activation of monocyte tissue migration

ROP17 is a serine-threonine kinase discharged from *T. gondii* rhoptry organelles into the host cell cytosol during invasion, and subsequently recruited onto the cytosolic face of the parasitophorous vacuole membrane (167). The catalytic triad of ROP17 is conserved, suggesting that ROP17 is likely a catalytically active kinase (169). Consistent with this prediction, previous

work from our group demonstrated that ROP17 is catalytically active *in vitro* (167). My work further determined that ROP17 kinase activity is required for *T. gondii* to enhance monocyte tissue migration, by showing that complementation with *rop17*^{D436A} and *rop17*^{K312A} catalytic triad mutants cannot restore the enhanced monocyte migration phenotype to *Δrop17* parasites.

Previous work identified the switch I region of host immunity-related GTPases as substrates for ROP17 and ROP18 phosphorylation (167). Because immunity-related GTPases are not connected with leukocyte migration (191), ROP17 likely phosphorylates a different substrate to activate tissue migration. I initially theorized that ROP17 could be involved in enhancing tissue migration due to the common presence of switch I regions in immunity-related GTPases and Rho GTPase (168). However, ROP17 could also activate Rho-dependent tissue migration by acting on Rho regulators, for exampling enhancing activity of a Rho GEF or neutralizing a Rho GAP or GDI, or even indirectly via Rho-Rac crosstalk (170) by potently inhibiting Rac activity. Several Rho regulators including the GEFs VAV and GEF-H1, the GAP DLC1 and RhoGD11 are known to be phosphoregulated (174) and thus are appealing candidate substrates for ROP17. However, phosphoregulation of Rho signaling pathway components has not been exhaustively studied (174), suggesting the relevant target could easily have not been previously shown to be phosphoregulated. Moreover, it remains possible that ROP17 functions far upstream of Rho, such at the level of GPCR signaling, or targets a different pathway as my inhibitor-based analysis of Rho/ROCK signaling may have been compounded by off-target effects. Future studies should thus take an unbiased approach to identifying ROP17 substrates.

Whether ROP17 is likely to mediate tissue migration from the parasitophorous vacuole or act earlier when still free in the host cytosol is uncertain. My working model is that ROP17 likely phosphorylates a substrate involved in Rho signaling. Activated Rho typically functions at the

plasma membrane (174). The parasitophorous vacuole to which ROP17 is recruited is derived from host cell plasma membrane, but substantially modified (192). Whether Rho is present or active on the parasitophorous vacuole membrane is uncertain. A series of N-terminal domains that mediate recruitment of ROP18 to the parasitophorous vacuole are well-established (193) and conserved in ROP17 (194). However, unlike in defense against vacuolar attack by host immunity-related GTPases mediated by the ROP5-ROP18-ROP17 complex (193), there is no intuitive intrinsic link between ROP17 promotion of tissue migration and parasitophorous vacuole localization. Accordingly, future studies should attempt to define whether ROP17 localization to the parasitophorous vacuole is needed for effective enhancement of monocyte tissue migration.

Infected monocytes promote dissemination by advancing parasite spread through tissues, rather than across endothelial barriers

The failure of the motility of infected monocytes to support robust transendothelial migration suggests that monocytes are ill-suited to act as Trojan horses that deliver *T. gondii* across the blood-brain barrier. Consistent with this idea, another study reported that infected monocytes adoptively transferred to recipient mice readily trafficked to the brain, but overwhelmingly remained in the vasculature and did not enter the brain parenchyma (30). This study proposed that CNS invasion is instead accomplished via the invasion of blood-brain barrier endothelial cells by extracellular *T. gondii* present in the bloodstream, which replicate within the endothelium and then subsequently egress into the parenchyma. Supporting this model, the study reported the presence of extracellular *T. gondii* parasites in the blood of mice fed tissue cysts and used intravital two-photon imaging to capture instances of blood-brain barrier invasion by parasites introduced intravenously (30). Whether these parasites approached the blood-brain

barrier as extracellular parasites or were delivered within leukocytes remains uncertain, as the intravital imaging assays did not include labeled leukocytes.

One intriguing hybrid of the direct parasite invasion of the blood-brain barrier model with the Trojan horse dissemination model is that infected monocytes could shuttle intracellular parasites throughout the bloodstream and thereby protect parasite cargo. Stalling or embolizing of infected monocytes in small capillaries could then provide an opportunity for parasites to egress out and directly invade the neighboring endothelium. Consistent with this model, a recent study suggested that endothelial adherence can prompt early *T. gondii* egress from monocytes (195). This model could also explain observations that *T. gondii* within the CNS tend to be found near small vessels (30,37).

I propose that the primary function of monocytes in advancing *T. gondii* dissemination is allowing parasites to rapidly move within and out of tissues (Figure 4.1). For example, immediately after traversing intestinal epithelium, *T. gondii* parasites encounter lamina propria monocytes and macrophages (28). This population includes many CX_3CR1-expressing macrophages that develop from inflammatory monocytes (115). Using intravital imaging, I showed that *T. gondii* infection enhanced the interstitial migration of CX_3CR1-expressing monocytes in the spleen, suggesting that migration of CX_3CR1^+ lamina propria cells is likely to be similarly enhanced by infection. Enhanced migration in infected CX_3CR1-expressing monocytes and descendant macrophages and DCs could enhance their entry into collecting lymphatics, or travel through lymph nodes and thus possibly increase the typically very low frequency of lymph node exit through efferent lymphatics (93). This route would eventually lead infected cells to the bloodstream via the lymphovenous valve (196) (Figure 4.1). Upon entering

the bloodstream, infected monocytes might then release parasites to invade endothelial cells and subsequently egress into tissues such as the brain as outlined above.

Notably, I did not test whether other leukocytes exhibited ROP17-dependent enhanced migration *in vivo*, or whether ROP17-dependent enhanced migration was relevant to parasite dissemination in a murine system that models natural infection routes with oral cyst inoculation. Future studies should test whether ROP17 promotes parasite dissemination after oral cyst inoculation.

Follow-up studies could then assess whether specific leukocyte types are targeted by ROP17-mediated enhanced migration. Monocytes are generally thought of as circulating cells that differentiate into macrophages or dendritic cells upon entering tissues. However, evidence suggests that at least some monocytes can extravasate into resting tissue, acquire antigen and transport it to lymph nodes without substantially differentiating (197). Accordingly, future work should test whether ROP17 activation of tissue migration is more potent in monocytes, macrophages, or dendritic cells, and further assess whether ROP17-enhanced migration of any of these cell types is particularly efficient at promoting *in vivo* dissemination after oral cyst inoculation. If undifferentiated monocytes are relevant targets *in vivo*, it would be further interesting to assess whether ROP17 activation of tissue migration is accompanied by pressure to differentiate into macrophages or dendritic cells. Finally, as $CCR2^{+}$ $Lyc6^{hi}$ inflammatory monocytes are specifically implicated in controlling acute toxoplasmosis (112,113), it would also be interesting to ascertain whether this specific monocyte subset is a target of ROP17-dependent enhanced migration.

Infected decouples matching of monocyte migratory mode to environment

Because all leukocytes express integrins that recognize ligands displayed in essentially all mammalian tissues, integrin-independent migration is presumably never forced *in vivo* by the impossibility of integrin-mediated adherence. However, integrin-independent migration may allow leukocytes migrate in a more rapid or energy efficient manner by overcoming the need for robust frictional forces or extensive cycles of adherence and de-adherence from substrates (129). Accordingly, leukocytes likely migrate through tissue interstitium *in vivo* in a hybrid fashion that incorporates different migratory modes as dictated by the immediate environments encountered (198,199). This plasticity is reflected by *in vitro* studies showing that macrophages match the adhesion-dependence of their migratory mode to the variety of 3-D matrix encountered **(**138**,**139**)**.

The data presented here indicate that *T. gondii*-infected monocytes migrate in an amoeboid manner even if presented with endothelium that should promote highly-adhesive integrin-dependent migration, as it is inherently ill-suited to be traversed in an amoeboid mode. This observation suggests that the parasite can interfere the matching of the host leukocytes' migratory strategy to environment. The mechanisms that control the transitions between leukocyte migratory modes are as yet unknown (199). Further investigations of the mechanism by which *T. gondii* ROP17 activates amoeboid migration in monocytes may provide insights into mechanisms that regulate the initiation of amoeboid migration in leukocytes. In addition, my findings identify toxoplasmosis as an intriguing physiological scenario where integrin-independent migration is not only possible if forced by genetic ablation of integrin functionality, but preferentially performed. This finding provides compelling evidence that integrin-independent migration of leukocytes is not only possible *in vivo,* but physiologically relevant.

Future Directions

This work shows that ROP17-dependent enhanced monocyte tissue migration promotes the systemic dissemination of *T. gondii* parasites. Further investigations into the mechanism by which ROP17 promotes monocyte tissue migration and the leukocytes and compartments most relevant to this phenotype *in vivo* following oral infection will illuminate how *T. gondii* disseminates and molecular mechanisms controlling leukocyte migration.

Mechanism of ROP17-enhanced tissue migration

This thesis established that ROP17 kinase activity allows *T. gondii* parasites to enhance the migration of infected monocytes through tissues. This is presumably achieved via the phosphorylation of a substrate other than the immunity-related GTPases previously identified as ROP17 substrates. Previous work also showed that ROP17 strongly prefers to phosphorylate threonine substrates, and has a subtle preference for surrounding hydrophobic residues (167). However, this motif cannot predict ROP17 substrates. Moreover, serine-threonine kinases are notoriously permissive *in vitro*. Accordingly, to define the mechanism by which ROP17 activates tissue migration and identify authentic substrates of ROP17 relevant to this phenotype, I propose three lines of investigation: testing whether ROP17 recruitment to the parasitophorous vacuole is required for its activity in enhancing tissue migration, identifying ROP17 interaction partners in live infected monocytes, and identifying ROP17 phosphorylation substrates in infected cells.

Parasitophorous vacuole targeting of ROP17

ROP18 contains an N-terminal series of three arginine-rich amphipathic helices (RAH domains) that target ROP18 to the parasitophorous vacuole membrane (193,200). Unsurprisingly given the function of ROP18 in defending the parasitophorous vacuole, disruption of this localization also disrupts ROP18 function in defending *T. gondii* from clearance in macrophages

(193). ROP17 similarly localizes to the parasitophorous vacuole (167) and contains a degenerate series of three N-terminal RAH domains that are sufficient to target constructs to the parasitophorous vacuole (194) (Figure 4.2). However, it is not immediately obvious that concentration of ROP17 activity at the parasitophorous vacuole would be necessary or even beneficial to enhance monocyte tissue migration.

ROP17 could influence Rho signaling by interacting with Rho or a Rho GTPase before being recruited to the parasitophorous vacuole, or by recruiting substrates to the parasitophorous vacuole where ROP17 would have access to substrates due to its situation on the membranes' cytosolic face. The amoeboid morphology of infected cells with constrictions appearing in many areas of the monocyte implies that signaling activity may not be constrained to the parasitophorous vacuole. Intriguingly, *ROP17* encodes two putative SUB2 cleavage motifs and processing at the second motif would disrupt the first RAH domain (Figure 4.2). In preliminary studies, I generated *ROP17* point mutants where either SUB2 motif is individually disrupted. Both SUB2 motif mutants were still processed into mature ROP17, indicating both motifs are functional processing sites (data not shown). I hypothesize that the dual SUB2 motifs might create two ROP17 variants for specific purposes: one to sit on the parasitophorous vacuole and assist ROP18, and one to remain cytosolic and manipulate host Rho signaling.

To test these models, I propose to complement *Δrop17* parasites with cMYC-tagged *ROP17* alleles where the arginines in the RAH domains are mutated to glutamates, as was previously done with ROP18 (193). Immunofluorescence can then be used to verify that these ROP17-RAH mutants traffic to rhoptries but are not recruited to the parasitophorous vacuole. I expect that disruption of RAH arginines will eliminate recruitment of ROP17 to the parasitophorous vacuole. If this is observed, monocytes infected with ROP17-RAH mutants can

then be used to test whether ROP17 variants that do not localize to the parasitophorous vacuole are still able to enhance monocyte migration through collagen matrices. If parasitophorous vacuole localization is important for enhancing monocyte migration, this can be used to narrow potential substrates identified in later studies to proteins that localize to the PVM.

If parasitophorous vacuole localization disruption does not restrict the ability of ROP17 to enhance monocyte migration, a similar approach could be used with *Δrop17* parasites complemented with ROP17 disrupted for the individual SUB2 motifs. This approach would test whether cleavage in the first RAH domain (resulting from cleavage at the second SUB2 motif) abrogates ROP17 targeting to the parasitophorous vacuole and enhancement of monocyte migration. If disruption of the second SUB2 motif and associated RAH domain is more disruptive to ROP17-dependent enhanced monocyte migration than disruption of the first SUB2 site, this would suggest that the two SUB2 processing sites on ROP17 produce functionally distinct ROP17 variants with roles likely determined by localization.

Identification of endogenous ROP17-interacting proteins

The permissive nature of serine-threonine kinase *in vitro* renders it challenging to determine whether substrates phosphorylated in such systems represent true physiological substrates. Accordingly, confirmation of interaction with ROP17 substrates under physiological conditions is a critical condition for assessing the veracity of putative substrates.

In pilot studies, I attempted to use pulldown of a cMYC-tagged ROP17 allele expressed by *T. gondii* to identify ROP17-interacting proteins in infected monocytes. Unfortunately, no host proteins were consistently enriched in ROP17-pulldowns as assessed by mass spectrometry of three independent experiments. The transient nature of kinase-substrate interactions makes such interactions challenging to detect via pulldown. Kinase-dead alleles of the related kinase

ROP18 increased the stability of interaction with IRG substrates, presumably caused by delays in the phosphor-transfer reaction trapping the substrate within ROP18 (186). However, both the D436A and K312A kinase dead ROP17-cMYC constructs I generated were not able to successfully pulldown ROP17 despite expressing well, rendering this approach intractable.

As an alternative approach better suited to identifying transient kinase-substrate interactions, I propose BirA-mediated biotinylation of proteins in proximity of ROP17 in infected monocytes. In this approach, the promiscuous biotin ligase BirA will be fused to ROP17 and used as bait to identify monocyte proteins that interact with ROP17 upon infection with these ROP17-BIRA *T. gondii*. Proteins that come into the proximity of the ROP17-BIRA fusion will be marked by biotinylation and can be detected by western blotting or mass spectroscopy following affinity chromatography capture. This approach has been successfully used to identify proteins present within the dense granules (201) and apical conoid compartment (190) of *T. gondii*. As infection never leads to faulty adherence or amoeboid morphology in the fibroblasts that *T. gondii* is routinely cultured in, it appears that this mechanism does not function in fibroblasts. Accordingly, I propose to perform a parallel assay in infected fibroblasts. Biotinylated proteins specific to or more abundantly labeled in monocytes than fibroblasts would be considered high priority candidates. Because biotin proximity labeling will likely identify many indirect interactions, high priority candidates would be further tested for ROP17-cMYC interaction by pulldown.

Unbiased identification of ROP17 phosphorylation substrates in monocytes

I propose attempting three independent unbiased approaches to identify potential substrates of ROP17 phosphorylation in infected monocytes or macrophages: the use of

sequence-independent phospho-threonine antibodies, a chemical genetic strategy relying upon manipulation of the ROP17 ATP gatekeeper pocket, and global phosphoproteomics.

In the simplest approach, I will collect lysates from RAW macrophages infected with *T. gondii* and probe these samples with several commercially available phospho-threonine antibodies. To identify events reliant on ROP17 phosphorylation, infection with wild-type RH *T. gondii* will be compared to infection with both *Δrop17* and kinase-dead *Δrop17 rop17*^{K312A} complemented parasites. To eliminate phosphorylation of immunity-related GTPases irrelevant to this phenotype, *Δrop18* parasites will also be used. Bands present or enriched in only monocytes or macrophages infected with wild-type *T. gondii*, but not *Δrop17*, kinase-dead *rop17*^{K312A}, or *Δrop18* parasites or uninfected controls would suggest ROP17 phosphorylation of a non-IRG target and could be sent for mass spectroscopy for protein identification. This approach is very simple to execute. Another advantage is that any detected phosphorylation events would occur within live infected cells. The primary disadvantage is that many phosphorylated threonine residues are detected by such antibodies and could easily mask the relevant ROP17-dependent events. If ROP17 phosphorylates Rho or a Rho regulator as I hypothesize, one strategy to circumvent this limitation could be performing a Rho pulldown on infected RAW lysates prior to antibody probing, thereby decreasing sample complexity and enriching for Rho and associated proteins.

If the antibody approach fails, I would then attempt a chemical genetic ATP gatekeeper pocket strategy. Briefly, in this strategy, ATP analogs are used to label the substrates of kinases engineered to accommodate these analogs via mutation of the gatekeeper residue of the ATP-binding pocket (202-204). In the presence of the ATP analogs introduced to semi-permeabilized cells, the engineered kinase thiophosphorylates substrates, which can be subsequently alkylated

and recognized by an thiophosphate ester-specific antibody (204). This approach has been previously used by our group to identify substrates for the *T. gondii* kinase CDPK1, which is highly unusual in that it naturally contains a glycine gatekeeper residue that is permissive to the ATP analogs used in this strategy (205). Glycine and alanine can both function as permissive gatekeeper residues. However, kinases often have to be engineered with compensatory mutations to maintain functionality in the presence of a permissive alanine or glycine gatekeeper (206).

I have identified the gatekeeper residue of ROP17 via sequence alignment to c-Src (Figure 4.2) and further determined that complementation of *Δrop17* parasites with *ROP17* mutant alleles featuring glycine or alanine gatekeepers can restore the enhanced collagen migration phenotype (data not shown). This successful complementation suggests that ROP17 can tolerative permissive gatekeepers. However, the robustness of these ROP17 gatekeeper mutants should be further confirmed with recombinant proteins with the *in vitro* kinase assay previously used by our group to show ROP17 activity (167). Should these assays confirm the activity of permissive gatekeeper ROP17 variants, I propose to introduce permissive ROP17 gatekeeper alleles into *Δcdpk1 T. gondii* to reduce background from naturally ATP-analog permissive CDPK1. RAW macrophages can then be infected and used in the ATP analog and alkylation schema outlined above, comparing *Δcdpk1 T. gondii* with and without permissive ROP17 alleles. ROP17 substrates can be identified by western blotting with the alkylated thiophosphate antibody and searching for bands present only upon expression of the permissive ROP17. Substrate identities would then be determined via immunoprecipitation with the alkylated thiophosphate antibody or an iodoacetyl resin that captures the labeled substrates (207), as was performed for CDPK1 (205). Because this gatekeeper ATP analog labeling strategy is performed under semi-permeabilized conditions, ROP17 will be exposed to many substrates

never encountered under physiological conditions. Accordingly, any candidate substrates identified from this approach would then be assessed for endogenous interaction with ROP17 in live cells using either pulldown or biotin labeling.

As a final approach, I propose performing comparative global phosphoproteomics to identify phosphopeptides that are enriched in monocytes infected with wild-type *T. gondii*, relative to monocytes infected with kinase-dead *ROP17*^{K312A} parasites. Due to their typical extreme low abundance, detecting phosphoproteins by mass spectroscopy is challenging (208). However, immobilized metal-ion affinity chromatography (IMAC) used in tandem with metal oxide affinity chromatography protocols have been extensively refined, allowing for enrichment of phosphopeptides from the background proteome sufficient enough to make global phosphoproteomics tractable (208). SILAC approaches further enable comparative quantification of events between samples (208). Notably, successful implementation of this strategy would identify both direct ROP17 substrates and phosphorylation events caused by downstream signaling cascades. Accordingly, it would again be critical to confirm direct interaction of ROP17 with any putative substrates.

Candidate substrates from these approaches would be assessed for direct ROP17 interaction and then analyzed by mass spectroscopy for ROP17-dependent phosphorylation comparing monocytes infected *T. gondii* expressing active and kinase-dead ROP17 alleles. To aid in detecting phosphorylation events, sampling can be focused on peptides predicted to be preferred by ROP17 as determined by a substrate motif previously generated by our group using a positional peptide scanning array (167). Functional implications of any identified phosphorylation events could then be further probed via the creation of corresponding phosphomimetic mutations and analyzing resultant changes in monocyte migration.

Assessing physiological roles of ROP17-enhanced tissue migration

The robust tissue migration of infected monocytes and macrophages suggests a role in advancing parasite spread through tissues. I demonstrated that ROP17 promotes interstitial migration of infected CX_3CR1-expressing cells in the spleen *in vivo*. However, because parasites first encounter monocytes in the intestinal lamina propria and rapidly spready beyond this compartment, I hypothesize that the major *in vivo* role of enhanced monocyte tissue migration lies in promoting parasite escape from the intestinal lamina propria.

To test this hypothesis, I propose assessing the dissemination of *Δrop17* parasites following oral inoculation with tissue cysts, which mimics the natural route of infection and leads to parasite invasion of the lamina propria. Unfortunately, this study cannot be performed with the ROP17 mutants used in my studies, as they were generated in a type I *T. gondii* background that does not form the tissue cysts in mice that are required for oral inoculation. Another group generated *Δrop17* parasites in a type II background that forms tissue cysts in mice (173). However, these mutants are also ill-suited to studying the lamina propria phase of toxoplasmosis, as the deletion of *ROP17* in this lineage led to a near complete loss of brain cyst formation (173).

To circumvent these limitations, I propose generating regulatable *ROP17* mutants in a cyst-competent *T. gondii* strain. Our group recently reported that an auxin-inducible degron (AID) system can be used to induce degradation of *T. gondii* proteins during murine infections by administering auxin to mice infected with parasites expressing the auxin receptor TIR1 and an AID-tagged knockdown target (209). To enable investigation of ROP17 function during natural infections, I would introduce TIR1 into a cyst-competent type II ME49 *T. gondii* strain developed in our lab that expresses both luciferase and mCherry. Subsequent introduction of a

ROP17-cMYC-AID allele into the resulting strain would enable auxin-inducible degradation of ROP17, which can be easily confirmed *in vitro*. To generate ROP17-deficient tissue cysts, this strain could then be inoculated into mice. Intravital luminescence imaging can be used to follow infection progression. Once parasites have colonized the CNS, auxin can be administered to the mice to induce ROP17 degradation and ROP17-deficient tissue cysts harvested for use in subsequent infections, in which auxin administration would be continued to maintain ROP17 degradation. Pitfalls to this approach include the possibility that TIR1/AID-induced ROP17 degradation would not be sufficiently severe to ablate ROP17 function, or that auxin may not robustly penetrate the blood-brain barrier. If these issues are encountered, alternative strategies could be pursued using a rapamycin-inducible dimerized Cre system already established in *T. gondii* (68), tamoxifen-inducible Cre-ER technology (210), or expression of Cre or CRISPR/Cas9 systems (187) under the expression of bradyzoite-specific *T. gondii* promoters (211) that would delay Cre or Cas9 expression until parasites differentiate into bradyzoites.

Once a robust regulatable ROP17 mutant is created in a cyst-competent lineage, this strain should be used to track parasite dissemination after oral cyst inoculation. I first propose using intravital luminescence imaging to track parasite dissemination for 1 month following oral inoculation of *ROP17*-deficient and control tissue cysts, coupled with daily administration of auxin or a vehicle control to maintain ROP17 status. Intravital luminescence imaging will be performed every 2 days for the first week, then every 5 days. After 30 days, mice will be sacrificed, and brain cyst burden assessed. Previous studies assessing a type II *Δrop17* mutant introduced into mice via intraperitoneal injection reported a near complete loss of brain cyst formation (173). Based upon my data suggesting that ROP17 promotes dissemination, I hypothesize that the observed loss of brain cysts was caused by a failure of the *Δrop17* parasites

to systemically disseminate. I accordingly predict that in this experiment, type II ROP17-deficient parasites introduced via cyst feeding will form no brain cysts, and intravital luminescence will show that they either fail to exit the abdominal cavity or exit the abdominal cavity with delayed kinetics and abundance. If the auxin-inducible strategy described above succeeds, this approach could then be complemented by another study in which auxin administration is discontinued after defined intervals to establish a time window in which ROP17-promoted dissemination is most important.

I next propose to use regulatable *ROP17* mutants in cyst competent lineages to identify leukocyte subsets that differentially migrate in response to oral infection with *ROP17*-deficient parasites. As above, mice will be orally inoculated with *ROP17*-ablated and control parasites. I will then collect mesenteric lymph nodes, peripheral blood, and spleens at early time-points after infection (1dpi, 2dpi, 3dpi, 5dpi). Samples will be split so that quantitative PCR can be used to establish parasite burden (expected to be very low) in each compartment at these early time points and flow cytometry used to identify infected leukocytes. Flow cytometry samples will be co-stained with a panel of markers selected to identify leukocyte subtypes and define the maturation status of any infected monocytes or monocyte-derived cells. The abundance of each leukocyte type in each compartment will be compared in mice infected with ROP17-proficient and ROP17-deficient *T. gondii*. I expect that leukocytes that are *in vivo* targets of ROP17-activated tissue migration would migrate to the lymph nodes and spleen in less abundance or with slower kinetics in ROP17-deficient parasite infections. After establishing the relevant leukocytes under physiological conditions, high dose tissue cyst infections could then be combined with intravital two-photon imaging to assess the *in vivo* motility of target infected leukocytes in the lamina propria.

Final Remarks

This work shows that *T. gondii* parasites use ACT1-dependent gliding motility to power productive invasion of diverse host cells, and ROP17-dependent activation of interstitial monocyte migration to spread through tissues. Future studies investigating which leukocytes and tissue compartments are targeted *in vivo* for ROP17-enhanced interstitial migration will illuminate how Trojan horses contribute to systemic *T. gondii* dissemination. In addition, probing the mechanism by which ROP17 manipulates monocyte migration such that a lowly-adhesive amoeboid mode is strongly favored over integrin-dependent modes may reveal fundamental mechanisms governing regulation of and transitions between leukocyte migratory strategies.

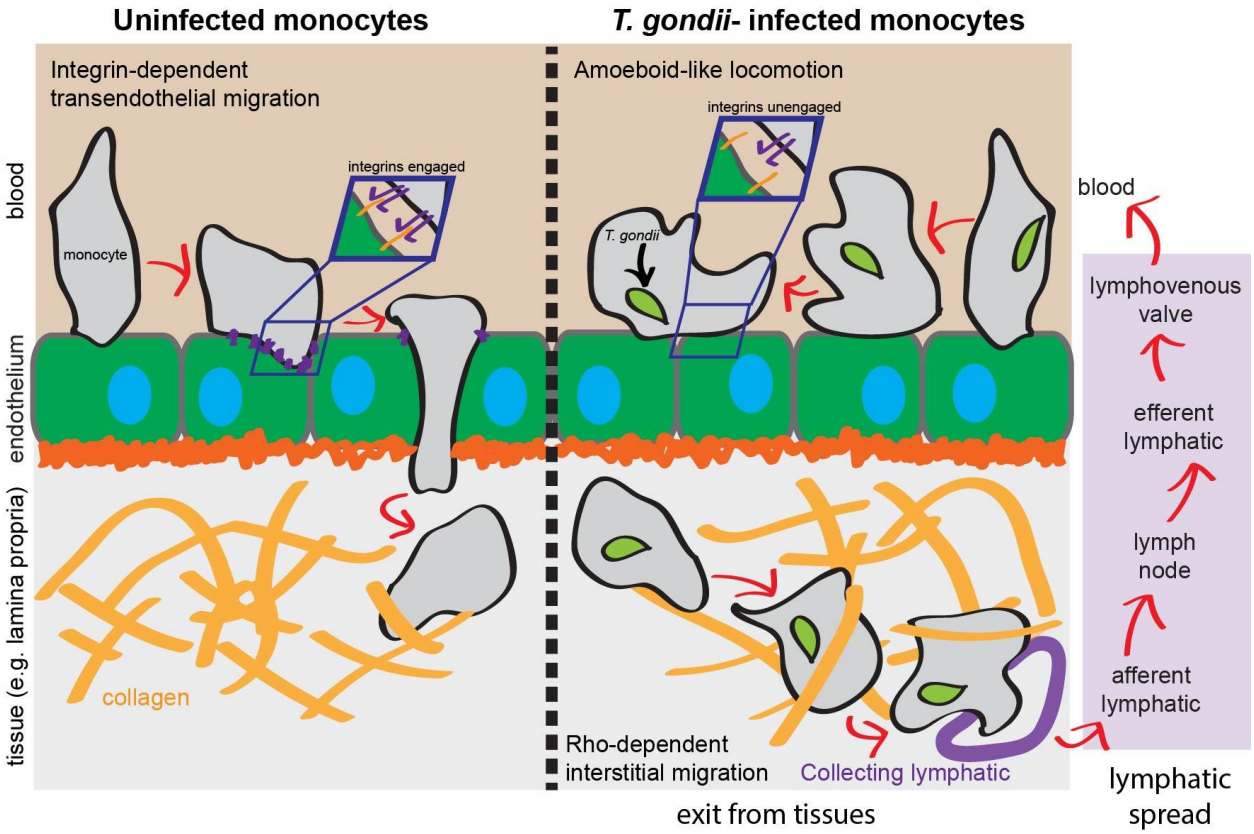

Figure 4.1: Model for monocyte contribution to *T. gondii* dissemination.

Infected monocytes inefficiently perform integrin-mediated adherence and transendothelial migration (left) but migrate through interstitial tissues with enhanced efficiency (right). Lymphatic drainage and eventual travel through the lymphovenous valve could allow migrating infected monocytes to deliver *T. gondii* into both secondary lymphoid tissues and the bloodstream.

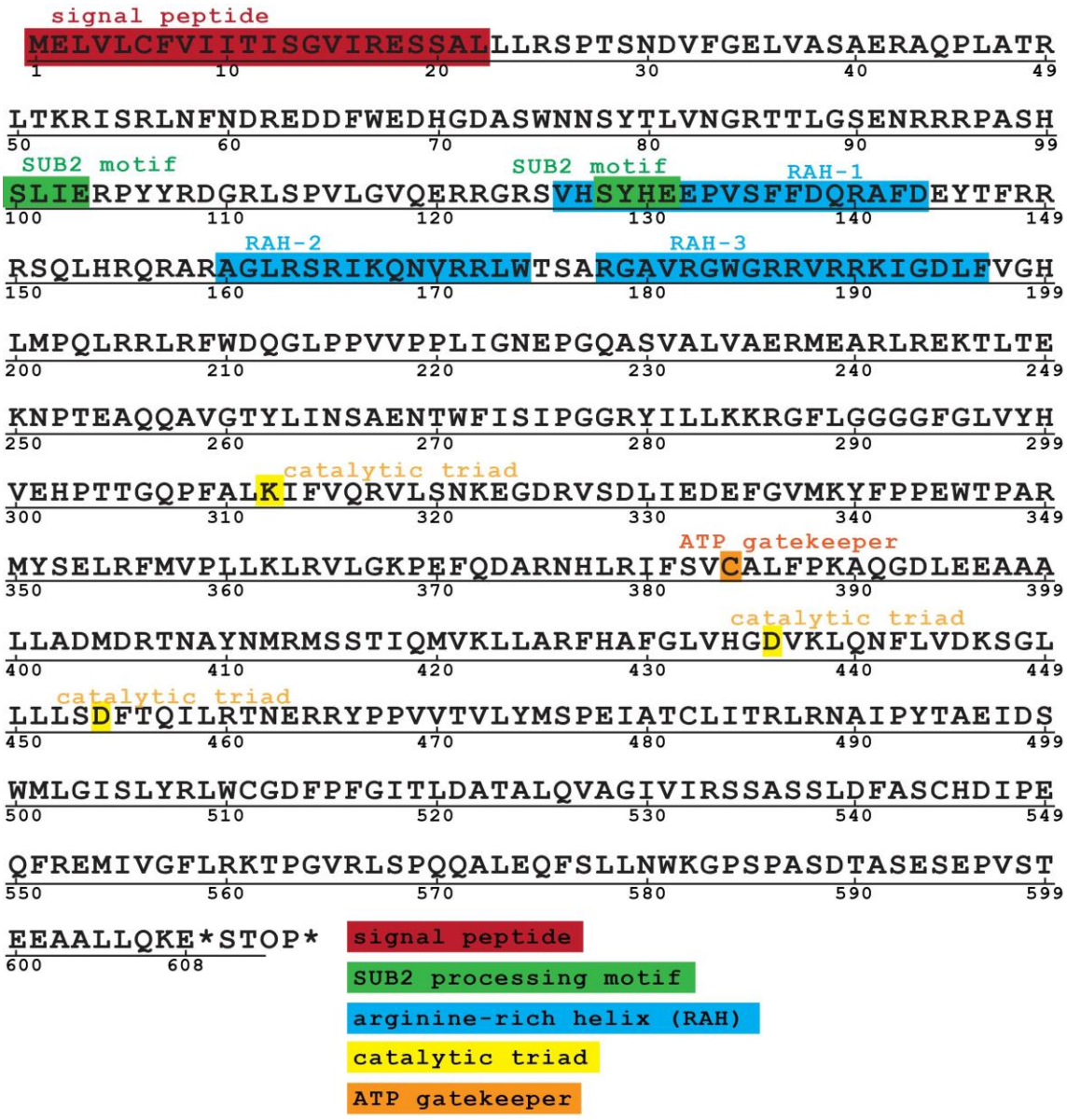

Figure 4.2: Annotated ROP17 amino acid sequence.

ROP17 amino acid sequence from genome sequence of type I *T. gondii* strain, GT1. Putative signal peptide sequence is highlighted in red, SUB2 processing motifs in green, arginine-rich amphipathic helices in blue, kinase catalytic triad residues in yellow, and the ATP gatekeeper pocket residue in orange.

References

1. Cowman, A. F., Healer, J., Marapana, D., and Marsh, K. (2016) *Cell* **167**, 610-624

2. Kotloff, K. L., Nataro, J. P., Blackwelder, W. C., Nasrin, D., Farag, T. H., Panchalingam, S., Wu, Y., Sow, S. O., Sur, D., Breiman, R. F., Faruque, A. S., Zaidi, A. K., Saha, D., Alonso, P. L., Tamboura, B., Sanogo, D., Onwuchekwa, U., Manna, B., Ramamurthy, T., Kanungo, S., Ochieng, J. B., Omore, R., Oundo, J. O., Hossain, A., Das, S. K., Ahmed, S., Qureshi, S., Quadri, F., Adegbola, R. A., Antonio, M., Hossain, M. J., Akinsola, A., Mandomando, I., Nhampossa, T., Acacio, S., Biswas, K., O'Reilly, C. E., Mintz, E. D., Berkeley, L. Y., Muhsen, K., Sommerfelt, H., Robins-Browne, R. M., and Levine, M. M. (2013) *Lancet* **382**, 209-222

3. Gibson, A. R., and Striepen, B. (2018) *Curr Biol* **28**, R193-R194

4. Blake, D. P., and Tomley, F. M. (2014) *Trends Parasitol* **30**, 12-19

5. Lassen, B., and Ostergaard, S. (2012) *Prev Vet Med* **106**, 258-265

6. Morrison, W. I. (2015) *Rev Sci Tech* **34**, 599-611

7. Montoya, J. G., and Liesenfeld, O. (2004) *Lancet* **363**, 1965-1976

8. Lindsay, D. S., and Dubey, J. P. (2007) *Toxoplasma Gondii*, 133-152

9. Dubey, J. P. (2006) *Vet Parasitol* **140**, 69-75

10. Frenkel, J. K., Dubey, J. P., and Miller, N. L. (1970) *Science* **167**, 893-896

11. Dubey, J. P. (2004) *Vet Parasitol* **126**, 57-72

12. Lindsay, D. S., Blagburn, B. L., and Dubey, J. P. (2002) *Vet Parasitol* **103**, 309-313

13. Watts, E., Zhao, Y., Dhara, A., Eller, B., Patwardhan, A., and Sinai, A. P. (2015) *mBio* **6**, e01155-01115

14. Dubey, J. P., Speer, C. A., Shen, S. K., Kwok, O. C., and Blixt, J. A. (1997) *The Journal of parasitology* **83**, 870-882

15. Dubey, J. P. (1997) *J Eukaryot Microbiol* **44**, 592-602

16. Luder, C. G. K., and Rahman, T. (2017) *Microb Cell* **4**, 203-211

17. Dobrowolski, J. M., and Sibley, L. D. (1996) *Cell* **84**, 933-939

18. Charron, A. J., and Sibley, L. D. (2004) *Traffic (Copenhagen, Denmark)* **5**, 855-867

19. Black, M. W., and Boothroyd, J. C. (2000) *Microbiol Mol Biol Rev* **64**, 607-623

20. Boyer, K., Hill, D., Mui, E., Wroblewski, K., Karrison, T., Dubey, J. P., Sautter, M., Noble, A. G., Withers, S., Swisher, C., Heydemann, P., Hosten, T., Babiarz, J., Lee, D., Meier, P., and McLeod, R. (2011) *Clinical infectious diseases : an official publication of the Infectious Diseases Society of America* **53**, 1081-1089

21. Luft, B. J., and Remington, J. S. (1992) *Clinical infectious diseases : an official publication of the Infectious Diseases Society of America* **15**, 211-222

22. Israelski, D. M., and Remington, J. S. (1993) *Current clinical topics in infectious diseases* **13**, 322-356

23. Pappas, G., Roussos, N., and Falagas, M. E. (2009) *International journal for parasitology* **39**, 1385-1394

24. Hill, D., and Dubey, J. P. (2002) *Clinical Microbiology and Infection* **8**, 634-640

25. Dubey, J. P., Miller, N. L., and Frenkel, J. K. (1970) *The Journal of experimental medicine* **132**, 636-662

26. Barragan, A., and Sibley, L. D. (2002) *The Journal of experimental medicine* **195**, 1625-1633

27. Dubey, J. P., Ferreira, L. R., Martins, J., and McLeod, R. (2012) *Parasitology* **139**, 1-13

28. Gregg, B., Taylor, B. C., John, B., Tait-Wojno, E. D., Girgis, N. M., Miller, N., Wagage, S., Roos, D. S., and Hunter, C. A. (2013) *Infect Immun* **81**, 1635-1643

29. Courret, N., Darche, S., Sonigo, P., Milon, G., Buzoni-Gâtel, D., and Tardieux, I. (2006) *Blood* **107**, 309-316

30. Konradt, C., Ueno, N., Christian, D. A., Delong, J. H., Pritchard, G. H., Herz, J., Bzik, D. J., Koshy, A. A., McGavern, D. B., Lodoen, M. B., and Hunter, C. A. (2016) *Nature Microbiology* **1**, 16001

31. Hitziger, N., Dellacasa, I., Albiger, B., and Barragan, A. (2005) *Cellular microbiology* **7**, 837-848

32. Sibley, L. D. (2010) *Current opinion in biotechnology* **21**, 592-598

33. Santiago-Tirado, F. H., and Doering, T. L. (2017) *PLoS Pathog* **13**, e1006680

34. Sumyuen, M. H., Garin, Y. J., and Derouin, F. (1995) *The Journal of parasitology* **81**, 327-329

35. Derouin, F., and Garin, Y. J. (1991) *Exp Parasitol* **73**, 460-468

36. Melzer, T. C., Cranston, H. J., Weiss, L. M., and Halonen, S. K. (2010) *J Neuroparasitology* **1**

37. Dellacasa-Lindberg, I., Hitziger, N., and Barragan, A. (2007) *Microbes and infection / Institut Pasteur* **9**, 1291-1298

38. Luder, C. G., Giraldo-Velasquez, M., Sendtner, M., and Gross, U. (1999) *Exp Parasitol* **93**, 23-32

39. Halonen, S. K., Lyman, W. D., and Chiu, F. C. (1996) *J Neuropathol Exp Neurol* **55**, 1150-1156

40. Cabral, C. M., Tuladhar, S., Dietrich, H. K., Nguyen, E., MacDonald, W. R., Trivedi, T., Devineni, A., and Koshy, A. A. (2016) *PLOS Pathogens* **12**, e1005447

41. Koshy, A. A., Dietrich, H. K., Christian, D. A., Melehani, J. H., Shastri, A. J., Hunter, C. A., and Boothroyd, J. C. (2012) *PLOS Pathogens* **8**, e1002825

42. Dzierszinski, F., Nishi, M., Ouko, L., and Roos, D. S. (2004) *Eukaryotic cell* **3**, 992-1003

43. Monnot, A. D., and Zheng, W. (2013) *Methods in molecular biology* **945**, 13-29

44. Louveau, A., Smirnov, I., Keyes, T. J., Eccles, J. D., Rouhani, S. J., Peske, J. D., Derecki, N. C., Castle, D., Mandell, J. W., Lee, K. S., Harris, T. H., and Kipnis, J. (2015) *Nature* **523**, 337-341

45. Aspelund, A., Antila, S., Proulx, S. T., Karlsen, T. V., Karaman, S., Detmar, M., Wiig, H., and Alitalo, K. (2015) *The Journal of experimental medicine* **212**, 991-999

46. Hakansson, S., Morisaki, H., Heuser, J., and Sibley, L. D. (1999) *Molecular biology of the cell* **10**, 3539-3547

47. Leung, J. M., Rould, M. A., Konradt, C., Hunter, C. A., and Ward, G. E. (2014) *PLoS ONE* **9**, e85763

48. Heintzelman, M. B. (2015) *Seminars in cell & developmental biology* **46**, 135-142

49. Sibley, L. D. (2004) *Science* **304**, 248-253

50. Lourido, S., Tang, K., and Sibley, L. D. (2012) *The EMBO journal* **31**, 4524-4534

51. Billker, O., Lourido, S., and Sibley, L. D. (2009) *Cell Host & Microbe* **5**, 612-622

52. Lovett, J. L., and Sibley, L. D. (2003) *Journal of Cell Science* **116**, 3009-3016

53. Carruthers, V. B., and Tomley, F. M. (2008) *Sub-cellular biochemistry* **47**, 33-45

54. Opitz, C., and Soldati, D. (2002) *Molecular microbiology* **45**, 597-604

55. Jacot, D., Tosetti, N., Pires, I., Stock, J., Graindorge, A., Hung, Y. F., Han, H., Tewari, R., Kursula, I., and Soldati-Favre, D. (2016) *Cell Host & Microbe* **20**, 731-743

56. Meissner, M., Schlüter, D., and Soldati, D. (2002) *Science (New York, N.Y.)* **298**, 837-840

57. Morisaki, J. H., Heuser, J. E., and Sibley, L. D. (1995) *Journal of cell science* **108 (Pt 6**, 2457-2464

58. Shen, B., and Sibley, L. D. (2012) *Current opinion in microbiology* **15**, 449-455

59. Gonzalez, V., Combe, A., David, V., Malmquist, N. A., Delorme, V., Leroy, C., Blazquez, S., Menard, R., and Tardieux, I. (2009) *Cell Host & Microbe* **5**, 259-272

60. Delorme-Walker, V., Abrivard, M., Lagal, V., Anderson, K., Perazzi, A., Gonzalez, V., Page, C., Chauvet, J., Ochoa, W., Volkmann, N., Hanein, D., and Tardieux, I. (2012) *Journal of Cell Science* **125**, 4333-4342

61. Frenal, K., Dubremetz, J. F., Lebrun, M., and Soldati-Favre, D. (2017) *Nature reviews. Microbiology* **15**, 645-660

62. Carruthers, V. B., and Sibley, L. D. (1997) *European journal of cell biology* **73**, 114-123

63. Besteiro, S., Dubremetz, J. F., and Lebrun, M. (2011) *Cellular microbiology* **13**, 797-805

64. Lamarque, M., Besteiro, S., Papoin, J., Roques, M., Vulliez-Le Normand, B., Morlon-Guyot, J., Dubremetz, J. F., Fauquenoy, S., Tomavo, S., Faber, B. W., Kocken, C. H., Thomas, A. W., Boulanger, M. J., Bentley, G. A., and Lebrun, M. (2011) *PLOS Pathogens* **7**, e1001276

65. Tyler, J. S., and Boothroyd, J. C. (2011) *PLOS Pathogens* **7**, e1001282

66. Tonkin, M. L., Roques, M., Lamarque, M. H., Pugniere, M., Douguet, D., Crawford, J., Lebrun, M., and Boulanger, M. J. (2011) *Science* **333**, 463-467

67. Dobrowolski, J. M., Niesman, I. R., and Sibley, L. D. (1997) *Cell motility and the cytoskeleton* **37**, 253-262

68. Andenmatten, N., Egarter, S., Jackson, A. J., Jullien, N., Herman, J. P., and Meissner, M. (2013) *Nature methods* **10**, 125-127

69. Egarter, S., Andenmatten, N., Jackson, A. J., Whitelaw, J. A., Pall, G., Black, J. A., Ferguson, D. J., Tardieux, I., Mogilner, A., and Meissner, M. (2014) *PLoS ONE* **9**, e91819

70. Bargieri, D. Y., Andenmatten, N., Lagal, V., Thiberge, S., Whitelaw, J. A., Tardieux, I., Meissner, M., and Ménard, R. (2013) *Nature communications* **4**, 2552

71. Barragan, A., and Sibley, L. D. (2003) *Trends Microbiol* **11**, 426-430

72. Frénal, K., Marq, J.-B., Jacot, D., Polonais, V., and Soldati-Favre, D. (2014) *PLoS pathogens* **10**, e1004504

73. Lamarque, M. H., Roques, M., Kong-Hap, M., Tonkin, M. L., Rugarabamu, G., Marq, J. B., Penarete-Vargas, D. M., Boulanger, M. J., Soldati-Favre, D., and Lebrun, M. (2014) *Nature communications* **5**, 4098

74. Skillman, K. M., Ma, C. I., Fremont, D. H., Diraviyam, K., Cooper, J. A., Sept, D., and Sibley, L. D. (2013) *Nature communications* **4**, 2285

75. Sahoo, N., Beatty, W., Heuser, J., Sept, D., and Sibley, L. D. (2006) *Molecular biology of the cell* **17**, 895-906

76. Daher, W., Plattner, F., Carlier, M. F., and Soldati-Favre, D. (2010) *PLOS Pathogens* **6**, e1001132

77. Mehta, S., and Sibley, L. D. (2011) *Molecular biology of the cell* **22**, 1290-1299

78. Skillman, K. M., Diraviyam, K., Khan, A., Tang, K., Sept, D., and Sibley, L. D. (2011) *PLOS Pathogens* **7**, e1002280

79. Vazquez-Torres, A., and Fang, F. C. (2000) *Current opinion in microbiology* **3**, 54-59

80. Vazquez-Torres, A., Jones-Carson, J., Baumler, A. J., Falkow, S., Valdivia, R., Brown, W., Le, M., Berggren, R., Parks, W. T., and Fang, F. C. (1999) *Nature* **401**, 804-808

81. Worley, M. J., Nieman, G. S., Geddes, K., and Heffron, F. (2006) *Proceedings of the National Academy of Sciences of the United States of America* **103**, 17915-17920

82. Drevets, D. A. (1999) *Infection and Immunity* **67**, 3512-3517

83. Join-Lambert, O. F., Ezine, S., Le Monnier, A., Jaubert, F., Okabe, M., Berche, P., and Kayal, S. (2005) *Cellular microbiology* **7**, 167-180

84. Drevets, D. A., Jelinek, T. A., and Freitag, N. E. (2001) *Infection and Immunity* **69**, 1344-1350

85. Sorrell, T. C., Juillard, P. G., Djordjevic, J. T., Kaufman-Francis, K., Dietmann, A., Milonig, A., Combes, V., and Grau, G. E. (2016) *Microbes and infection* **18**, 57-67

86. Charlier, C., Nielsen, K., Daou, S., Brigitte, M., Chretien, F., and Dromer, F. (2009) *Infection and Immunity* **77**, 120-127

87. Ueno, N., and Lodoen, M. B. (2015) *Current opinion in microbiology* **26**, 53-59

88. Chretien, F., Lortholary, O., Kansau, I., Neuville, S., Gray, F., and Dromer, F. (2002) *The Journal of infectious diseases* **186**, 522-530

89. Santiago-Tirado, F. H., Onken, M. D., Cooper, J. A., Klein, R. S., and Doering, T. L. (2017) *mBio* **8**

90. Pinheiro, N. F., Jr., Hermida, M. D., Macedo, M. P., Mengel, J., Bafica, A., and dos-Santos, W. L. (2006) *Infection and Immunity* **74**, 3912-3921

91. Figueira, C. P., Carvalhal, D. G., Almeida, R. A., Hermida, M., Touchard, D., Robert, P., Pierres, A., Bongrand, P., and dos-Santos, W. L. (2015) *Scientific Reports* **5**, 12862

92. Steigerwald, M., and Moll, H. (2005) *Infection and Immunity* **73**, 2564-2567

93. Randolph, G. J., Angeli, V., and Swartz, M. A. (2005) *Nature reviews. Immunology* **5**, 617-628

94. Bierly, A. L., Shufesky, W. J., Sukhumavasi, W., Morelli, A. E., and Denkers, E. Y. (2008) *J Immunol* **181**, 8485-8491

95. Lambert, H., Hitziger, N., Dellacasa, I., Svensson, M., and Barragan, A. (2006) *Cellular microbiology* **8**, 1611-1623

96. Lambert, H., Vutova, P. P., Adams, W. C., Loré, K., and Barragan, A. (2009) *Infection and immunity* **77**, 1679-1688

97. Weidner, J. M., Kanatani, S., Hernández-Castañeda, M. A., Fuks, J. M., Rethi, B., Wallin, R. P. A., and Barragan, A. (2013) *Cellular microbiology* **15**, 1735-1752

98. Fuks, J. M., Arrighi, R. B. G., Weidner, J. M., Kumar Mendu, S., Jin, Z., Wallin, R. P. A., Rethi, B., Birnir, B., and Barragan, A. (2012) *PLoS pathogens* **8**, e1003051

99. Kanatani, S., Fuks, J. M., Olafsson, E. B., Westermark, L., Chambers, B., Varas-Godoy, M., Uhlen, P., and Barragan, A. (2017) *PLOS Pathogens* **13**, e1006739

100. Weidner, J. M., Kanatani, S., Uchtenhagen, H., Varas-Godoy, M., Schulte, T., Engelberg, K., Gubbels, M. J., Sun, H. S., Harrison, R. E., Achour, A., and Barragan, A. (2016) *Cellular microbiology* **18**, 1537-1550

101. Sidik, S. M., Huet, D., and Lourido, S. (2018) *Nat Protoc* **13**, 307-323

102. Sluchanko, N. N., and Gusev, N. B. (2010) *Biochemistry (Mosc)* **75**, 1528-1546

103. Shi, C., and Pamer, E. G. (2011) *Nature reviews. Immunology* **11**, 762-774

104. Tacke, F., and Randolph, G. J. (2006) *Immunobiology* **211**, 609-618

105. Geissmann, F., Jung, S., and Littman, D. R. (2003) *Immunity* **19**, 71-82

106. Cook, J. H., Ueno, N., and Lodoen, M. B. (2018) *J Biol Chem*

107. Harker, K. S., Ueno, N., Wang, T., Bonhomme, C., Liu, W., and Lodoen, M. B. (2013) *Journal of leukocyte biology* **93**, 789-800

108. Ueno, N., Harker, K. S., Clarke, E. V., McWhorter, F. Y., Liu, W. F., Tenner, A. J., and Lodoen, M. B. (2014) *Cellular microbiology* **16**, 580-595

109. Daneman, R., and Prat, A. (2015) *Cold Spring Harb Perspect Biol* **7**, a020412

110. Ley, K., Laudanna, C., Cybulsky, M. I., and Nourshargh, S. (2007) *Nature reviews. Immunology* **7**, 678-689

111. Lambert, H., Dellacasa-Lindberg, I., and Barragan, A. (2011) *Microbes and infection / Institut Pasteur* **13**, 96-102

112. Dunay, I. R., Damatta, R. A., Fux, B., Presti, R., Greco, S., Colonna, M., and Sibley, L. D. (2008) *Immunity* **29**, 306-317

113. Dunay, I. R., Fuchs, A., and Sibley, L. D. (2010) *Infection and immunity* **78**, 1564-1570

114. Dunay, I. R., and Sibley, L. D. (2010) *Current opinion in immunology* **22**, 461-466

115. Zigmond, E., and Jung, S. (2013) *Trends Immunol* **34**, 162-168

116. Gordon, S., and Taylor, P. R. (2005) *Nature reviews. Immunology* **5**, 953-964

117. Da Gama, L. M., Ribeiro-Gomes, F. L., Guimaraes, U., Jr., and Arnholdt, A. C. (2004) *Microbes and infection* **6**, 1287-1296

118. Coombes, J. L., Charsar, B. A., Han, S. J., Halkias, J., Chan, S. W., Koshy, A. A., Striepen, B., and Robey, E. A. (2013) *Proceedings of the National Academy of Sciences of the United States of America* **110**, E1913-1922

119. Liu, C. H., Fan, Y. T., Dias, A., Esper, L., Corn, R. A., Bafica, A., Machado, F. S., and Aliberti, J. (2006) *J Immunol* **177**, 31-35

120. Hunter, C. A., and Sibley, L. D. (2012) *Nature Reviews Microbiology* **10**, 766-778

121. Lämmermann, T., and Germain, R. N. (2014) *Seminars in immunopathology* **36**, 227-251

122. Lammermann, T., Bader, B. L., Monkley, S. J., Worbs, T., Wedlich-Soldner, R., Hirsch, K., Keller, M., Forster, R., Critchley, D. R., Fassler, R., and Sixt, M. (2008) *Nature* **453**, 51-55

123. Kanatani, S., Uhlen, P., and Barragan, A. (2015) *PLoS ONE* **10**, e0139104

124. Marshall, B. T., Long, M., Piper, J. W., Yago, T., McEver, R. P., and Zhu, C. (2003) *Nature* **423**, 190-193

125. Kansas, G. S. (1996) *Blood* **88**, 3259-3287

126. Chan, J. R., Hyduk, S. J., and Cybulsky, M. I. (2001) *The Journal of experimental medicine* **193**, 1149-1158

127. Berlin, C., Bargatze, R. F., Campbell, J. J., von Andrian, U. H., Szabo, M. C., Hasslen, S. R., Nelson, R. D., Berg, E. L., Erlandsen, S. L., and Butcher, E. C. (1995) *Cell* **80**, 413-422

128. Calderwood, D. A., and Ginsberg, M. H. (2003) *Nature Cell Biology* **5**, 694-697

129. Renkawitz, J., and Sixt, M. (2010) *EMBO reports* **11**, 744-750

130. Lammermann, T., Afonso, P. V., Angermann, B. R., Wang, J. M., Kastenmuller, W., Parent, C. A., and Germain, R. N. (2013) *Nature* **498**, 371-375

131. Woolf, E., Grigorova, I., Sagiv, A., Grabovsky, V., Feigelson, S. W., Shulman, Z., Hartmann, T., Sixt, M., Cyster, J. G., and Alon, R. (2007) *Nature Immunology* **8**, 1076-1085

132. Paluch, E. K., Aspalter, I. M., and Sixt, M. (2016) *Annual review of cell and developmental biology* **32**, 469-490

133. Fackler, O. T., and Grosse, R. (2008) *The Journal of cell biology* **181**, 879-884

134. Paluch, E. K., Aspalter, I. M., and Sixt, M. (2016) *Annu Rev Cell Dev Biol* **32**, 469-490

135. Hynes, R. O. (2002) *Cell* **110**, 673-687

136. Humphries, J. D., Byron, A., and Humphries, M. J. (2006) *J Cell Sci* **119**, 3901-3903

137. Renkawitz, J., Schumann, K., Weber, M., Lammermann, T., Pflicke, H., Piel, M., Polleux, J., Spatz, J. P., and Sixt, M. (2009) *Nat Cell Biol* **11**, 1438-1443

138. Cougoule, C., Van Goethem, E., Le Cabec, V., Lafouresse, F., Dupré, L., Mehraj, V., Mège, J.-L., Lastrucci, C., and Maridonneau-Parini, I. (2012) *European Journal of Cell Biology* **91**, 938-949

139. Van Goethem, E., Poincloux, R., Gauffre, F., Maridonneau-Parini, I., and Le Cabec, V. (2010) *The Journal of Immunology* **184**, 1049-1061

140. Carruthers, V., and Boothroyd, J. C. (2007) *Current opinion in microbiology* **10**, 83-89

141. Lebrun, M., Michelin, A., El Hajj, H., Poncet, J., Bradley, P. J., Vial, H., and Dubremetz, J. F. (2005) *Cellular microbiology* **7**, 1823-1833

142. Alexander, D. L., Mital, J., Ward, G. E., Bradley, P., and Boothroyd, J. C. (2005) *PLoS pathogens* **1**, e17

143. Ryning, F. W., and Remington, J. S. (1978) *Infection and Immunity* **20**, 739-743

144. Mital, J., Meissner, M., Soldati, D., and Ward, G. E. (2005) *Molecular biology of the cell* **16**, 4341-4349

145. Brossier, F., Jewett, T. J., Lovett, J. L., and Sibley, L. D. (2003) *The Journal of biological chemistry* **278**, 6229-6234

146. Toyama, S. (1988) *The Journal of Cell Biology* **107**, 1499-1504

147. Gordon, J. L., and Sibley, L. D. (2005) *BMC genomics* **6**, 179

148. Buguliskis, J. S., Brossier, F., Shuman, J., and Sibley, L. D. (2010) *PLOS Pathogens* **6**, e1000858

149. Shen, B., Buguliskis, J. S., Lee, T. D., and Sibley, L. D. (2014) *mBio* **5**, e01795-01714

150. Harker, K. S., Ueno, N., and Lodoen, M. B. (2015) *Parasite immunology* **37**, 141-149

151. Dubey, J. P., Speer, C. A., Shen, S. K., Kwok, O. C., and Blixt, J. A. (1997) *J Parasitol* **83**, 870-882

152. Joeris, T., Muller-Luda, K., Agace, W. W., and Mowat, A. M. (2017) *Mucosal Immunol* **10**, 845-864

153. Olafsson, E. B., Varas-Godoy, M., and Barragan, A. (2018) *Cell Microbiol* **20**

154. Fuks, J. M., Arrighi, R. B., Weidner, J. M., Kumar Mendu, S., Jin, Z., Wallin, R. P., Rethi, B., Birnir, B., and Barragan, A. (2012) *PLoS Pathog* **8**, e1003051

155. Daniels, B. P., Cruz-Orengo, L., Pasieka, T. J., Couraud, P.-O., Romero, I. A., Weksler, B., Cooper, J. A., Doering, T. L., and Klein, R. S. (2013) *Journal of neuroscience methods* **212**, 173-179

156. van Kooyk, Y., and Figdor, C. G. (2000) *Current Opinion in Cell Biology* **12**, 542-547

157. Onken, M. D., Mooren, O. L., Mukherjee, S., Shahan, S. T., Li, J., and Cooper, J. A. (2014) *Cytoskeleton (Hoboken, N.J.)* **71**, 695-706

158. Belin, B. J., Goins, L. M., and Mullins, R. D. (2014) *Bioarchitecture* **4**, 189-202

159. Charras, G., and Paluch, E. (2008) *Nat Rev Mol Cell Biol* **9**, 730-736

160. Wolf, K., Alexander, S., Schacht, V., Coussens, L. M., von Andrian, U. H., van Rheenen, J., Deryugina, E., and Friedl, P. (2009) *Seminars in cell & developmental biology* **20**, 931-941

161. Weber, M., and Sixt, M. (2013) *Methods Mol Biol* **1013**, 215-226

162. Shang, X., Marchioni, F., Sipes, N., Evelyn, C. R., Jerabek-Willemsen, M., Duhr, S., Seibel, W., Wortman, M., and Zheng, Y. (2012) *Chem Biol* **19**, 699-710

163. Martiny-Baron, G., Kazanietz, M. G., Mischak, H., Blumberg, P. M., Kochs, G., Hug, H., Marme, D., and Schachtele, C. (1993) *J Biol Chem* **268**, 9194-9197

164. Rizvi, S. A., Neidt, E. M., Cui, J., Feiger, Z., Skau, C. T., Gardel, M. L., Kozmin, S. A., and Kovar, D. R. (2009) *Chem Biol* **16**, 1158-1168

165. Nolen, B. J., Tomasevic, N., Russell, A., Pierce, D. W., Jia, Z., McCormick, C. D., Hartman, J., Sakowicz, R., and Pollard, T. D. (2009) *Nature* **460**, 1031-1034

166. Hakimi, M. A., Olias, P., and Sibley, L. D. (2017) *Clin Microbiol Rev* **30**, 615-645

167. Etheridge, Ronald D., Alaganan, A., Tang, K., Lou, Hua J., Turk, Benjamin E., and Sibley, L. D. (2014) *Cell Host & Microbe* **15**, 537-550

168. Ihara, K., Muraguchi, S., Kato, M., Shimizu, T., Shirakawa, M., Kuroda, S., Kaibuchi, K., and Hakoshima, T. (1998) *The Journal of biological chemistry* **273**, 9656-9666

169. Talevich, E., and Kannan, N. (2013) *BMC Evol Biol* **13**, 117

170. Guilluy, C., Garcia-Mata, R., and Burridge, K. (2011) *Trends in cell biology* **21**, 718-726

171. Swirski, F. K., Nahrendorf, M., Etzrodt, M., Wildgruber, M., Cortez-Retamozo, V., Panizzi, P., Figueiredo, J. L., Kohler, R. H., Chudnovskiy, A., Waterman, P., Aikawa, E., Mempel, T. R., Libby, P., Weissleder, R., and Pittet, M. J. (2009) *Science* **325**, 612-616

172. Renkawitz, J., and Sixt, M. (2010) *EMBO Rep* **11**, 744-750

173. Fox, B. A., Rommereim, L. M., Guevara, R. B., Falla, A., Hortua Triana, M. A., Sun, Y., and Bzik, D. J. (2016) *mBio* **7**, e00193-00116

174. Hodge, R. G., and Ridley, A. J. (2016) *Nature Reviews Molecular Cell Biology* **17**, 496-510

175. Weksler, B. B., Subileau, E. A., Perrière, N., Charneau, P., Holloway, K., Leveque, M., Tricoire-Leignel, H., Nicotra, A., Bourdoulous, S., Turowski, P., Male, D. K., Roux, F., Greenwood, J., Romero, I. A., and Couraud, P. O. (2005) *FASEB journal : official publication of the Federation of American Societies for Experimental Biology* **19**, 1872-1874

176. Kreisel, D., Nava, R. G., Li, W., Zinselmeyer, B. H., Wang, B., Lai, J., Pless, R., Gelman, A. E., Krupnick, A. S., and Miller, M. J. (2010) *Proceedings of the National Academy of Sciences of the United States of America* **107**, 18073-18078

177. Zinselmeyer, B. H., Dempster, J., Wokosin, D. L., Cannon, J. J., Pless, R., Parker, I., and Miller, M. J. (2009) *Methods in enzymology* **461**, 349-378

178. Kowarz, E., Loscher, D., and Marschalek, R. (2015) *Biotechnol J* **10**, 647-653

179. Alaganan, A., Fentress, S. J., Tang, K., Wang, Q., and Sibley, L. D. (2014) *Proceedings of the National Academy of Sciences of the United States of America* **111**, 1126-1131

180. Pfefferkorn, E. R., and Kasper, L. H. (1983) *Exp Parasitol* **55**, 207-218

181. Dubey, J. P. (1992) *The Journal of parasitology* **78**, 151-153

182. Tobin, C. M., and Knoll, L. J. (2012) *Infect Immun* **80**, 55-61

183. Huynh, M. H., and Carruthers, V. B. (2009) *Eukaryotic cell* **8**, 530-539

184. Khan, A., Shaik, J. S., Behnke, M., Wang, Q., Dubey, J. P., Lorenzi, H. A., Ajioka, J. W., Rosenthal, B. M., and Sibley, L. D. (2014) *BMC genomics* **15**, 1168

185. Behnke, M. S., Khan, A., Wootton, J. C., Dubey, J. P., Tang, K., and Sibley, L. D. (2011) *Proceedings of the National Academy of Sciences of the United States of America* **108**, 9631-9636

186. Fentress, S. J., Behnke, M. S., Dunay, I. R., Mashayekhi, M., Rommereim, L. M., Fox, B. A., Bzik, D. J., Taylor, G. A., Turk, B. E., Lichti, C. F., Townsend, R. R., Qiu, W., Hui, R., Beatty, W. L., and Sibley, L. D. (2010) *Cell Host & Microbe* **8**, 484-495

187. Shen, B., Brown, K. M., Lee, T. D., and Sibley, L. D. (2014) *mBio* **5**, e01114-01114

188. Drewry, L. L., and Sibley, L. D. (2015) *mBio* **6**, e00557

189. Whitelaw, J. A., Latorre-Barragan, F., Gras, S., Pall, G. S., Leung, J. M., Heaslip, A., Egarter, S., Andenmatten, N., Nelson, S. R., Warshaw, D. M., Ward, G. E., and Meissner, M. (2017) *BMC Biol* **15**, 1

190. Long, S., Brown, K. M., Drewry, L. L., Anthony, B., Phan, I. Q. H., and Sibley, L. D. (2017) *PLOS Pathogens* **13**, e1006379

191. Taylor, G. A., Feng, C. G., and Sher, A. (2007) *Microbes and infection* **9**, 1644-1651

192. Suss-Toby, E., Zimmerberg, J., and Ward, G. E. (1996) *Proceedings of the National Academy of Sciences of the United States of America* **93**, 8413-8418

193. Fentress, S. J., Steinfeldt, T., Howard, J. C., and Sibley, L. D. (2012) *Cellular microbiology* **14**, 1921-1933

194. Reese, M. L., and Boothroyd, J. C. (2009) *Traffic* **10**, 1458-1470

195. Baba, M., Batanova, T., Kitoh, K., and Takashima, Y. (2017) *Sci Rep* **7**, 5675

196. Randolph, G. J., Ivanov, S., Zinselmeyer, B. H., and Scallan, J. P. (2017) *Annu Rev Immunol* **35**, 31-52

197. Jakubzick, C., Gautier, E. L., Gibbings, S. L., Sojka, D. K., Schlitzer, A., Johnson, T. E., Ivanov, S., Duan, Q., Bala, S., Condon, T., van Rooijen, N., Grainger, J. R., Belkaid, Y., Ma'ayan, A., Riches, D. W., Yokoyama, W. M., Ginhoux, F., Henson, P. M., and Randolph, G. J. (2013) *Immunity* **39**, 599-610

198. Petrie, R. J., and Yamada, K. M. (2016) *Current Opinion in Cell Biology* **42**, 7-12

199. Schmidt, S., and Friedl, P. (2010) *Cell and Tissue Research* **339**, 83-92

200. Labesse, G., Gelin, M., Bessin, Y., Lebrun, M., Papoin, J., Cerdan, R., Arold, S. T., and Dubremetz, J. F. (2009) *Structure* **17**, 139-146

201. Nadipuram, S. M., Kim, E. W., Vashisht, A. A., Lin, A. H., Bell, H. N., Coppens, I., Wohlschlegel, J. A., and Bradley, P. J. (2016) *mBio* **7**

202. Witucki, L. A., Huang, X., Shah, K., Liu, Y., Kyin, S., Eck, M. J., and Shokat, K. M. (2002) *Chemistry & biology* **9**, 25-33

203. Lourido, S., Zhang, C., Lopez, M. S., Tang, K., Barks, J., Wang, Q., Wildman, S. A., Shokat, K. M., and Sibley, L. D. (2013) *Journal of Medicinal Chemistry* **56**, 3068-3077

204. Allen, J. J., Li, M., Brinkworth, C. S., Paulson, J. L., Wang, D., Hubner, A., Chou, W. H., Davis, R. J., Burlingame, A. L., Messing, R. O., Katayama, C. D., Hedrick, S. M., and Shokat, K. M. (2007) *Nature methods* **4**, 511-516

205. Lourido, S., Jeschke, G. R., Turk, B. E., and Sibley, L. D. (2013) *ACS Chemical Biology* **8**, 1155-1162

206. Blethrow, J., Zhang, C., Shokat, K. M., and Weiss, E. L. (2004) *Curr Protoc Mol Biol* **Chapter 18**, Unit 18 11

207. Blethrow, J. D., Glavy, J. S., Morgan, D. O., and Shokat, K. M. (2008) *Proceedings of the National Academy of Sciences of the United States of America* **105**, 1442-1447

208. von Stechow, L., Francavilla, C., and Olsen, J. V. (2015) *Expert Rev Proteomics* **12**, 469-487

209. Brown, K. M., and Sibley, L. D. (2018) *Cell Host & Microbe*

210. Metzger, D., and Chambon, P. (2001) *Methods* **24**, 71-80

211. Paredes-Santos, T. C., Tomita, T., Yan Fen, M., de Souza, W., Attias, M., Vommaro, R. C., and Weiss, L. M. (2016) *Microbes and infection* **18**, 39-47